MODELING, STABILITY ANALYSIS AND CONTROL SYSTEM DESIGN OF A SMALL-SIZED TILTROTOR UAV

A THESIS SUBMITTED TO
THE GRADUATE SCHOOL OF NATURAL AND APPLIED SCIENCES
OF
MIDDLE EAST TECHNICAL UNIVERSITY

BY

FERİT ÇAKICI

IN PARTIAL FULFILLMENT OF THE REQUIREMENTS
FOR
THE DEGREE OF MASTER OF SCIENCE
IN
ELECTRICAL AND ELECTRONICS ENGINEERING

FEBRUARY 2009

Approval of the thesis:

MODELING, STABILITY ANALYSIS AND CONTROL SYSTEM DESIGN OF A SMALL-SIZED TILTROTOR UAV

submitted by **FERİT ÇAKICI** in partial fulfillment of the requirements for the degree of **Master of Science in Electrical and Electronics Engineering Department, Middle East Technical University** by,

Prof. Dr. Canan Özgen
Dean, Gradute School of **Natural and Applied Sciences** _____

Prof. Dr. İsmet Erkmen
Head of Department, **Electrical and Electronics Engineering** _____

Prof. Dr. M. Kemal Leblebicioğlu
Supervisor, **Electrical and Electronics Engineering, METU** _____

Examining Committee Members:

Prof. Dr. M. Kemal Özgören
Mechanical Engineering, METU _____

Prof. Dr. M. Kemal Leblebicioğlu
Electrical and Electronics Engineering, METU _____

Prof. Dr. Aydan Erkmen
Electrical and Electronics Engineering, METU _____

Assist. Prof. Dr. Afşar Saranlı
Electrical and Electronics Engineering, METU _____

Assist. Prof. Dr. İlkay Yavrucuk
Aerospace Engineering, METU _____

Date: **05.02.2009**

I hereby declare that all information in this document has been obtained and presented in accordance with academic rules and ethical conduct. I also declare that, as required by these rules and conduct, I have fully cited and referenced all material and results that are not original to this work.

Name, Last name : FERİT ÇAKICI

Signature :

ABSTRACT

MODELING, STABILITY ANALYSIS AND CONTROL SYSTEM DESIGN OF A SMALL-SIZED TILTROTOR UAV

Çakıcı, Ferit

M.Sc., Department of Electrical and Electronics Engineering

Supervisor: Prof. Dr. M. Kemal Leblebicioğlu

February 2009, 126 pages

Unmanned Aerial Vehicles (UAVs) are remotely piloted or self-piloted aircrafts that can carry cameras, sensors, communications equipment or other payloads. Tiltrotor UAVs provide a unique platform that fulfills the needs for ever-changing mission requirements by combining the desired features; hovering like a helicopter and reaching high forward speeds like an airplane. In this work, the conceptual design and aerodynamical model of a realizable small-sized Tiltrotor UAV is constructed, the linearized state-space models are obtained around the trim points for airplane, helicopter and conversion modes, controllers are designed using Linear Quadratic Regulator (LQR) methods and gain-scheduling is employed to obtain a simulation for the whole flight envelope. The ideas for making a real flying model are established according to simulation results.

Keywords: UAV, Tiltrotor, LQR, Control, Optimization.

ÖZ

DÖNER-ROTORLU (TILTROTOR) MİNİ İHA MODELLEMESİ, KARARLILIK ANALİZİ VE KONTROL SİSTEMİ TASARIMI

Çakıcı, Ferit

Yüksek Lisans, Elektrik ve Elektronik Mühendisliği Bölümü

Tez Yöneticisi: Prof. Dr. M. Kemal Leblebicioğlu

Şubat 2009, 126 sayfa

İnsansız Hava Araçları (İHA) kameralar, algılayıcılar, iletişim araçları ve diğer faydalı yükleri taşıyabilen, uzaktan kumanda ile veya kendi kendine uçabilen hava araçlarıdır. Döner-rotorlu İHA'lar yapısal olarak sahip olduğu helikopter ve uçak modlarıyla, bu hava araçlarının havada asılı kalma ve yüksek seyir hızı gibi tercih edilen özelliklerini bünyesinde barındıran bir hava platformu olarak, kullanım alanlarındaki değişken ihtiyaçlara cevap verebilecek bir yapıya sahiptir. Bu çalışmada, model uçak malzemeleriyle üretilebilecek döner-rotorlu bir mini İHA'nın kavramsal tasarımı yapılmış, aerodinamik modeli oluşturulmuş, helikopter, uçak ve geçiş modları için denge noktaları hesaplanarak doğrusal modelleri elde edilmiş, LQR (Linear Quadratic Regulator) yöntemiyle doğrusal kontrolcüler tasarlanmış ve bütün uçuş zarfı için kazanç ayarlama (Gain-scheduling) yöntemiyle kontrol sisteminin benzetimi gerçekleştirilmiştir. Elde edilen sonuçlar çerçevesinde, gerçek bir modelin prototipinin oluşturulmasına yönelik fikirler öne sürülmüştür.

Anahtar Kelimeler: İHA, Döner-Rotor, Optimal, Kontrol, Optimizasyon.

Everyone believes the test results, except the person who made the measurements, and nobody believes the theoretical results, except the person who calculated them. This work is dedicated to colleagues, who make both theoretical and test results believable.

ACKNOWLEDGEMENTS

The author wishes to express his deepest gratitude to his supervisor Prof. Dr. M. Kemal Leblebicioğlu for his guidance, advice, criticism, encouragements and insight throughout this research.

The author also would like to thank H. Erdem Akın and Yakup Ertaş for their support and encouragements throughout this work. Also, the technical assistance and long last patience of Zafer Kaya was invaluable.

TABLE OF CONTENTS

LIST OF TABLES

TABLES

LIST OF FIGURES

FIGURES

LIST OF SYMBOLS AND ABBREVIATIONS

SYMBOLS

F_I : Inertial reference frame, inertial axes.

F_E : Earth reference frame, Earth surface axes.

F_{EC} : Earth reference frame, Earth center axes.

F_V : Vehicle-carried reference frame, vehicle-carried axes.

F_B : Body-fixed reference frame, body axes.

F_{WI} : Wings frame.

F_{HT} : Horizontal tail frame.

F_{VT} : Vertical tail frame.

F_{PR} : Propeller frame.

F_{AF} : Airfoil frame.

$m_B\,(kg)$: Mass of the aircraft.

$I_B\,(kg\,m^2)$: Inertia tensor of the aircraft in body axes.

$S\,(m^2)$: Crossectional surface area of the fuselage.

$X, Y, Z\,(N)$: Net forces in body frame.

$L, M, N\,(Nm)$: Net moments in body frame.

$u, v, w\,(m/s)$: Linear velocities in body frame.

$p, q, r\,(\deg/s)$: Angular velocities in body frame.

$\phi, \theta, \psi\,(\deg)$: Euler angles (roll, pitch, yaw) in vehicle-carried frame.

$x_e, y_e, z_e\,(m)$: Location of the origin of the vehicle-carried frame in the Earth axes.

$T\,(K)$: Temperature of the atmosphere.

$\rho\,(kg/m^3)$: Air density in the atmosphere.

$\mu\,(kg/m\,s)$: Viscosity in the atmosphere.

$a\,(m/s)$: Speed of sound in the atmosphere.

$g\left(m/s^2\right)$: Gravitational acceleration in vehicle-carried frame.

Ma : Mach number.

Re : Reynolds number.

$q_\infty\left(Pa\right)$: Dynamic air pressure.

$\Omega_x\left(RPM\right)$: Rotational speed of the propeller X.

$\theta_x\left(\deg\right)$: Tilt angle of the propeller X.

$r_0\left(m\right)$: Root length of a blade.

$R\left(m\right)$: Span length of a blade.

$V_i\left(m/s\right)$: Velocity of inflow air sucked by propeller.

B : Tip-loss factor.

$A\left(m^2\right)$: Disc area of the propeller.

μ : Advance ratio of the propeller.

C_T : Thrust coefficient of the propeller.

C_M : Torque coefficient of the propeller.

C_P : Power coefficient of the propeller.

$c\left(m\right)$: Chord-length of the airfoil.

$V_\infty\left(m/s\right)$: Freestream air velocity.

${}^{AF}V_\infty\left(m/s\right)$: Air velocity in airfoil frame.

${}^{AF}\alpha_\infty\left(\deg\right)$: Angle of attack in airfoil frame.

$\alpha_0\left(\deg\right)$: Zero-lift angle of attack of the airfoil.

C_L : Lift coefficient of the airfoil.

C_D : Drag coefficient of the airfoil.

C_M : Moment coefficient of the airfoil.

$dL\left(N/m\right)$: Section lift of the airfoil per unit span.

$dD\left(N/m\right)$: Section drag of the airfoil per unit span.

$dM\left(N\right)$: Section moment of the airfoil per unit span.

C_l : Section lift coefficient of the airfoil.

C_d : Section drag coefficient of the airfoil.

C_m : Section moment coefficient of the airfoil.

x : States vector.

u : Control inputs vector.

Q : States weighting matrix of LQR.

R : Inputs weighting matrix of LQR.

K : Full-state feedback gain matrix of LQR.

P : State transition matrix of LQR.

ABBREVIATIONS

UAV	: Unmanned aerial vehicle.
LQR	: Linear quadratic regulator.
NACA	: National Advisory Committee on Aeronautics.
DOF	: Degrees of freedom.
AoA	: Angle of attack.
c.g.	: Center of gravity.
IGE	: In ground effect.
RPM	: Revolutions per minute.
ISA	: International standard atmosphere.
WGS	: World geodetic system.
AF	: Airfoil.
WI	: Wings.
HT	: Horizontal tail.
VT	: Vertical tail.
PR	: Propeller.
CW	: Clock-wise rotation.
CCW	: Counter clock-wise rotation.
NB	: The number of blades in a propeller.
GPS	: Generalized pattern search.
CFD	: Computational fluid dynamics.
H.O.T.	: Higher order terms.
ARE	: Algebraic Riccati equation.
CE	: Control effort.
PSD	: Power spectrum density.

CHAPTER 1

INTRODUCTION

Aerial vehicles have proved their usefulness in military (combat, deployment of units, patrolling, surveillance, reconnaissance, etc.) and civil areas (transport, search and rescue, fire-fighting, etc.) of application over a hundred years, with enhancing their capabilities over time, and fulfilling ever-changing requirements. Starting with aerostats, following with aerodynes, they have become one of the major subjects of the scientifical research community; always using the latest technology with big budgets.

The most popular aerial vehicles, helicopters and airplanes have become available in easing human life, and providing a large range of abilities with mass-numbered productions. The low speed limits of airplanes and high speed limits of helicopters have made their usage areas different from each other. Although, a lot of effort has been spent to combine the advantages of these aircrafts into one platform with eliminating disadvantages; like tiltwings and tailsitters, and none has been successful enough to go into production, until tiltrotors.

A tiltrotor aircraft combined the vertical lift capability of a helicopter with the speed and range of a turboprop airplane. As the name implies, a tiltrotor aircraft uses tiltable rotating propellers, or proprotors, for lift and propulsion. For vertical flight, the proprotors are angled to direct their thrust upwards providing lift. In this mode of operation the aircraft is essentially identical to a helicopter. As the aircraft gains forward speed, the proprotors are slowly tilted forward, with the blades eventually becoming perpendicular to the ground. In this mode, the wings provide the lift, and the wings' greater efficiency helps the tiltrotor achieve its high speed. In this mode, the aircraft is essentially a turboprop aircraft. Although the choice of using a

comparable helicopter instead of a tiltrotor does not seem to be feasible for today, according to Leishman [1], it sure holds its potential for the future.

Aside from cargo and transport missions, unmanned aerial vehicles (UAVs) have become popular with accomplishing a number of military roles like reconnaissance and attack, and a growing number of civil usages, for over a few decades. UAVs have lowered the operating costs and potential risks, and extended their capabilities with eliminating the need for an onboard human pilot. UAVs can be remotely controlled or flown autonomously based on pre-programmed flight plans or more complex dynamic automation systems. Small-sized UAVs of airplane and helicopter types have been developed and are currently in use in many mission-specific areas.

Being inspired by the capabilities of Tiltrotors and UAVs, the leading idea discussed in this thesis is based on the conceptual design of a small-sized Tiltrotor UAV.

1.1. Purpose and Scope of the Thesis

This study aims to assert an initial conceptual design for a small-sized Tiltrotor UAV, explore its dynamics, and determine control strategies and requirements for a manufacturable model that can be realized with the hobbyist's model airplane parts. With that purpose, simulation programs are prepared in order to obtain the numerical results for the design phases.

The geometrical design of the aircraft is realized with modeling of all the components individually, and then combining them together in order to form the full aircraft model. Then, aerodynamical model is constructed based on the geometrical model, and it is used to simulate the aircraft in flight, with the purpose of obtaining the forces and moments generated. Trim points have been calculated for navigation states, that encapsulates the entire flight envelope. Analytic and numerical linearization techniques are utilized in order to obtain linearized state-space models around the trim points. The stability characteristics of the aircraft are examined from the linearized models, with the inspection of the eigenvalues. An LQR (Linear Quadratic Regulator) based optimal control system is designed in order to control the Tiltrotor UAV for the overall flight envelope.

When the aircraft gains forward speed in level flight, it is expected that the trim points will guide Tiltrotor UAV from helicopter mode to conversion mode, and when

the cruise speed is reached, finally to the airplane mode. In these mode transitions, the trends in the trim input values are expected to tell us, how the conversion is accomplished from the control point of view. Considering the power requirements, less power should be required in the airplane mode and descends, much power in the helicopter mode and ascends, and in-between power levels for the conversion modes.

Although the main textbooks about helicopters and airplanes make certain assumptions, for the sake of simplicity, these assumptions are avoided wherever possible, for the sake of revealing the true characteristics of this conceptual aircraft.

1.2. Previous Works

The number of scientifical studies about tiltrotors and tiltrotor UAVs found in the literature is less then helicopters and airplanes, because of the chronological development phases of these types of aircrafts.

Early Tiltrotor studies started in the 1940's. Later, Bell Helicopter Company developed the first successful Tiltrotor XV-3 in 1960's, yielding the development of the XV-15 by Bell/Army/NASA Team in 1973. The experience gained from the XV-15 fostered the V-22 Osprey. Bell, teamed with AgustaWestland, is currently developing the commercial BA609, and the firm has also developed a Tiltrotor UAV, the TR918 Eagle Eye (Bell [2]). Current research on the four-rotor version of the V-22 with two tandem sets of fixed wings and four tilting rotors is still in progress.

An innovative conceptual design study for a heavy lift Mono-Tiltrotor has been proposed by Preator [3], that integrates a tilting coaxial-rotor, an aerodynamically deployed folding wing, and an efficient cargo handling system. T-Wing: a tandem-wing tailsitter UAV concept demonstator has been implemented by Castillo [25], with LQR control.

Linear modeling and stability analysis for a tiltrotor has been performed by Kleinhesselink [4] and Klein [5]. It is shown that Tiltrotors, V-22 and XV-15 have similar unstable characteristics in the helicopter modes, and similar stable characteristics in the airplane modes.

Hobbyist's model propellers' performance has been investigated by Merchant [6], which are proprietary informations for manufacturers.

LQR control of a quadrotor has been implemented by Cowling [7], and a small-sized helicopter model is controlled with LQR by Karasu [8].

1.3. Contributions

The main contribution aimed in this thesis, is the introduction of the conceptual design of a small-sized Tiltrotor UAV, which may perform well in reconnaissance, surveillance, search-rescue and disaster observation missions, with its vertical take off-landing and high-speed, efficient level flight capabilities.

Also, with the help of GUI-based softwares prepared in this work, modeling, trimming, linearization, investigation of stability characteristics, and control system design have become easy, allowing the designer to make any trade-offs for the initial design, in order to meet the desired performance specifications.

Tiltrotors have helicopter-like controls in the helicopter mode, helicopter-airplane-like controls in the conversion modes, and airplane-like controls in the airplane mode. The idea asserted in this thesis for controls, is that two tiltrotors where RPMs and tilts can be set independent of each other, for all modes of operations.

Tiltrotor UAV's aerodynamical simulations are conducted using look-up tables of aerodynamical coefficients of airfoils, instead of using simplified formulas, due to the increased nonlinearity of these coefficients in small-scale, in order to obtain more realistic results.

A general trim algorithm is proposed in order to obtain trim conditions for the overall flight envelope. In addition, an LQR based control system design for tiltrotors is proposed.

This work was presented (Çakıcı [26]) in the 50th Annual Conference of Turkish National Committee of Automatic Control (TOK 2008) on 13-15 November 2008, which was organized by Istanbul Technical University, in Istanbul, Turkey.

1.4. Outline of the Chapters

Chapter 1: This chapter makes an introduction, sets the purpose, determines the scope and gives information about relevant previous studies.

Chapter 2: This chapter reveals the mathematical modeling and underlying ideas for composing the geometrical and aerodynamical model of the conceptual Tiltrotor UAV. First, the reference frames and variables are defined. The assumptions and espousals are introduced. Then, the models for environment, motion, fuselage, propeller, wings and airfoils are derived.

Chapter 3: In this chapter, stability analysis is performed with identifying the nature of the trim algorithm, linearization concepts, and inspection of the eigenvalues of the linearized system to observe its stability characteristics.

Chapter 4: This chapter contains the underlying theorems and methods used in designing the control system of the Tiltrotor UAV. LQR is discussed as the control system for the linearized models.

Chapter 5: In this chapter, the modeling and simulation programs prepared in this study are explained, with the addition of implementation methods of theoretical background, which was set in Chapter 3 and Chapter 4.

Chapter 6: In this chapter, the simulations performed and their results are presented with comments and discussions.

Chapter 7: The studies conducted for this thesis are criticized and summarized as a conclusion.

Chapter 8: The ideas for the future works that may follow this research are stated in this chapter.

CHAPTER 2

MATHEMATICAL MODELING

Since the dynamics of the aerial vehicles are very complex, the accurate models for a large portion of the flight envelope are difficult to collect. However, some techniques have been developed like mathematical modeling and system identification, different but complementary techniques. By mathematical modeling, the linear models at trim points are calculated. The main drawback of this technique is the requirement of many physical parameters. The system identification technique requires the treatment of the time response data or the frequency-response data obtained from the flight tests. The main problem with this technique is the difficulty of simulating the full envelope and realizing the flight tests, which are expensive and time-consuming. By combining these two techniques, accurate models may be generated for the flight simulations.

Since the small-sized Tiltrotor UAV is a conceptual design, only the mathematical modeling technique is used in this thesis.

2.1. Reference Frames

When formulating and solving problems in flight dynamics, a number of frames of reference must be used for specifying variables such as relative positions, velocities, components of vectors (forces, velocities, accelerations etc.), and elements of matrices (aerodynamic derivatives, inertia tensor etc.). The equations of motion may be written from the standpoint of an observer fixed in any of the reference frames; the choice being only a matter of convenience and preference, and formulae must be available for transforming quantities of interest from one frame to another (Etkin [9]).

Note that, for every frame of interest, x-axis is denoted by red, y-axis is denoted by green and z-axis is denoted by blue color.

2.1.1. Inertial Reference Frame (Inertial Axes, F_I)

In every dynamics problem, there must be an inertial reference frame, either explicitly defined, or lurking implicitly in the background. This frame is fixed, or in uniform rectilinear translation relative to the distant stars.

It is called the inertial frame, because Newton's Law of Inertia holds in it, along with his other laws; Law of Acceleration and Law of Reciprocal Actions. An inertial reference frame is a coordinate system that is not accelerating and not rotating, which means having constant linear velocity, including standing still as shown in Figure 1. An object within this frame will only change its velocity if an actual non-zero net force is applied to it.

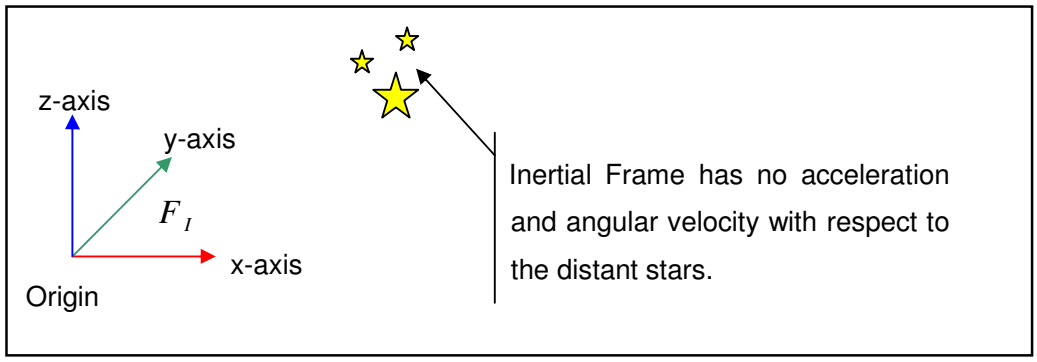

Figure 1. Inertial frame.

2.1.2. Earth Reference Frame (Earth Surface Axes, F_E)

Since hypersonic and space flight is out of the scope of this study, the rotation of the Earth relative to F_I can be neglected, and any reference frame fixed to the Earth can be used as an inertial frame. There are two Earth-fixed frames of interest as shown in Figure 2,

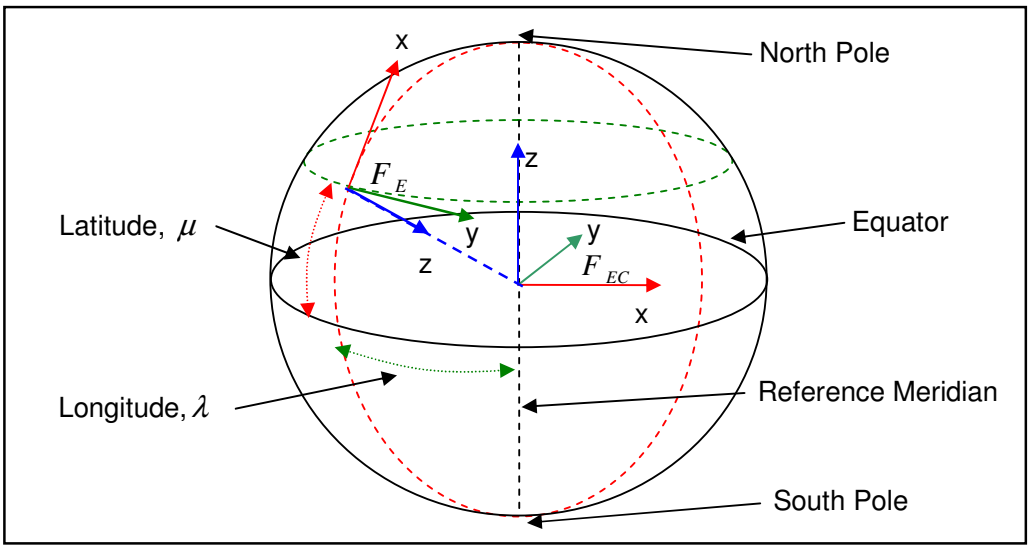

Figure 2. Earth frames.

- Earth Center Frame, F_{EC}, is used when Earth's rotation is considered,

- Earth Surface Frame, F_E, is used with its origin close to the vehicle, and z-axis directed vertically downward from the surface to the center of the Earth, x-y axis is the local horizontal plane, where x-axis points to the north and y-axis points to the east.

In this study, small velocities and short distances are considered on the surface of the Earth, so the Earth surface frame, F_E, is used with flat-Earth approximation.

2.1.3. Vehicle-Carried Reference Frame (Vehicle Carried Axes, F_V)

This is a reference frame in which, the origin is attached to the vehicle at the center of gravity (c.g) as shown in Figure 3. Z-axis is directed vertically downward, i.e., in the same direction of the local g (gravitational acceleration) vector. The other axes are directed parallel to the Earth frame's corresponding axes. Since the origin of the Earth frame is in close proximity to the vehicle, the curvature of the Earth is considered to be negligible, with flat-Earth approximation.

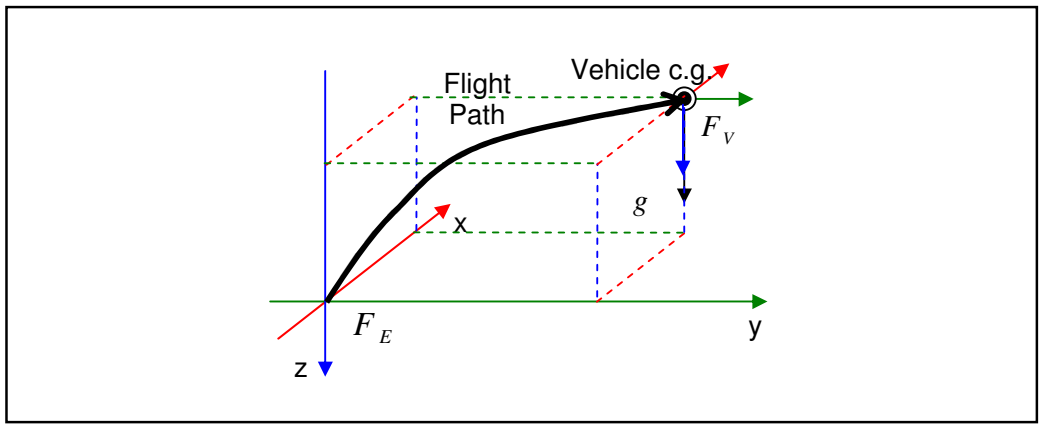

Figure 3. Vehicle-carried frame.

2.1.4. Body-Fixed Reference Frame (Body Axes, F_B)

Any set of axes fixed in a rigid body is a body-fixed reference frame. The body axis system (Figure 4) is the conventional NACA (National Advisory Committee on Aeronautics) orthogonal aircraft axis system. The origin of the body axes is the mass c.g. A particular set of body axes with special properties are principal axes of inertia, denoted by F_B. Looking from the cockpit, the nose of the aircraft points the x-axis, right side points y-axis and z-axis points downward according to right hand rule. The conventional variables associated with the body frame are given in Table 1.

Table 1. Body frame variables.

	Force	*Linear Velocity*	*Moment*	*Angular Velocity*
x-axis	X	u	L	p
y-axis	Y	v	M	q
z-axis	Z	w	N	r
Units	$\left(kg\ m/s^2 = N\right)$	$\left(m/s\right)$	$\left(kg\ m^2/s^2 = Nm\right)$	$\left(\deg/s\right)$

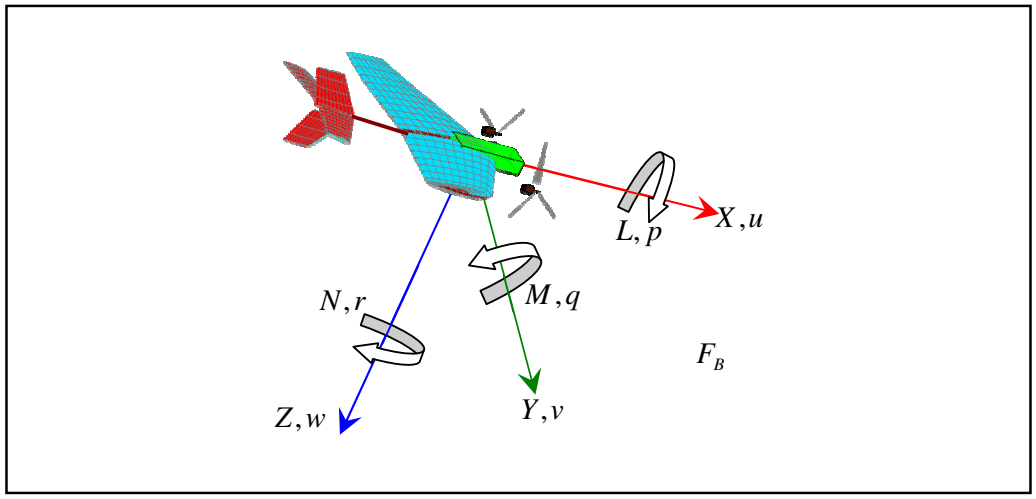

Figure 4. Body frame and variables.

2.1.5. Rotations Between Frames

Consider two frames F_V and F_B. F_V is fixed and F_B is the rotated frame about an axis of F_V with a constant angle as shown in Figure 5. This is achieved by a rotation matrix $Rot(angle, axis)$. This matrix is obtained by writing the principal axis of F_B in terms of the principle axis of F_V, meaning dot products of corresponding principal axes:

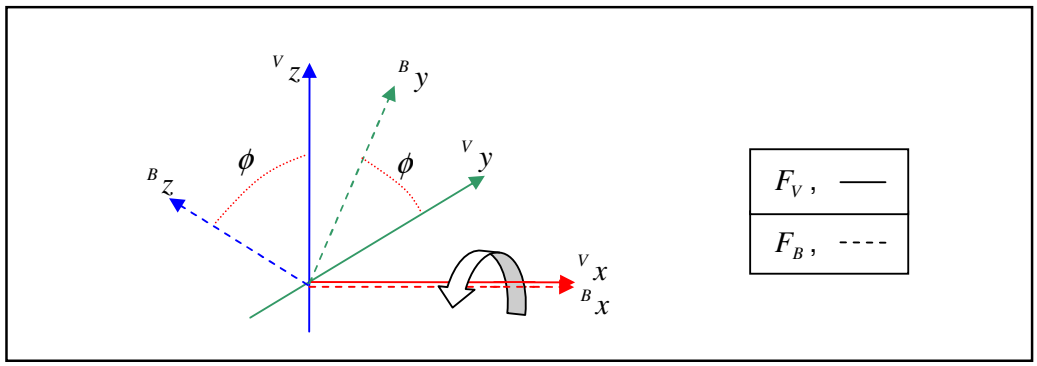

Figure 5. Rotation about x-axis of F_V.

$$Rot(\phi, {}^{V}x) = {}^{V}R_B = \begin{bmatrix} {}^{V}x_B & {}^{V}y_B & {}^{V}z_B \end{bmatrix} = \begin{bmatrix} x_B \cdot x_V & y_B \cdot x_V & z_B \cdot x_V \\ x_B \cdot y_V & y_B \cdot y_V & z_B \cdot y_V \\ x_B \cdot z_V & y_B \cdot z_V & z_B \cdot z_V \end{bmatrix}.$$

Since the dot product equals the multiplication of magnitudes of the vectors and the cosine of the angle between them;

$$a \cdot b = |a||b| \cos(\alpha_{ab}),$$

Considering only the principal axes, which have the magnitude of 1;

$$|a| = 1,\ |b| = 1,\ a \cdot b = \cos(\alpha_{ab}).$$

the equation becomes

$$Rot(\phi, {}^{V}x) = \begin{bmatrix} \cos(\alpha_{x_B x_V}) & \cos(\alpha_{y_B x_V}) & \cos(\alpha_{z_B x_V}) \\ \cos(\alpha_{x_B y_V}) & \cos(\alpha_{y_B y_V}) & \cos(\alpha_{z_B y_V}) \\ \cos(\alpha_{x_B z_V}) & \cos(\alpha_{y_B z_V}) & \cos(\alpha_{z_B z_V}) \end{bmatrix} = \begin{bmatrix} \cos(0) & \cos(90^\circ) & \cos(90^\circ) \\ \cos(90^\circ) & \cos(\phi) & \cos(90^\circ + \phi) \\ \cos(90^\circ) & \cos(90^\circ - \phi) & \cos(\phi) \end{bmatrix},$$

$$Rot(\phi, {}^{V}x) = \begin{bmatrix} 1 & 0 & 0 \\ 0 & \cos(\phi) & -\sin(\phi) \\ 0 & \sin(\phi) & \cos(\phi) \end{bmatrix}.$$

Making the same calculations for the other axes yields the following results;

$$Rot(\theta, {}^{V}y) = \begin{bmatrix} \cos(\theta) & 0 & \sin(\theta) \\ 0 & 1 & 0 \\ -\sin(\theta) & 0 & \cos(\theta) \end{bmatrix},\ Rot(\psi, {}^{V}z) = \begin{bmatrix} \cos(\psi) & -\sin(\psi) & 0 \\ \sin(\psi) & \cos(\psi) & 0 \\ 0 & 0 & 1 \end{bmatrix}.$$

Any vector ${}^{V}V$ in F_V can be represented as ${}^{B}V$ in F_B, with the following rotation formula;

$${}^{B}V = Rot(angle, axis) \cdot {}^{V}V.$$

When making rotations between frames, **X-Y-Z fixed Euler angles**, which are also named as **roll, pitch, yaw angles** are used, where each of 3 rotations takes place

about an axis in the fixed reference frame. The order of rotations is roll-pitch-yaw, since fixed angles are used, rotation matrices are pre-multiplied (Craig [24]),

$$ {}^{V}R_{B} = Rot(\psi,\, z-axis)\cdot Rot(\theta,\, y-axis)\cdot Rot(\phi,\, x-axis), $$

$$ {}^{V}R_{B} = \begin{bmatrix} \cos(\psi)\cos(\theta) & -\sin(\psi)\cos(\phi)+\cos(\psi)\sin(\theta)\sin(\phi) & \sin(\psi)\sin(\phi)+\cos(\psi)\sin(\theta)\cos(\phi) \\ \sin(\psi)\cos(\theta) & \cos(\psi)\cos(\phi)+\sin(\psi)\sin(\theta)\sin(\phi) & -\cos(\psi)\sin(\phi)+\sin(\psi)\sin(\theta)\cos(\phi) \\ -\sin(\theta) & \cos(\theta)\sin(\phi) & \cos(\theta)\cos(\phi) \end{bmatrix}. $$

where ${}^{B}R_{V} = {}^{V}R_{B}'$.

2.2. Models

The following assumptions and espousals are made while obtaining the models;

- IGE (In Ground Effect) condition is not considered in Tiltrotor UAV model, due to the placement of rotors, having them high from the ground more than 2 times the diameter of the rotor. The aircraft operates out of ground effect.
- Components of the Tiltrotor UAV are assumed to have no interaction between each other. The airframe is out of propeller wake influence.
- The conversion assumes quasi-steady motion. The higher order propeller, control and inflow dynamics are much faster than the fuselage motions and have time to reach their steady state well within the typical time constants of the whole aircraft response modes.
- The blades of the propellers are assumed to be rigid, having no feathering, flapping, lead and lag motion.
- Inflow through the propeller is uniform.
- RPM for the propellers is a constant direct input, governor is not used as in the real airplanes.
- The wings are considered to be rigid, having no deflection under stress.
- Wings and propeller blades have constant NACA 0012 airfoil sections.

- Medium variables are calculated for Ankara, Turkey (39°52'N, 32°52'E, Altitude: 850 m. Temperature: 25 °C) with the atmosphere at rest. These variables are assumed to be fixed for all simulations.

- The centripetal and Coriolis acceleration, associated with the Earth's rotation are neglected, assuming flat-Earth approximation.

2.2.1. Environmental Model

The medium that the aircraft experiences, has many variables like temperature, pressure, density, viscosity, speed of sound and gravitational acceleration. The environmental model (Figure 6) is used to determine the atmospheric variables and gravitational acceleration of the Earth, which are used in other models as inputs.

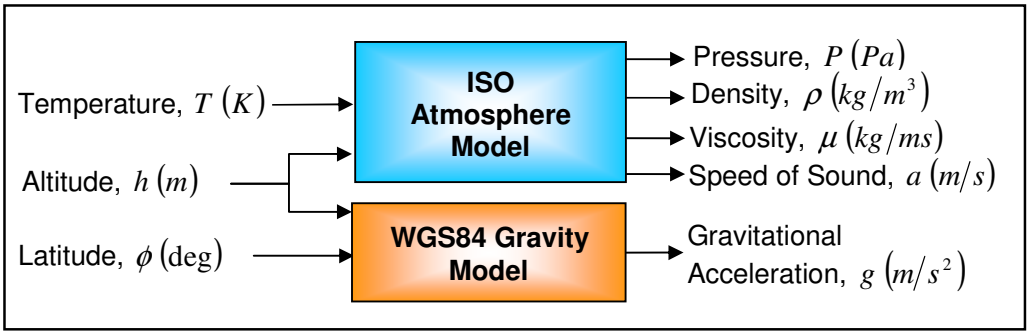

Figure 6. Environmental model.

2.2.1.1. Atmosphere Model

The International Standard Atmosphere (ISA [10]) is an atmospheric model of how the pressure, temperature, density, and viscosity of the Earth's atmosphere change over a wide range of altitudes. It consists of tables of values at various altitudes, plus some formulas by which those values were derived. The ISA model divides the atmosphere into layers with linear temperature distributions. The other values are computed from basic physical constants and relationships.

2.2.1.2. Gravity Model

The precise strength of the Earth's gravity varies depending on latitude and altitude due to the Earth's geoid shape. Sea-level gravitational acceleration increases from about $9.780\ m/s^2$ at the equator to about $9.832\ m/s^2$ at the poles, so an object will weigh about 0.5% more at the poles than at the equator. The approximated values of g, as a function of latitude μ and altitude h is obtained by using the WGS (World Geodetic System) 84 ellipsoidal gravity formula:

$$g = 9.780327\left(1 + 0.0053024\sin^2\mu - 0.0000058\sin^2 2\mu\right) - 3.086\times10^{-6}h,$$

where

$g\ (m/s^2)$: gravitational acceleration,

$h\ (m)$: altitude,

$\mu\ (\deg)$: latitude.

2.2.2. Motion Model (6-DOF)

The equations of motion have been derived in the body frame, whose orientation is defined according to the vehicle-carried frame, which was defined in the inertial frame, where Newton's laws are valid. The application of Newton's laws of motion to an aircraft in flight, leads to the assembly of a set of nonlinear differential equations for the evolution of the aircraft response trajectory and attitude with time.

The motion of a rigid body in 3-dimensions is governed by its mass m_B and inertia tensor I_B, including aerodynamic loads, gravitational forces and inertial forces and moments. A dynamic relationship is formed in the following fashion, in order to obtain the nonlinear dynamics of the motion;

$$\dot{x} = F(x, u, t),$$

where

x: state variables, u: input variables, t: time.

In flight dynamics, there are 12 variables used as state variables. They can be categorized as shown in Table 2.

Table 2. State variables for motion model, $x = [u\ v\ w\ p\ q\ r\ \phi\ \theta\ \psi\ x_e\ y_e\ z_e]^t$.

DYNAMICS						KINEMATICS					
TRANSLATION (m/s)			ROTATION (rad/s)			ROTATION (rad)			TRANSLATION (m)		
u	v	w	p	q	r	ϕ	θ	ψ	x_e	y_e	z_e

The input variables for the motion of a vehicle are the net forces and moments acting on the vehicle. The input variables are defined as shown in Table 3.

Table 3. Input variables for motion model, $u = [X\ Y\ Z\ L\ M\ N]^t$.

FORCES, (N)			MOMENTS, (Nm)		
X	Y	Z	L	M	N

2.2.2.1. Translational Kinematics

Considering the translational motion of the aircraft, this is direct transformation changing linear velocities (u, v, w), from F_B into F_V:

$$\begin{bmatrix} \dot{x}_e \\ \dot{y}_e \\ \dot{z}_e \end{bmatrix} = {}^{V}R_B \begin{bmatrix} u \\ v \\ w \end{bmatrix},$$

$$\begin{bmatrix} \dot{x}_e \\ \dot{y}_e \\ \dot{z}_e \end{bmatrix} = \begin{bmatrix} \cos\psi\cos\theta & -\sin\psi\cos\phi+\cos\psi\sin\theta\sin\phi & \sin\psi\sin\phi+\cos\psi\sin\theta\cos\phi \\ \sin\psi\cos\theta & \cos\psi\cos\phi+\sin\psi\sin\theta\sin\phi & -\cos\psi\sin\phi+\sin\psi\sin\theta\cos\phi \\ -\sin\theta & \cos\theta\sin\phi & \cos\theta\cos\phi \end{bmatrix} \begin{bmatrix} u \\ v \\ w \end{bmatrix}.$$

2.2.2.2. Rotational Kinematics

This transformation is obtained by sequential transformation of axes and angular velocities, as shown by Etkin [10]:

$$\begin{bmatrix} \dot{\phi} \\ \dot{\theta} \\ \dot{\psi} \end{bmatrix} = \begin{bmatrix} 1 & \sin\phi\tan\theta & \cos\phi\tan\theta \\ 0 & \cos\phi & -\sin\phi \\ 0 & \sin\phi\sec\theta & \cos\phi\sec\theta \end{bmatrix} \begin{bmatrix} p \\ q \\ r \end{bmatrix}.$$

2.2.2.3. Translational Dynamics

Considering that the mass of the aircraft is constant, the state variables related to translational dynamics can be calculated according to Newton's Second Law: the summation of all external forces acting on a rigid body is equal to the time rate of change of the linear momentum of the body:

$$\sum F = \frac{d}{dt}(m\,V),$$
$$F_B = m_B\, a_B = m_B\left(\dot{V}_B + w_B \times V_B\right),$$

$$\begin{bmatrix} X \\ Y \\ Z \end{bmatrix} + m_B \begin{bmatrix} \cos\psi\cos\theta & \sin\psi\cos\theta & -\sin\theta \\ -\sin\psi\cos\phi+\cos\psi\sin\theta\sin\phi & \cos\psi\cos\phi+\sin\psi\sin\theta\sin\phi & \cos\theta\sin\phi \\ \sin\psi\sin\phi+\cos\psi\sin\theta\cos\phi & -\cos\psi\sin\phi+\sin\psi\sin\theta\cos\phi & \cos\theta\cos\phi \end{bmatrix} \begin{bmatrix} 0 \\ 0 \\ g \end{bmatrix}$$
$$= m_B \left(\begin{bmatrix} \dot{u} \\ \dot{v} \\ \dot{w} \end{bmatrix} + \begin{bmatrix} p \\ q \\ r \end{bmatrix} \times \begin{bmatrix} u \\ v \\ w \end{bmatrix} \right).$$

After performing some calculations and leaving the derivatives of the state variables alone at the left side, we obtain

$$\begin{bmatrix} \dot{u} \\ \dot{v} \\ \dot{w} \end{bmatrix} = \begin{bmatrix} rv - qw - g\sin\theta + \dfrac{X}{m_B} \\ pw - ru + g\cos\theta\sin\phi + \dfrac{Y}{m_B} \\ qu - pv + g\cos\theta\cos\phi + \dfrac{Z}{m_B} \end{bmatrix}.$$

2.2.2.4. Rotational Dynamics

Considering that the inertia tensor I_B, is not changing when expressed in the body frame (i.e. $\dot{I}_B = 0$), applying Euler's formula; the summation of the external moments acting on a rigid body is equal to the time rate of change of the angular momentum:

$$\sum M = \begin{bmatrix} L \\ M \\ N \end{bmatrix} = \frac{d}{dt}(H_B) = \dot{H}_B + w_B \times H_B = \dot{I}_B w_B + I_B \dot{w}_B + w_B \times I_B w_B ,$$

where $H_B = I_B w_B$, $\frac{d}{dt} H_B = I_B \dot{w}_B + w_B \times I_B w_B$. After consecutive calculations;

$$\begin{bmatrix} \dot{p} \\ \dot{q} \\ \dot{r} \end{bmatrix} = I_B^{-1} \begin{bmatrix} L \\ M \\ N \end{bmatrix} - I_B^{-1} \begin{bmatrix} -I_{XZ}pq - I_{YZ}q^2 + I_{ZZ}qr + I_{XY}pr - I_{YY}qr + I_{YZ}r^2 \\ I_{XX}pr - I_{XY}qr - I_{XZ}r^2 + I_{XZ}p^2 + I_{YZ}pq - I_{ZZ}pr \\ -I_{XY}p^2 + I_{YY}pq - I_{YZ}pr - I_{XX}pq + I_{XY}q^2 + I_{XZ}rq \end{bmatrix}.$$

2.2.2.5. Equations of Motion

The equations of motion for a rigid body are constructed according to the block diagram model shown in Figure 7. resulting the following matrix form;

$$\frac{d}{dt}\begin{bmatrix} u \\ v \\ w \\ p \\ q \\ r \\ \phi \\ \theta \\ \psi \\ x_e \\ y_e \\ z_e \end{bmatrix} = \begin{bmatrix} rv - qw - g\sin\theta \\ pw - ru + g\sin\phi\cos\theta \\ qu - pv + g\cos\phi\cos\theta \\ -I_B^{-1}\begin{bmatrix} -I_{XZ}pq - I_{YZ}q^2 + I_{ZZ}qr + I_{XY}pr - I_{YY}qr + I_{YZ}r^2 \\ I_{XX}pr - I_{XY}qr - I_{XZ}r^2 + I_{XZ}p^2 + I_{YZ}pq - I_{ZZ}pr \\ -I_{XY}p^2 + I_{YY}pq - I_{YZ}pr - I_{XX}pq + I_{XY}q^2 + I_{XZ}rq \end{bmatrix} \\ \begin{bmatrix} 1 & \sin\phi\tan\theta & \cos\phi\tan\theta \\ 0 & \cos\phi & -\sin\phi \\ 0 & \sin\phi\sec\theta & \cos\phi\sec\theta \end{bmatrix}\begin{bmatrix} p \\ q \\ r \end{bmatrix} \\ \begin{bmatrix} \cos\psi\cos\theta & -\sin\psi\cos\phi + \cos\psi\sin\theta\sin\phi & \sin\psi\sin\phi + \cos\psi\sin\theta\cos\phi \\ \sin\psi\cos\theta & \cos\psi\cos\phi + \sin\psi\sin\theta\sin\phi & -\cos\psi\sin\phi + \sin\psi\sin\theta\cos\phi \\ -\sin\theta & \cos\theta\sin\phi & \cos\theta\cos\phi \end{bmatrix}\begin{bmatrix} u \\ v \\ w \end{bmatrix} \end{bmatrix} + \begin{bmatrix} \frac{1}{m_B}\begin{bmatrix} X \\ Y \\ Z \end{bmatrix} \\ I_B^{-1}\begin{bmatrix} L \\ M \\ N \end{bmatrix} \\ \begin{bmatrix} 0 \\ 0 \\ 0 \\ 0 \\ 0 \\ 0 \end{bmatrix} \end{bmatrix}.$$

According to Figure 7, if we know about the world (gravitational acceleration) and aircraft (net forces, net moments, mass, inertia tensor) dynamics, then we can calculate the state variables (linear velocities, angular velocities, angular position and translational position) in the world.

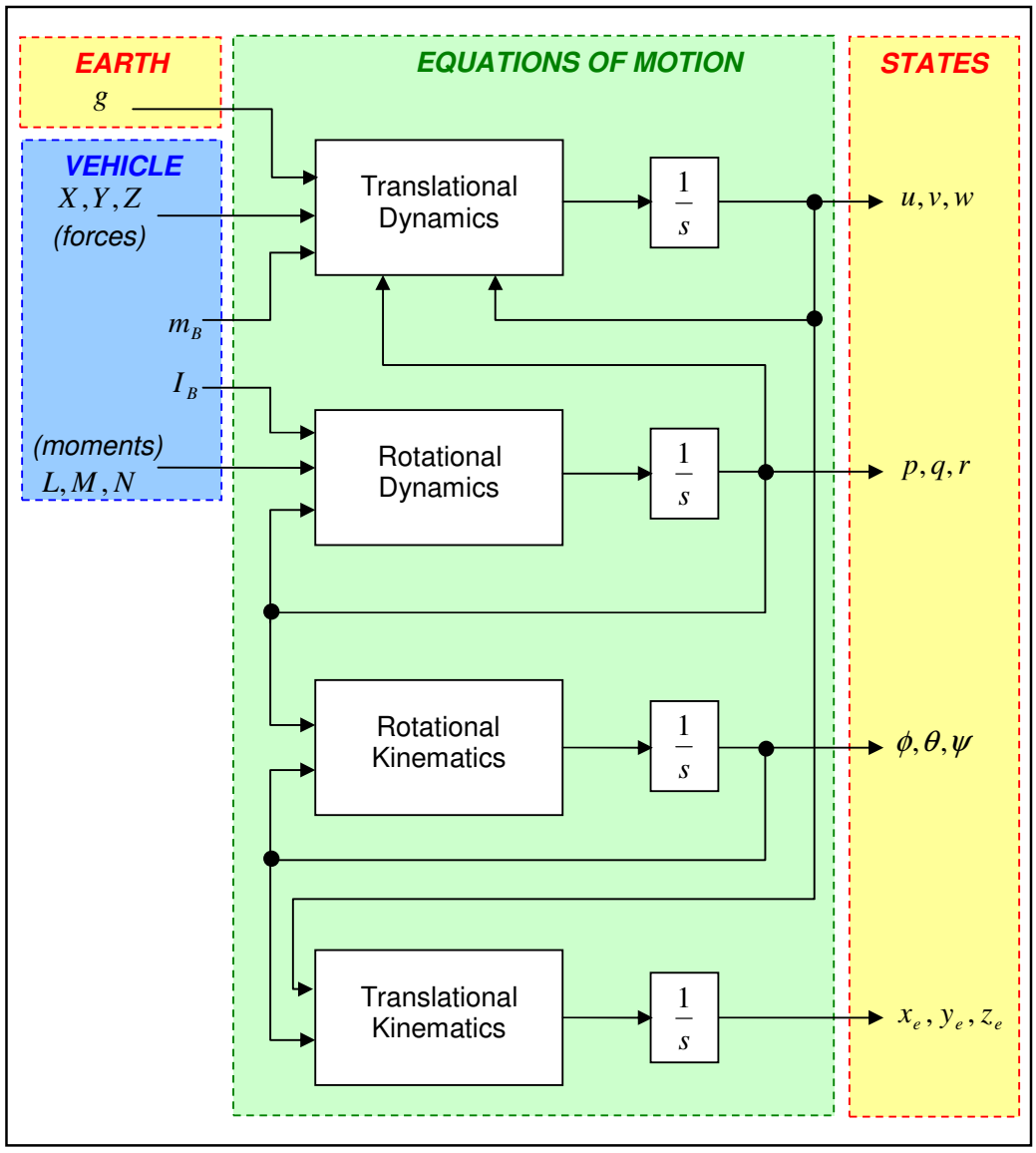

Figure 7. Motion model.

2.2.3. Tiltrotor Model

The tiltrotor simulation model created in this study is named as “Tiltrotor UAV“. It has a mass and an inertia tensor, which is calculated at the c.g. of the body. These values are determined according to avionics equipments’ and mechanical part's total masses, and distribution of these masses in the aircraft’s total volume.

2.2.3.1. Conceptual Design

Tiltrotor UAV has two force generating plants stationed at the both sides of the body. These powerplants are like propellers on a real tiltrotor aircraft, which provide thrust with a tilt angle. The control variables, both rotational speeds Ω_1, Ω_2 (RPM) and tilt angles θ_1, θ_2 $(\deg)$ of the propellers are can be set independent of each other, but they are not completely independent, from the control point of view.

The fuselage of Tiltrotor UAV carries all of the avionics equipments (battery, power unit, processor unit, GPS, INS, RF Link) inside, and constitutes a structural frame to hold other parts (propellers and wings) together. Two identical wings are stationed at the both sides of the fuselage in order to provide the main source of lift. Horizontal and vertical tail wings are fixed at the back of the aircraft in order to increase stability by providing the aircraft pitch and yaw moments. The main properties and components of Tiltrotor UAV are presented in the Figure 8,9.

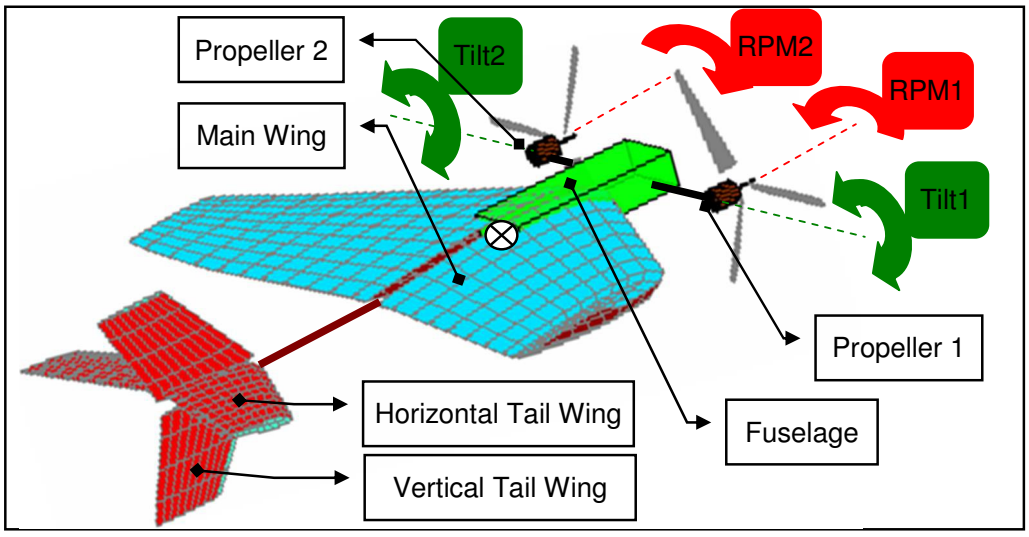

Figure 8. Tiltrotor UAV’s components.

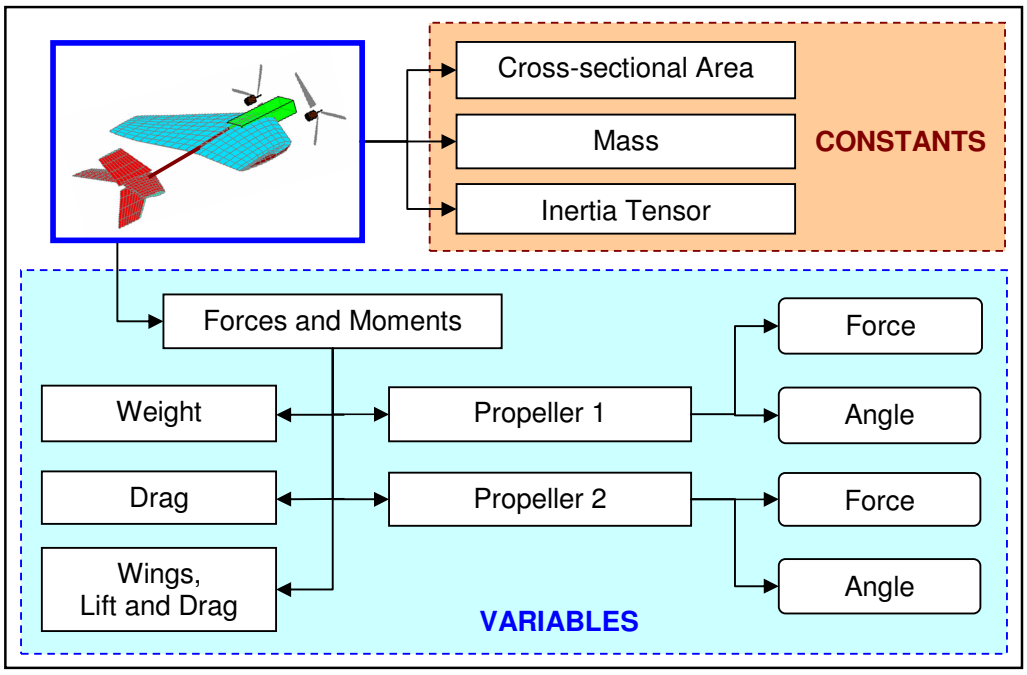

Figure 9. Tiltrotor UAV's properties.

2.2.3.2. Physical Design

Tiltrotor UAV model is constructed using Component Designer and UAV Designer programs explained in Chapter 5. First, the c.g. of the aircraft is calculated according to the design reference frame, the inertia tensor is obtained for the c.g. The list of components and their physical parameters used in Tiltrotor UAV are listed in Table 4.

The chord length $c(m)$ for the main wings is designed to be large, in order to provide more pitch moment in the conversion mode, so that the fuselage of the Tiltrotor UAV tilts more easily. Typical helicopter main rotor's blade twists are on the order of 10°, and the proprotor blades have a blade twist magnitude of 40° for the XV-15, 47° for the V-22 (Kleinhesselink [4]). The blade twists for tiltrotors are neither optimal for a helicopter nor an airplane, instead the proprotor twists are a compromise between helicopter performance and airplane performance. Considering this compromise, the blade twists for the propeller blades are chosen to be 45°.

Table 4. The physical parameters of the Tiltrotor UAV's components.

Name	*Mass (kg)*	*C.G. (m)*	*Inertia Tensor (kg m^2)*	*Features*
Fuselage	1	$\begin{bmatrix}0\\0\\0\end{bmatrix}$	$\begin{bmatrix}0.0042 & 0 & 0\\0 & 0.0217 & 0\\0 & 0 & 0.0242\end{bmatrix}$	-
Main Wings	0.7	$\begin{bmatrix}-0.1718\\0\\-0.0105\end{bmatrix}$	$\begin{bmatrix}0.1868 & 0 & -0.0044\\0 & 0.0564 & 0\\-0.0044 & 0 & 0.2410\end{bmatrix}$	Airfoil : NACA0012 Wing Span: 2 m Dihedral : -20 deg at 0.7 m. $c_{root}: 0.75m, c_{tip} = 0.3m$
Horizontal Tail	0.25	$\begin{bmatrix}-0.0919\\0\\0\end{bmatrix}$	$\begin{bmatrix}0.0196 & 0 & 0\\0 & 0.0054 & 0\\0 & 0 & 0.0248\end{bmatrix}$	Airfoil : NACA0012 Wing Span: 0.8 m $c_{root}: 0.3m, c_{tip} = 0.2m$
Vertical Tail	0.25	$\begin{bmatrix}-0.0900\\0\\0\end{bmatrix}$	$\begin{bmatrix}0.0077 & 0 & 0\\0 & 0.0056 & 0\\0 & 0 & 0.0129\end{bmatrix}$	Airfoil : NACA0012 Wing Span: 0.6 m $c_{root}: 0.3m, c_{tip} = 0.2m$
Propeller 1	0.4	$\begin{bmatrix}-0.0525\\0\\0\end{bmatrix}$	$\begin{bmatrix}0.0021 & 0 & 0\\0 & 0.0027 & 0\\0 & 0 & 0.027\end{bmatrix}$	Airfoil : NACA0012 Blade Root: 0.05 m Blade Tip: 0.35 m Twist : 45 deg Rot : CCW
Propeller 2	0.4	$\begin{bmatrix}-0.0525\\0\\0\end{bmatrix}$	$\begin{bmatrix}0.0021 & 0 & 0\\0 & 0.0027 & 0\\0 & 0 & 0.027\end{bmatrix}$	Airfoil : NACA0012 Blade Root: 0.05 m Blade Tip: 0.35 m Twist : 45 deg Rot : CW

The components designed in Component Designer program are placed at the desired positions and orientations as listed in Table 5, according to the design reference frame. The combination of these components gives the resultant mass and center of gravity and inertia tensor of the Tiltrotor UAV.

Due to Tiltrotor UAV's unique geometrical design, it has helicopter modes, conversion modes and airplane modes of operation. XV-15 and V-22 achieves mode transitions with changing the thrust vectors of the tiltrotors, and the fuselage is kept parallel to the Earth surface. Tiltrotor UAV achieves mode transitions with changing the fuselage pitch with the help of tiltrotors as shown in Figure 10.

Table 5. The locations of components of the Tiltrotor UAV.

Component			*Tiltrotor UAV*	
Name	*Position (m)*	*Orientation (deg)*	*Mass (kg)*	*Inertia Tensor (kg m^2)*
Fuselage	$[0.1 \quad 0 \quad 0]$	$[0 \quad 0 \quad 0]$	3	$\begin{bmatrix} 0.3506 & 0 & -0.0061 \\ 0 & 0.7193 & 0 \\ -0.0061 & 0 & 1.0463 \end{bmatrix}$
Main Wings	$[0 \quad 0 \quad 0]$	$[0 \quad 0 \quad 0]$		
Vertical Tail	$[-1 \quad 0 \quad 0]$	$[90 \quad 0 \quad 0]$		
Horizontal Tail	$[-1 \quad 0 \quad 0]$	$[0 \quad -10 \quad 0]$		
Propeller 1	$[0.35 \quad 0.4 \quad 0]$	$[0 \quad 0 \quad 0]$		
Propeller 2	$[0.35 \quad -0.4 \quad 0]$	$[0 \quad 0 \quad 0]$		

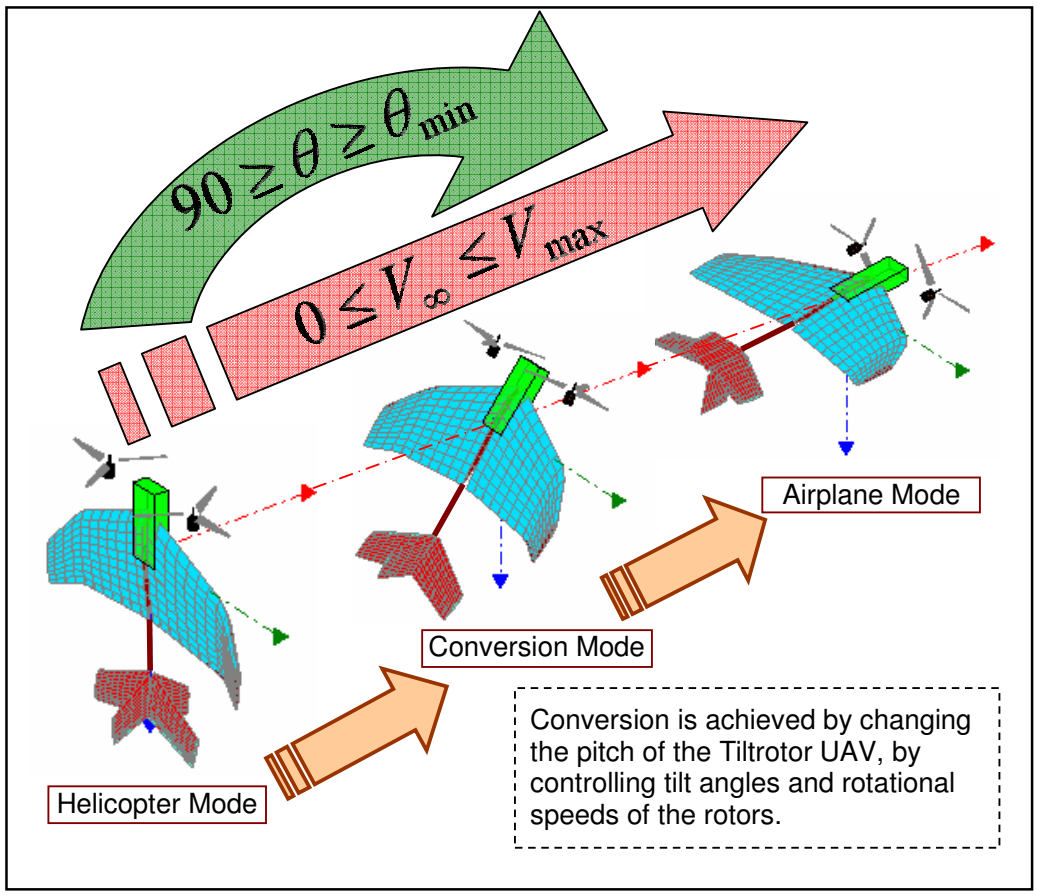

Figure 10. Mode transitions of Tiltrotor UAV.

2.2.3.3. Equations of Tiltrotor UAV Model

The net forces and moments acting on the c.g. of the Tiltrotor UAV (Figure 11) is calculated with summing all of the force and moments, resulted on the components:

$$ {}^{B}F = {}^{B}R_{FU} \cdot {}^{FU}F + {}^{B}R_{HT} \cdot {}^{HT}F + {}^{B}R_{VT} \cdot {}^{VT}F + {}^{B}R_{WT} \cdot {}^{WI}F + {}^{B}R_{PR1} \cdot {}^{PR1}F + {}^{B}R_{PR2} \cdot {}^{PR2}F , $$

$$ \begin{aligned} {}^{B}M = {}^{B}P_{FU} \times {}^{B}R_{FU} \cdot {}^{FU}F + {}^{B}P_{WI} \times {}^{B}R_{WI} \cdot {}^{WI}F + {}^{B}R_{WI} \cdot {}^{WI}M + \\ {}^{B}P_{HT} \times {}^{B}R_{HT} \cdot {}^{HT}F + {}^{B}R_{HT} \cdot {}^{HT}M + {}^{B}P_{VT} \times {}^{B}R_{VT} \cdot {}^{VT}F + {}^{B}R_{VT} \cdot {}^{VT}M + \\ {}^{B}P_{PR1} \times {}^{B}R_{PR1} \cdot {}^{PR1}F + {}^{B}R_{PR1} \cdot {}^{PR1}M + {}^{B}P_{PR2} \times {}^{B}R_{PR2} \cdot {}^{PR2}F + {}^{B}R_{PR2} \cdot {}^{PR2}M \end{aligned} . $$

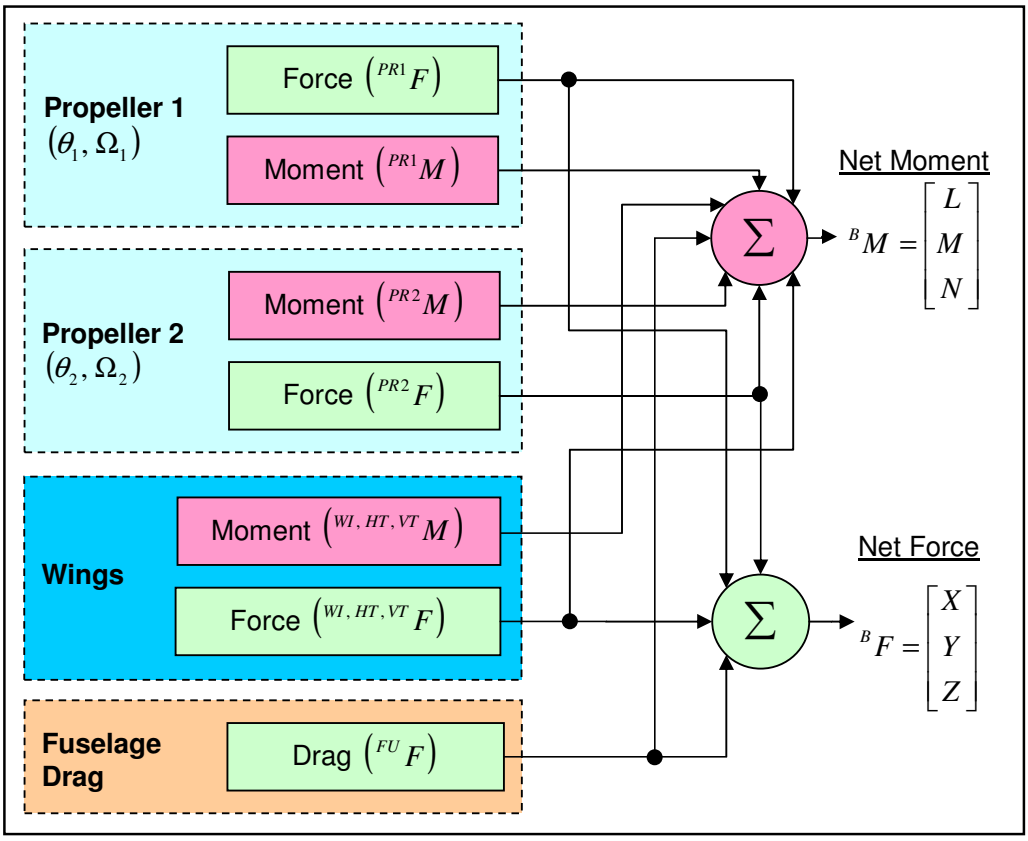

Figure 11. Tiltrotor UAV model.

2.2.4. Drag Model

Drag is the resultant force exerted on a moving object in a fluid, in the opposite direction of the movement. Objects having a reference area moving through a fluid will experience a drag force proportional to their respective drag coefficients, C_d:

$$D = -\frac{1}{2}\rho V^2 S C_d,$$

where, $S(m^2)$: projected frontal area, $V(m/s^2)$: Velocity perpendicular to the projected frontal area.

The drag coefficient for a cube: 1.05, for a large rectangular prism: 0.82, for a short rectangular prism: 1.15 are given in the reference [29]. Since the fuselage was modeled as a rectangular prism of desired dimensions, $C_d = 1.00$ is used as an average. Bertin [30] showed that, the drag coefficient changes according the Reynolds number and Mach number, but since the fuselage considered in this model is small in dimensions, which will result in small drag force, drag coefficient is assumed to be fixed, for simplification. So, the drag force is a result of the interaction between the crossectional area of the fuselage and the incoming air. $S = [S_x \quad S_y \quad S_z](m^2)$ are the effective frontal, side and vertical drag areas of the fuselage and ${}^{B}V = [u \quad v \quad w](m/s^2)$ are the fuselage velocities with respect to the air (see Karasu [8]). So the fuselage drag is calculated as follows, with $C_d = 1.00$:

$${}^{FU}F = \begin{bmatrix} X_D \\ Y_D \\ Z_D \end{bmatrix} = -\frac{1}{2}\rho \begin{bmatrix} S_x\, u^2 \\ S_y\, v^2 \\ S_z\, w^2 \end{bmatrix}.$$

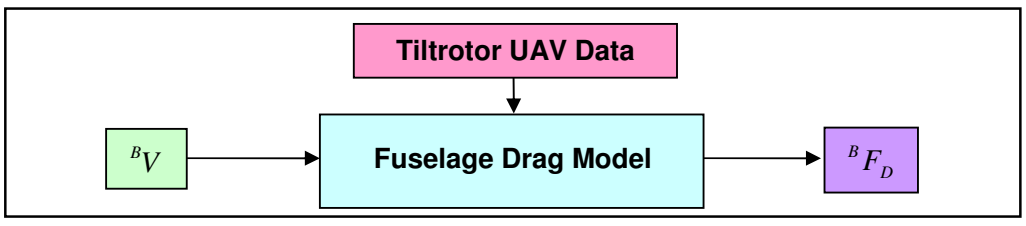

Figure 12. Fuselage drag model.

2.2.5. Wings Model

Tiltrotor UAV has two identical wings, located at the both sides of the body. The wings axis, F_{WI} is defined for the wings, whose origin is stationed at the c.g. of the wings. The center of F_{WI} is placed at ${}^{B}P_{WI}$, with respect to the aircraft c.g. Each wing starts from r_0, extending to R spanwise, and it is composed of airfoil sections as seen in Figure 13.

The primary objective of the wings is to overcome weight, so that we can use the propellers only to provide forward thrust, in the level flight.

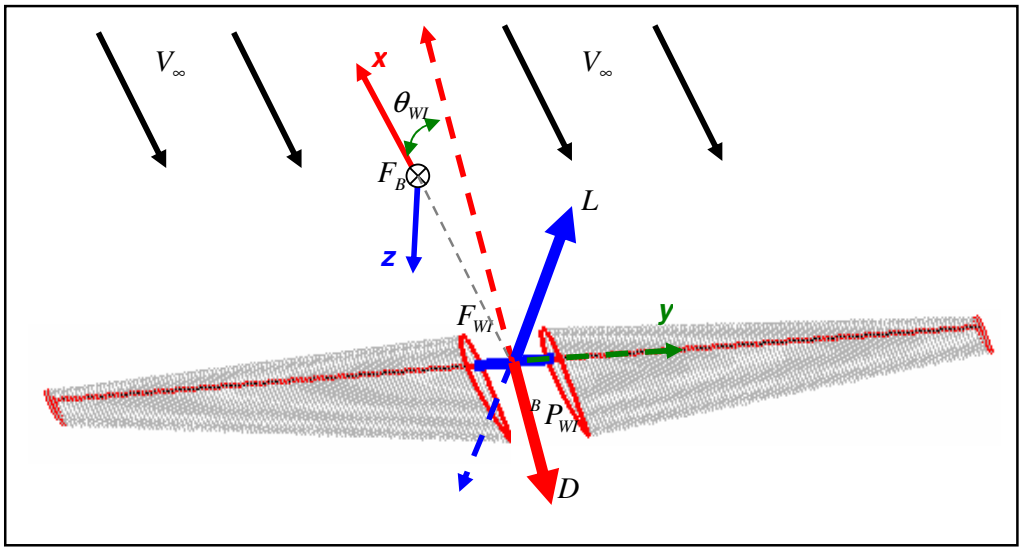

Figure 13. Wings.

The blade element theory (BET, Leishman [11]) is used in order to calculate the aerodynamics of the wings. The BET assumes that each blade section acts as a quasi-two dimensional airfoil to produce aerodynamic forces and moments. Wings' resultant forces and moments can be obtained by integrating the sectional airloads at each wing element over the spanlength of the wing.

2.2.5.1. Inflow Dynamics

In order to obtain the inputs for the airfoil dynamics (Figure 14), inflow and angle of attack must be determined for every airfoil section. The aerial velocity of every airfoil (AF) is calculated with considering inertial velocity ${}^{B}V$, angular velocity ${}^{B}W$ and the location of AF in F_B ;

$${}^{AF}V = {}^{AF}R_B\left({}^{B}W \times \left({}^{B}P_{WI} + {}^{B}R_{WI}\ {}^{WI}P_{AF}\right) + {}^{B}V\right),$$

where ${}^{WI}R_B = Rot(\theta_{WI},\ y\ of\ F_B)$.

When calculating the air inflow velocity, considering AF is stationary, there are two components of interest which are tangential and parallel velocities. The aerodynamic forces are assumed to arise solely from the velocity and angle of attack normal to the leading edge of the blade section. The effect of the radial component velocity is ignored in accordance with the independence principle (Leishman [11]).

$$V_T = -{}^{AF}V_x,$$

$$V_P = -{}^{AF}V_z.$$

Then the inflow angle is;

$$\phi = \arctan\left(\frac{V_P}{V_T}\right) = \arctan\left(\frac{{}^{AF}V_z}{{}^{AF}V_x}\right).$$

Then the angle of attack becomes;

$${}^{AF}\alpha_\infty = {}^{AF}\theta - \phi.$$

Also the air inflow velocity is calculated as follows;

$${}^{AF}V_\infty = \sqrt{{}^{AF}V_x{}^2 + {}^{AF}V_z{}^2}\ .$$

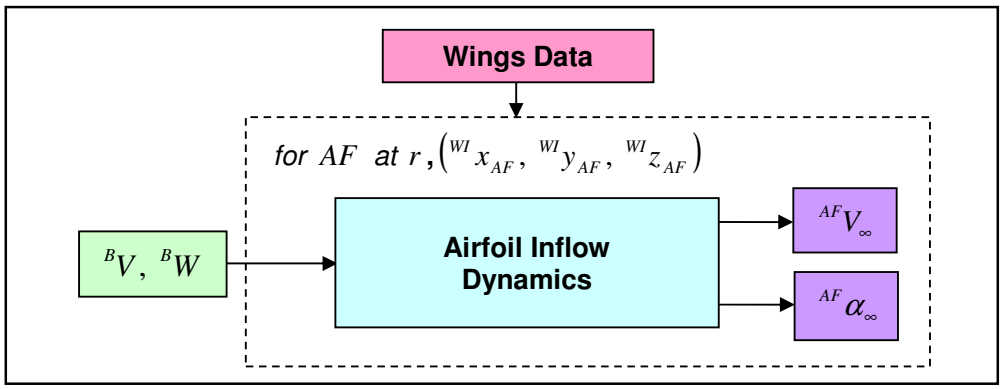

Figure 14. Wing airfoil inflow model.

2.2.5.2. Airfoil Dynamics

Since we have calculated inflow and angle of attack for the airfoils, we can use them as inputs for the airfoil model obtained in Chapter 2.2.7., which will result in the forces and moments on the airfoil as shown in Figure 15.

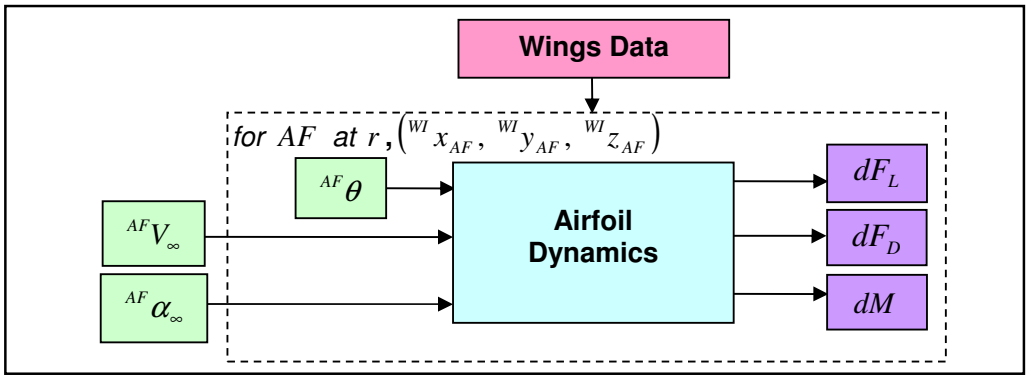

Figure 15. Wing airfoil dynamics.

2.2.5.3. Integration of Forces and Moments

The integration of all of the forces and moments for all airfoil sections of the wings gives the net forces and net moments as shown in Figure 16. Calculating the net forces of the wings;

$$^{WI}F = \int_{r_0}^{R} {}^{WI}R_{AF} \begin{bmatrix} -dF_D \\ 0 \\ -dF_L \end{bmatrix} dy + \int_{-r_0}^{-R} {}^{WI}R_{AF} \begin{bmatrix} -dF_D \\ 0 \\ -dF_L \end{bmatrix} dy .$$

Calculating the net moment of the wings:

$$^{WI}M = \int_{-r_0}^{-R} \begin{bmatrix} {}^{WI}x_{AF} \\ {}^{WI}y_{AF} \\ {}^{WI}z_{AF} \end{bmatrix} \times {}^{WI}R_{AF} \begin{bmatrix} -dF_D \\ 0 \\ -dF_L \end{bmatrix} + {}^{WI}R_{AF} \begin{bmatrix} 0 \\ dM \\ 0 \end{bmatrix} dy + \int_{r_0}^{R} \begin{bmatrix} {}^{WI}x_{AF} \\ {}^{WI}y_{AF} \\ {}^{WI}z_{AF} \end{bmatrix} \times {}^{WI}R_{AF} \begin{bmatrix} -dF_D \\ 0 \\ -dF_L \end{bmatrix} + {}^{WI}R_{AF} \begin{bmatrix} 0 \\ dM \\ 0 \end{bmatrix} dy .$$

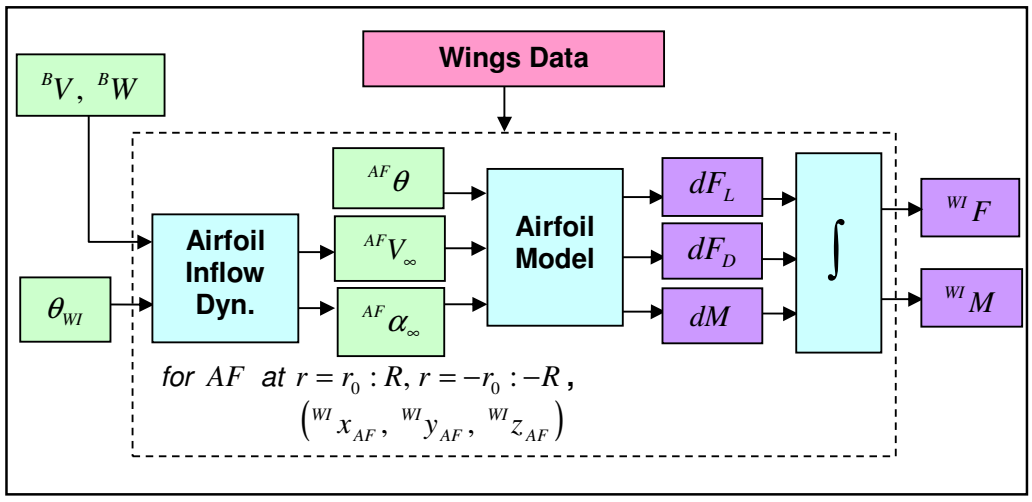

Figure 16. Wings model.

2.2.6. Propeller Model

Tiltrotor UAV has two propellers, located at the both sides of the body. Each propeller has a power plant, rotating with a given RPM, turning the blades. One of the propellers is rotated CW, and the other one is rotated CCW in order to balance the moment generated due to rotation.

We define a new axis system, ${}^{B}F_{PR}$ for each propeller, whose origin is at the hub center and positioned at ${}^{B}P_{PR}$. Also, it may be tilted around y-axis of ${}^{B}F_{PR}$, independent of each other.

Each propeller has NB (number of blades) identical blades, which starts from r_0, extending to R spanwise. Every blade has identical structures, and composed of identical airfoil sections with a geometrical twist angle and position as seen in Figure 17.

The inputs for the propeller model, are the angular speed generated by the power plant $\Omega\,(RPM)$ and angular position of the propeller $\theta_{TILT}\,(\deg)$ as shown in Figure 18. The outputs of the propeller model are the forces ${}^{PR}F$, $[X_{PR} \quad Y_{PR} \quad Z_{PR}]$ and moments ${}^{PR}M$, $[L_{PR} \quad M_{PR} \quad N_{PR}]$ defined in F_{PR}.

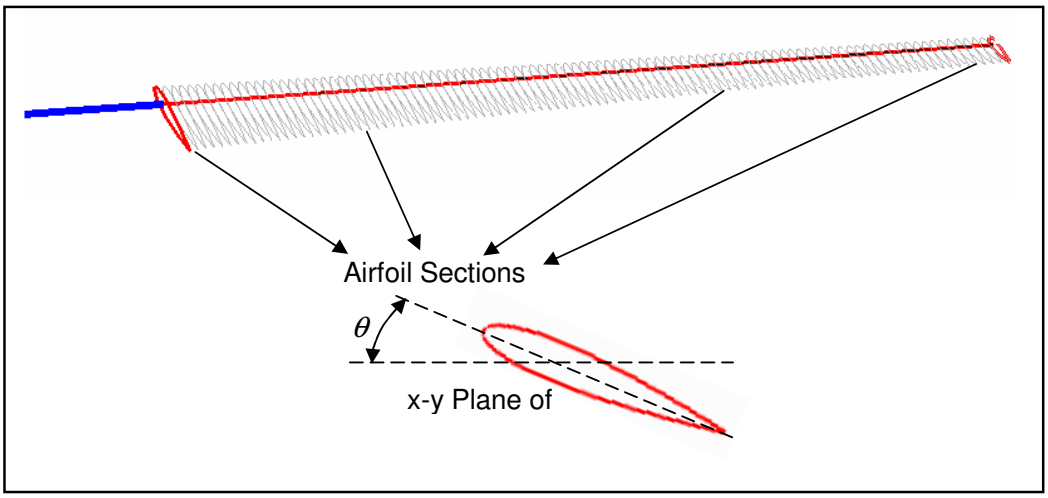

Figure 17. Propeller blade.

The blade element theory (BET - Leishman [11]) forms the basis of most modern analysis of rotor aerodynamics. The BET assumes that each blade section acts as a quasi-two dimensional airfoil to produce aerodynamic forces and moments. Propeller outputs can be obtained by integrating the sectional airloads at each blade element over the length of the blade and averaging the result over a rotor revolution.

2.2.6.1. Inflow Dynamics

In order to calculate the forces and moments generated by the propeller, V_∞ and α_∞ must be determined for every airfoil section of every blade according to current situation (aircraft's velocities and tilt angle of main rotor).

Inertial velocity of the F_{PR} is calculated considering tilt angle θ_{TILT} of the propeller, angular velocity ${}^{B}W$ and translational velocity ${}^{B}V$ of the Tiltrotor UAV:

$${}^{PR}V = {}^{PR}R_B\left({}^{B}W \times {}^{B}P_{PR} + {}^{B}V\right),$$

where

$${}^{PR}R_B = Rot(\theta_{TILT},\ y\ of\ F_{PR}).$$

Inertial velocity of the airfoil is calculated considering Ω (RPM, rotational velocity, CCW around x-axis of F_{PR}), location of the airfoil r (radius in the y-z plane of F_{PR}), angular position of the airfoil ϕ, inertial velocity of the propeller ${}^{PR}V$, and the induced velocity, V_i. Induced inflow velocity is multiplied by -1, since it was defined as the speed of the air sucked by the propeller;

$${}^{AF}V = {}^{AF}R_{PR}\left(Rot(\phi,\ x\ of\ F_{PR})\,{}^{PR}V + \begin{bmatrix} \frac{60}{2\pi}\Omega r & 0 & -V_i \end{bmatrix}' \right),$$

$$\begin{bmatrix} V_T \\ V_R \\ V_P \end{bmatrix} = -{}^{AF}V\ .$$

The effect of the radial component of velocity V_R, on the aerodynamic calculations is ignored in accordance with the independence principle (Leishman [11]). So, ${}^{AF}V_\infty$ and ${}^{AF}\alpha_\infty$ is calculated as follows;

$${}^{AF}V_\infty = \sqrt{{V_P}^2 + {V_T}^2},\ {}^{AF}\phi = \arctan(V_P/V_T),\ {}^{AF}\alpha_\infty = {}^{AF}\theta - {}^{AF}\phi.$$

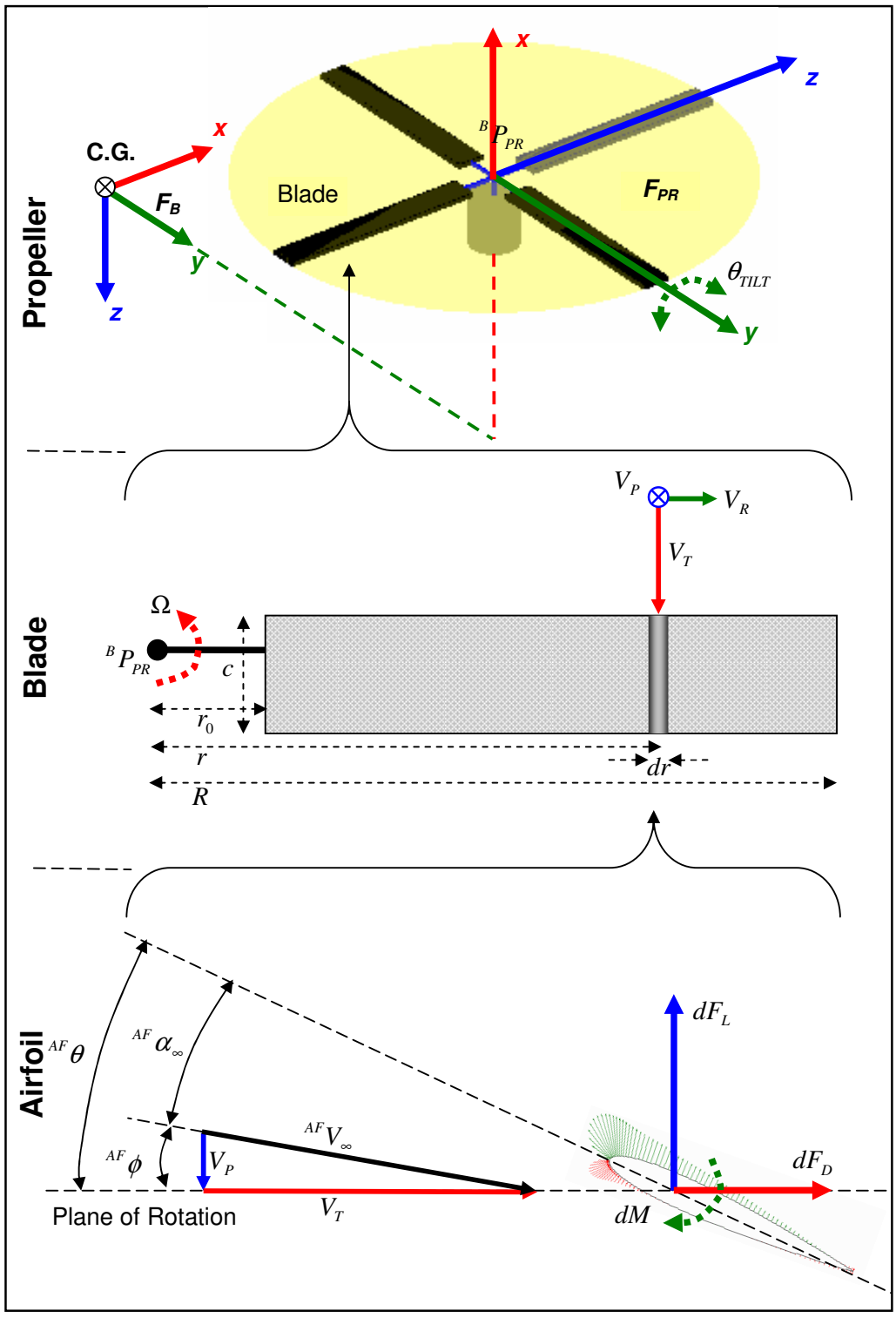

Figure 18. Propeller and variables.

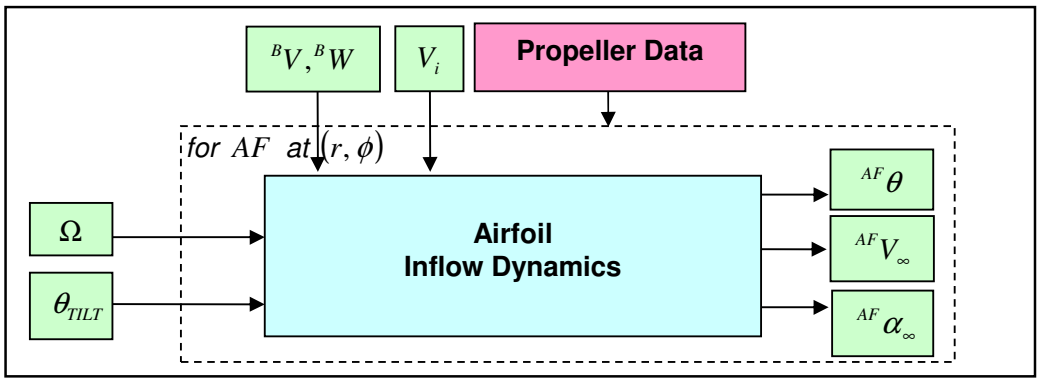

Figure 19. Airfoil inflow dynamics.

2.2.6.2. Airfoil Dynamics

Since we have calculated inflow velocity and angle of attack for the airfoils, we can use them as inputs for the airfoil dynamics obtained in Chapter 2.2.7., which will result the forces and moments (Figure 20) on the airfoil.

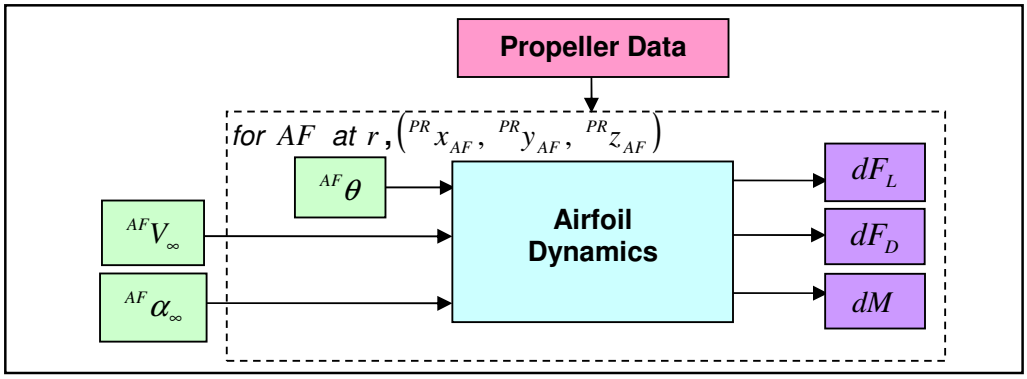

Figure 20. Wing airfoil dynamics.

2.2.6.3. Integration of Forces and Moments

Using the forces on the airfoil sections are calculated in Chapter 2.2.7., we can take the integral of airfoil forces spanwise and radially, then take the mean of it and then

multiply it with the number of blades. This results the average forces and moments generated by the propeller.

The formation of trailed vortex at the tip of each blade produces a high local inflow over the tip region and effectively reduces the lifting capability there. This is referred to as a tip loss. A simple tip loss factor B is used to account for this physical effect such that the product BR corresponds to an effective blade radius. Although, B changes with inflow and number of blades, a good approximation is $B = 0.95$ (Leishman [11]).

$R_e = B \cdot R$.

The forces generated by the propeller is calculated as follows:

$$^{PR}F = \begin{bmatrix} ^{PR}X \\ ^{PR}Y \\ ^{PR}Z \end{bmatrix} = NB\frac{1}{2\pi}\int_0^{2\pi}\int_{r_0}^{R_e}\begin{bmatrix} -dF_L(\phi,r) \\ dF_D(\phi,r)\cos(\phi) \\ -dF_D(\phi,r)\sin(\phi) \end{bmatrix} dr\ d\phi\ .$$

In order to calculate the moments, we take the integral of the product of the moment arms and forces. In the presence of a change in the rotational speed, this change it is multiplied with the inertia tensor:

$$^{PR}M = \begin{bmatrix} ^{PR}L \\ ^{PR}M \\ ^{PR}N \end{bmatrix} = NB\frac{1}{2\pi}\int_0^{2\pi}\int_{r_0}^{R_e}\begin{bmatrix} -dF_L(\phi,r)\sin(\phi)r \\ dF_L(\phi,r)\cos(\phi)r \\ dF_D(\phi,r)r \end{bmatrix} dr\ d\phi + I_{PR}\begin{bmatrix} \frac{d}{dt}\left(\frac{60}{2\pi}\Omega\right) \\ 0 \\ 0 \end{bmatrix}.$$

2.2.6.4. Conservation of Momentum

The propeller produces upward thrust by driving a column of air downwards through the rotor plane. In other words, the rotor disc supports a thrust created by the action of the air on the blades. By Newton's law, there must be an equal and opposite reaction of the rotor on the air. As a result, the air in the rotor wake acquires a velocity increment, directed opposite to the thrust direction (Johnson [12]). A relationship between the thrust produced and the velocity communicated to the air

can be obtained by the application of Newtonian mechanics – the laws of conservation of mass, momentum and energy – to the overall process. This approach is referred as the momentum theory for propellers, corresponding essentially to the theory set out by Glauert for aircraft propellers (Seddon [13]).

In momentum theory for propellers, the rotor is conceived as an "actuator disc", across which there is a sudden increase of pressure, uniformly spread. In hover, the column of air passing through the disc is a clearly defined streamtube above and below the disc; outside this streamtube the air is assumed to be undisturbed and no rotation is imparted to the flow.

When we consider the air mass flow rate, $\dot{m}$, through the actuator disc area A;

$$\dot{m} = \rho A U,$$

where

$$U = {}^{PR}V_x + V_i.$$

The application of the conservation of momentum for the mass flow rate, in a normal direction to the disc gives;

$$T = \dot{m}\left({}^{PR}V_x + V_{i\infty}\right) - \dot{m}\left({}^{PR}V_x\right) = \dot{m}V_{i\infty}.$$

By applying the conservation of energy, we obtain;

$$\begin{aligned} T\left({}^{PR}V_x + V_i\right) &= \frac{1}{2}\dot{m}\left({}^{PR}V_x + V_{i\infty}\right)^2 - \frac{1}{2}\dot{m}\left({}^{PR}V_x\right)^2 \\ \dot{m}V_{i\infty}\left({}^{PR}V_x + V_i\right) &= \frac{1}{2}\dot{m}\left(2V_{i\infty}\,{}^{PR}V_x + {V_{i\infty}}^2\right) \\ 2\,{}^{PR}V_x + 2V_i &= 2\,{}^{PR}V_x + V_{i\infty} \\ 2V_i &= V_{i\infty} \end{aligned} \quad .$$

So the momentum rate becomes;

$$T = 2\dot{m}V_i = 2\rho A V_i\left({}^{PR}V_x + V_i\right).$$

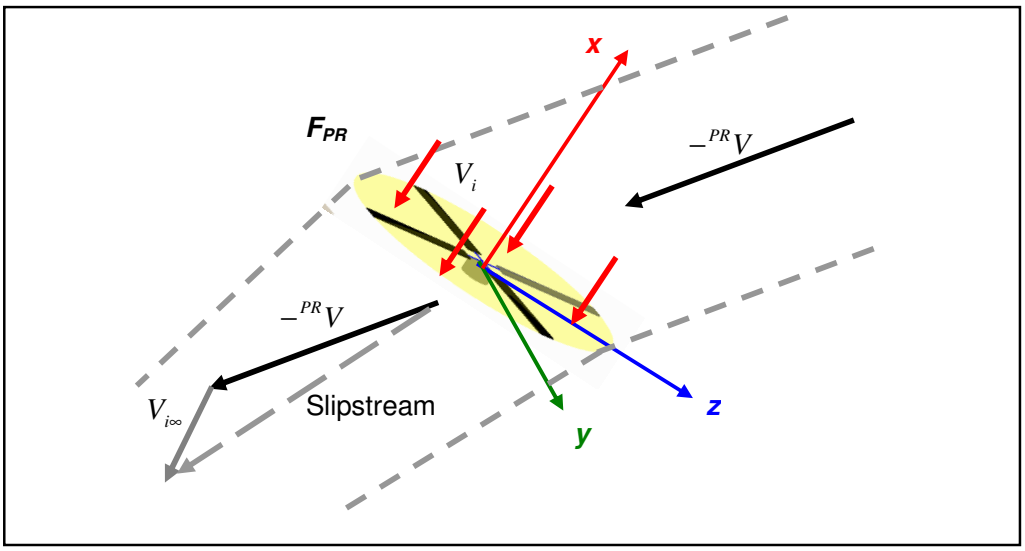

Figure 21. Propeller inflow dynamics.

Since the momentum rate is equal to force, it is equal to the thrust of the propeller, which is also a function of V_i:

$${}^{PR}F_x(V_i) = 2\rho A V_i \left({}^{PR}V_x + V_i\right).$$

In order to find the value of V_i, we minimize the function below;

$$V_i = \arg\min_{V_i}\left(\left|f(V_i)\right|\right),$$

where

$$f(V_i) = -{}^{PR}F_x(V_i) + 2\rho A V_i \left({}^{PR}V_x + V_i\right).$$

Generalized Pattern Search (GPS, Nacedal [14]) is used in order to solve this minimization problem.

With the inclusion of the dynamic inflow model, the propeller model becomes as shown in Figure 22.

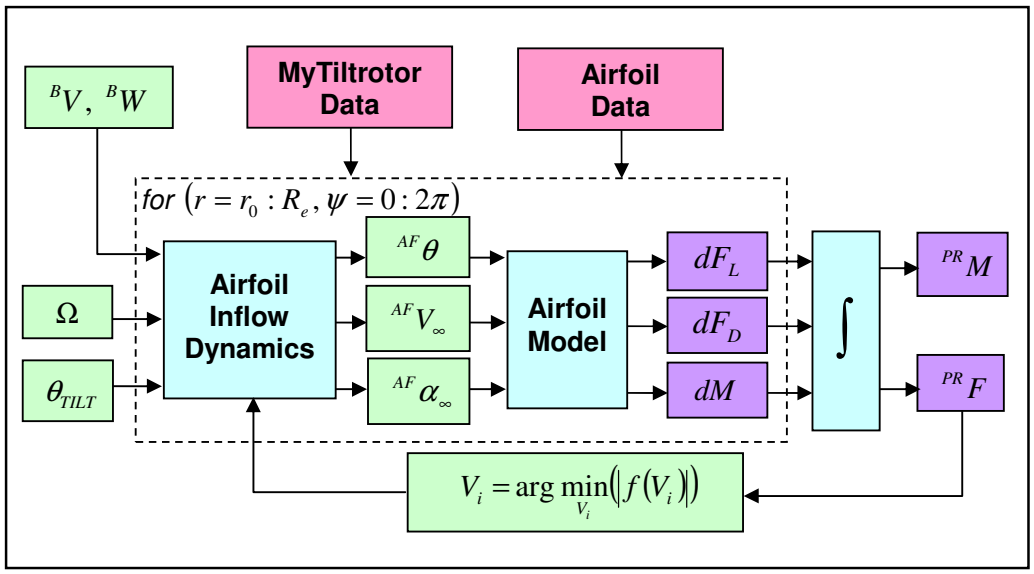

Figure 22. Propeller model.

2.2.7. Airfoil Model

An airfoil (in American English, or aerofoil in British English) is the shape of a wing or blade (of a propeller, rotor or turbine) or sail as seen in cross-section.

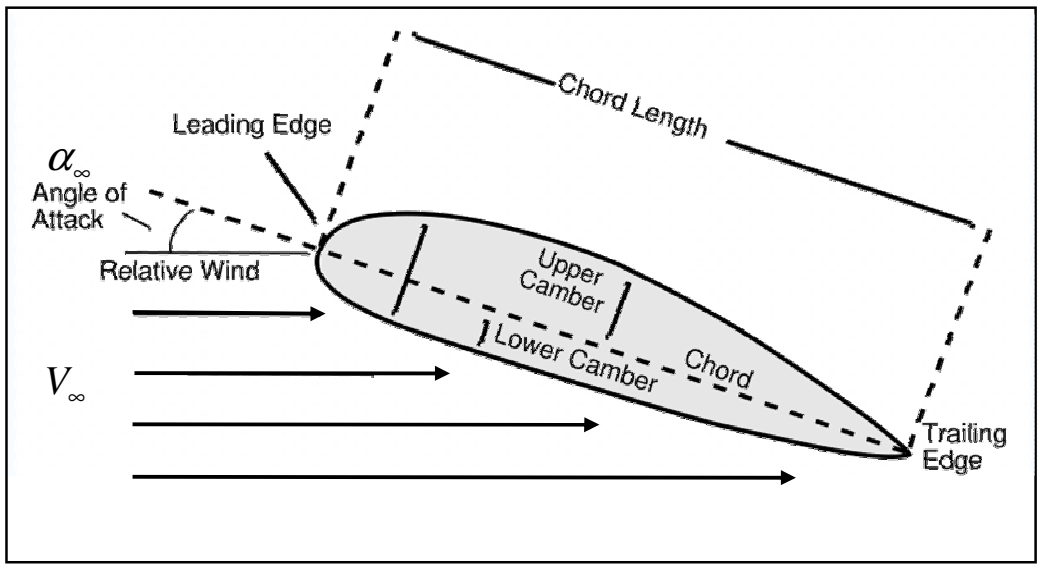

Figure 23. Airfoil properties.

An airfoil shaped body moved through a fluid produces a force perpendicular to the motion is called lift. Subsonic flight airfoils have a characteristic shape with a rounded leading edge, followed by a sharp trailing edge (Figure 23), often with asymmetric camber.

The input variables for an airfoil are the freestream velocity ($V_\infty\,(m/s)$, relative air velocity), angle of attack ($\alpha(\deg)$) and pitch angle ($\theta(\deg)$). Calculations made together with atmospheric variables and airfoil data result in sectional lift ($dF_l\,(N/m)$), sectional drag ($dF_d\,(N/m)$) and sectional moment ($dM\,(N)$). The inputs and outputs of an airfoil are shown in Figure 24.

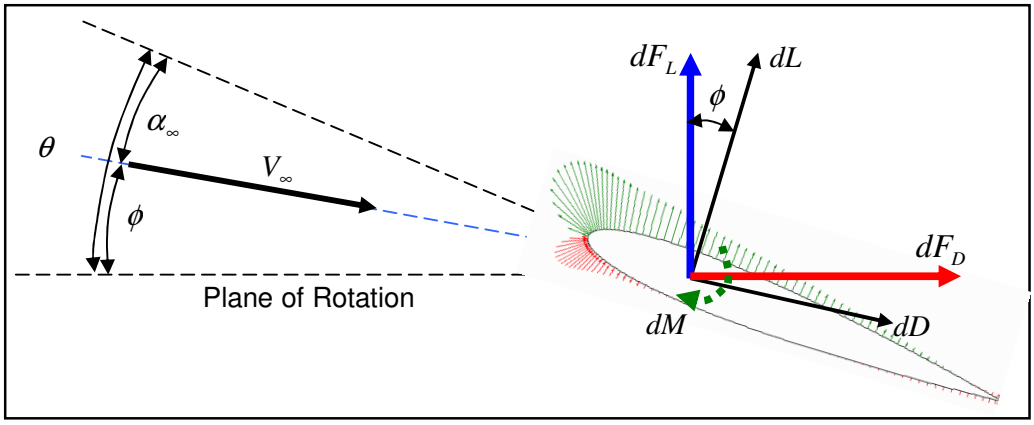

Figure 24. Airfoil aerodynamic variables.

2.2.7.1. Aerodynamic Variables

The ratio of the speed of the airflow to that of the speed of sound (a) is called the **Mach number** and can be interpreted as a ratio of inertial forces in the fluid to forces resulting from compressibility. In order to avoid compressibility related problems like, wave drag and shock induced stall at the transonic speeds, the airfoils in the simulation are operated in the subsonic region. The Mach number is calculated as follows,

$$Ma = \frac{V_\infty}{a}.$$

In fluid mechanics, the **Reynolds number** is the ratio of inertial forces to viscous forces and, consequently, it quantifies the relative importance of these two types of forces for the given flow conditions. It is one of the most important dimensionless numbers in fluid dynamics and is used, usually along with other dimensionless numbers, to provide a criterion for determining dynamic similitude. When two geometrically similar flow patterns, in perhaps different fluids with possibly different flow rates, have the same values for the relevant dimensionless numbers, then they are said to be dynamically similar, and will have similar flow geometry. The Reynolds number is calculated as follows;

$$\mathrm{Re} = \frac{inertial \;\; forces}{viscous \;\; forces} = \frac{\rho V_\infty{}^2 / c}{\mu V_\infty / c^2} = \frac{\rho V_\infty c}{\mu}.$$

Dynamic pressure is calculated with the following formula for all airfoil sections of the propeller blades and wings,

$$q_\infty = \frac{1}{2}\rho_\infty V_\infty{}^2.$$

2.2.7.2. Aerodynamic Coefficients

As an airfoil travels through the air, the air is separated into two regions on the upper and lower surface of the airfoil, considering laminar flow for low Reynolds numbers below the speed of sound. When the angle of attack is positive for a symmetrical airfoil, the air on the upper surface travels a longer path than on the lower surface. Since the air separated on the leading edge must combine on the trailing edge, the air on the upper surface travels faster than on the lower surface. This results a higher air speed on the upper surface, resulting lower pressure. This pressure distribution is shown in Figure 25, for 5 degrees of angle of attack of NACA 0012 symmetrical airfoil.

The resultant forces and moments acting on a typical section of the blade are the net result of the action of the distributed pressure and viscous shear forces. These forces and moments are obtained by integrating the local values of pressure and shear stress acting normal and parallel to the surface around the airfoil (Leishman [11]). The aerodynamic coefficients C_L, C_D, C_M are formed in the following fashion;

$$C_L = \frac{L}{q_\infty S},\ C_D = \frac{D}{q_\infty S},\ C_M = \frac{M}{q_\infty Sc},$$

where $L(N)$: lift, $D(N)$: drag, $M(Nm)$: moment, $S(m^2)$: crossectional area, $c(m)$: chord length, resulting in dimensionless numbers.

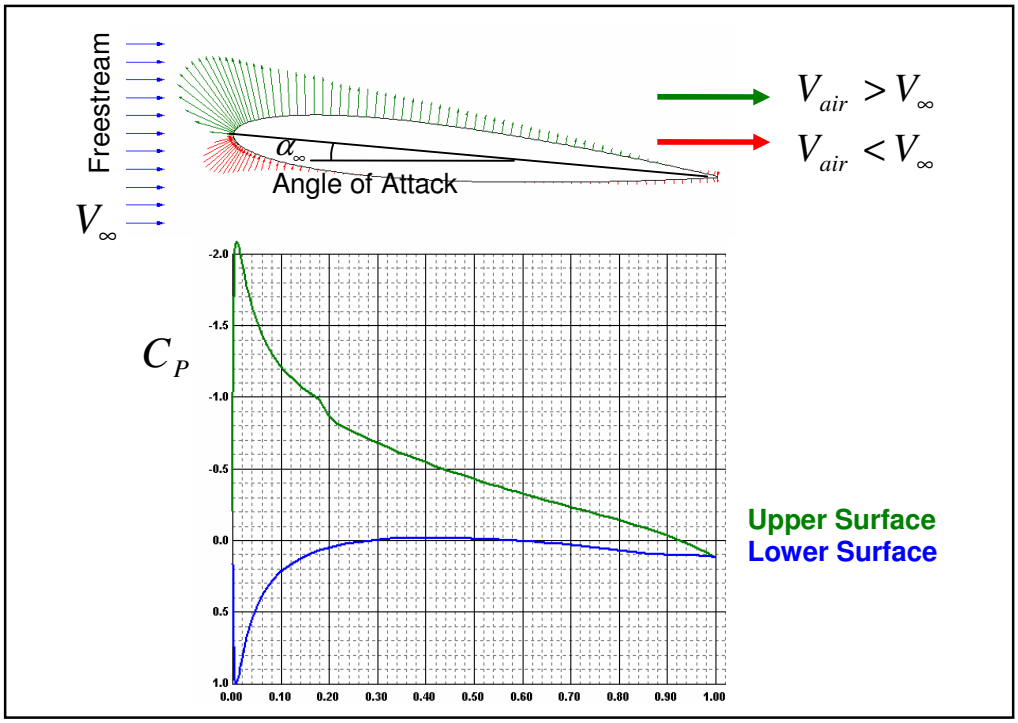

Figure 25. Airfoil pressure distributions.

Although the calculations for lift, drag and moment are straightforward, the calculation of pressure distributions of air, over the airfoil's surface depend on the geometry of the airfoil involving CFD (Computational Fluid Dynamics) solutions, which is out of the scope of this work. In order to overcome this difficulty, a simulation program, XFOIL (Drela [15]) is used in order to obtain the sectional aerodynamic coefficients for different airfoils. Sectional aerodynamical coefficients are defined for unit span as follows (Leishman [11]):

$$C_l = \frac{dL}{q_\infty c},\ C_d = \frac{dD}{q_\infty c},\ C_m = \frac{dM}{q_\infty c^2},$$

where $dL(N/m)$: lift per unit span, $dD(N/m)$: drag per unit span, $M(N)$: moment per unit span, $c(m)$: chord length, resulting in dimensionless C_l, C_d, C_m. Sectional aerodynamical coefficients will be used throughout the simulations and called simply as aerodynamical coefficients.

XFOIL simulations are run for a range of angles of attack, with respect to different Reynolds numbers, and C_l, C_d and C_m surfaces are obtained as shown in Figure 26. Since XFOIL does not give results for the high angles of attack ranges, the present data is interpolated according to the results of experimental data obtained by Sheldahl [16] and formulas for high angle of attack presented by Leishman [11]:

$C_l = 1.1\sin(2(\alpha - \alpha_0))$, α_0 : zero lift angle of attack,

$C_d = 1.135 - 1.05\cos(2(\alpha - \alpha_0))$,

$C_m = -0.5\sin(\alpha - \alpha_0) + 0.11\sin(2(\alpha - \alpha_0))$.

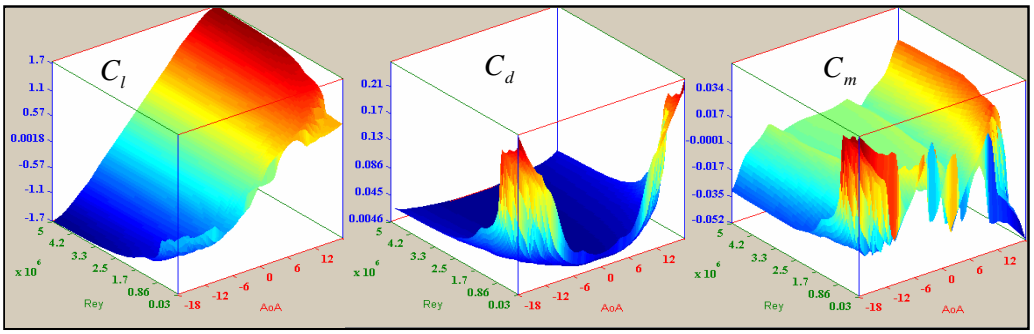

Figure 26. Aerodynamic coefficient surfaces for NACA0012.

The aerodynamic coefficient surfaces are used as look up tables, throughout Tiltrotor UAV simulations as,

$$\begin{bmatrix} C_l \\ C_d \\ C_m \end{bmatrix} = f_{XFOIL}(\alpha, \mathrm{Re}, AF).$$

2.2.7.3. Forces and Moments

The forces and moments per span length for the airfoil sections are calculated as follows;

$$dL = C_l \, q_\infty \, c \,,$$

$$dD = C_d \, q_\infty \, c \,,$$

$$dM = C_m \, q_\infty \, c^2 \,,$$

The lift dL and drag dD act perpendicular and parallel to the resultant flow velocity V_∞. These forces can be resolved perpendicular and parallel to the rotor disk plane giving;

$$\phi = \theta - \alpha \,,$$

$$dF_L = dL\cos\phi - dD\sin\phi \,,$$

$$dF_D = dL\sin\phi + dD\cos\phi \,.$$

The full model for an airfoil section is summarized as,

$$\begin{bmatrix} dF_L \\ dF_D \\ dM \end{bmatrix} = \frac{1}{2}\rho V_\infty^2 c \begin{bmatrix} C_l\cos(\theta-\alpha) - C_d\sin(\theta-\alpha) \\ C_l\sin(\theta-\alpha) + C_d\cos(\theta-\alpha) \\ C_m c \end{bmatrix}$$

where, $\begin{bmatrix} C_l \\ C_d \\ C_m \end{bmatrix} = f_{XFOIL}(\alpha, \mathrm{Re}, AF)$, $\mathrm{Re} = \dfrac{\rho V_\infty c}{\mu}$.

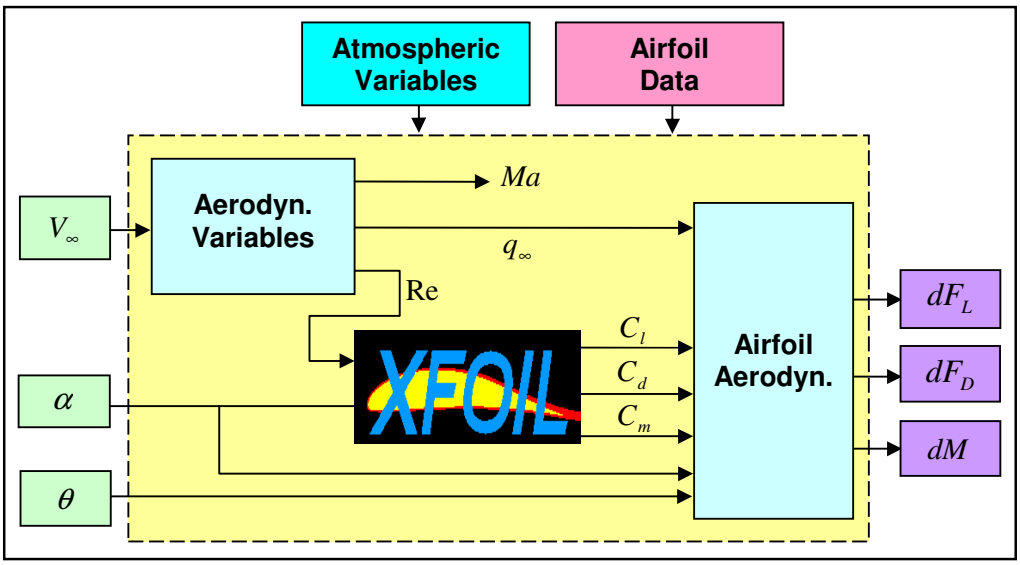

Figure 27. Airfoil dynamics.

CHAPTER 3

TRIMMING, LINEARIZATION AND STABILITY ANALYSIS

The mechanics of aircraft flight can be described in terms of three aspects – trim, linearization and stability. These three make up the flying characteristics of the aircraft.

Stability analysis requires linearization about a trim point and an examination of the eigenvalues and eigenvectors of the system. This is useful when examining the system responses to step inputs, frequency response and other stability characteristics of a dynamic system. The main assumption underlying in the stability and trim analysis is that the higher order rotor and inflow dynamics are much faster than the fuselage motions and have time to reach their steady state well within the typical time constants of the whole aircraft response modes (Padfield [17]).

The trim and stability analysis can be based on one of the three possible axes systems: wind axes, stability axes, and body axes. Although each system is valid, there are two reasons for using the body axes system in this study. First, the other systems loose their significance in hover. Second, aircrafts are equipped with inertial measurement units like gyros and accelerometers, giving measurements in body axes.

3.1. Trimming

The general principle of flight with any aircraft is that the aerodynamic, inertial and gravitational forces and moments about three mutually perpendicular axes are in balance at all times. When this balance is achieved, the aircraft is said to be trimmed. An aircraft is trimmed when the resultant forces and moments on the aircraft are zero, for a non-rotational flight. More generally, the trim can be defined

as the equilibrium point, where the rates of the aerodynamic state variables are zero.

The derived variables in the motion model, can be divided into two groups as aerodynamic and navigation variables. The aerodynamic variables are $[u, v, w, p, q, r, \phi, \theta]$, which are used in aerodynamical calculations, where the remaining variables $[\psi, x_e, y_e, z_e]$ are used in navigation calculations, as shown in Figure 28. Because, ignoring the changes in the medium variables like wind, pressure and gravitational acceleration, the heading angle and the position of the aircraft have no effect on aerodynamical calculations.

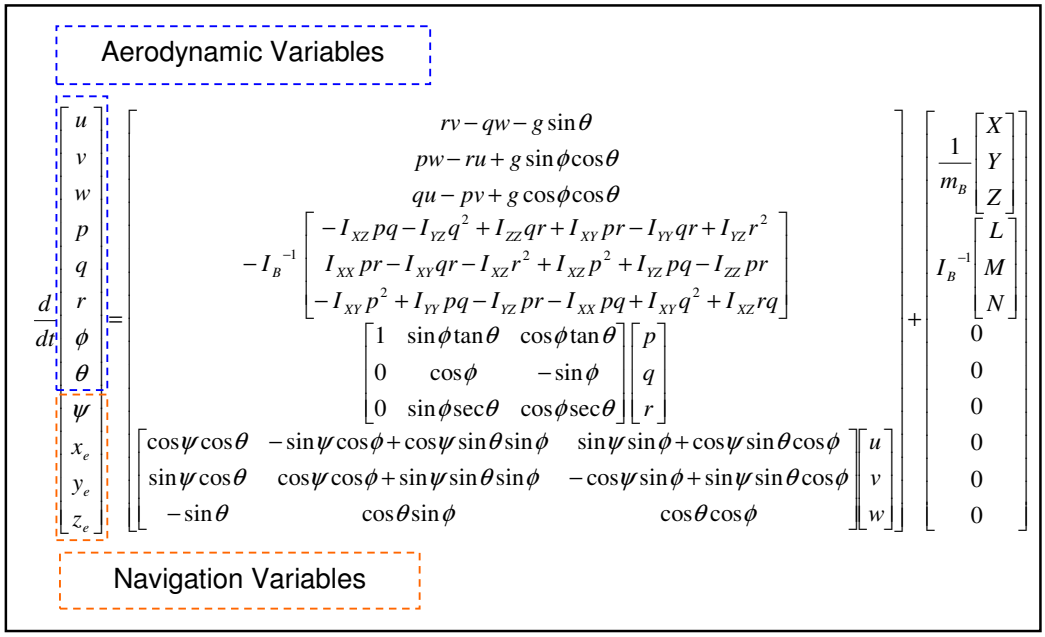

Figure 28. Aerodynamic and navigation variables in the motion model.

The physical meaning of trim point is the equilibrium point of aircraft motion that is to be the nulling of the aerodynamic variable derivatives. At the trim point, the rates of change of the Euler angles ϕ and θ are both zero $\dot{\phi} = \dot{\theta} = 0$, so that the gravitational force components are constant. If $\dot{\phi} \neq \dot{\theta} \neq 0$, then the weight vector in the body axes would be changing in time, resulting changes in the aerodynamic

variables. The heading angle ψ, is not important in the flight dynamics; it will be used only for navigation purposes.

The trim problem concerns the determination of control inputs $[\Omega_{1e}, \theta_{1e}, \theta_{2e}, \Omega_{2e}]$, Euler angles $[\phi_e, \theta_e]$, translational and rotational velocities $[u_e, v_e, w_e, p_e, q_e, r_e]$ required to hold the aircraft in equilibrium. The aircraft may be climbing, turning at large angles of incidence and sideslip, but if the Euler angles, translational and rotational velocities are constant with the controls fixed, then the aircraft is in trim. Since trim is an aerodynamical equilibrium, the derivatives of the aerodynamic variables are set to zero. Therefore, navigation variables determine the flight condition, where we want to reach the trim, so they are prescribed by the navigation algorithm. If we rewrite the motion model for the trim point:

$$\begin{bmatrix} X_e \\ Y_e \\ Z_e \\ L_e \\ M_e \\ N_e \end{bmatrix} = \begin{bmatrix} m_B\left(-r_e v_e + q_e w_e + g\sin\theta_e\right) \\ m_B\left(-p_e w_e + r_e u_e - g\sin\phi_e\cos\theta_e\right) \\ m_B\left(-q_e u_e + p_e v_e - g\cos\phi_e\cos\theta_e\right) \\ -I_{XZ}p_e q_e - I_{YZ}q_e^2 + I_{ZZ}q_e r_e + I_{XY}p_e r_e - I_{YY}q_e r_e + I_{YZ}r_e^2 \\ I_{XX}p_e r_e - I_{XY}q_e r_e - I_{XZ}r_e^2 + I_{XZ}p_e^2 + I_{YZ}p_e q_e - I_{ZZ}p_e r_e \\ -I_{XY}p_e^2 + I_{YY}p_e q_e - I_{YZ}p_e r_e - I_{XX}p_e q_e + I_{XY}q_e^2 + I_{XZ}r_e q_e \end{bmatrix},$$

$$LHS = RHS$$

with transformations

$$\begin{bmatrix} p_e \\ q_e \\ r_e \end{bmatrix} = \begin{bmatrix} -\dot{\psi}_e \sin\theta_e \\ \dot{\psi}_e \sin\phi_e \cos\theta_e \\ \dot{\psi}_e \cos\phi_e \cos\theta_e \end{bmatrix},$$

$$\begin{bmatrix} u_e \\ v_e \\ w_e \end{bmatrix} = \begin{bmatrix} \cos\psi_e\cos\theta_e & \sin\psi_e\cos\theta_e & -\sin\theta_e \\ -\sin\psi_e\cos\phi_e + \cos\psi_e\sin\theta_e\sin\phi_e & \cos\psi_e\cos\phi_e + \sin\psi_e\sin\theta_e\sin\phi_e & \cos\theta_e\sin\phi_e \\ \sin\psi_e\sin\phi_e + \cos\psi_e\sin\theta_e\cos\phi_e & -\cos\psi_e\sin\phi_e + \sin\psi_e\sin\theta_e\cos\phi_e & \cos\theta_e\cos\phi_e \end{bmatrix} \begin{bmatrix} \dot{x}_e \\ \dot{y}_e \\ \dot{z}_e \end{bmatrix},$$

where

$$\begin{bmatrix} X_e \\ Y_e \\ Z_e \end{bmatrix} = {}^{B}F\left(\Omega_{1e}, \theta_{1e}, \theta_{2e}, \Omega_{2e}, u_e, v_e, w_e, p_e, q_e, r_e, \phi_e, \theta_e\right),$$

$$\begin{bmatrix} L_e \\ M_e \\ N_e \end{bmatrix} = {}^{B}M\left(\Omega_{1e}, \theta_{1e}, \theta_{2e}, \Omega_{2e}, u_e, v_e, w_e, p_e, q_e, r_e, \phi_e, \theta_e\right).$$

So, there are 12 equations, 16 variables $(\Omega_{1e}, \theta_{1e}, \theta_{2e}, \Omega_{2e}, u_e, v_e, w_e, p_e, q_e, r_e, \phi_e, \theta_e, \dot{\psi}_e, \dot{x}_e, \dot{y}_e, \dot{z}_e)$, $\psi_e = 0$ being fixed, then we need to prescribe 4 variables in order to obtain a trim solution. A conventional selection of the prescribed variables, as stated by Padfield [17], are:

$V_{fe}\ (m/s)$: flight speed,

$\gamma_{fe}\ (\deg)$: flight path angle,

$\dot{\psi}_e\ (\deg/s)$: turn rate,

$\beta_e\ (\deg)$: side-slip angle.

These variables require the definitions of new frames and variables, other than already defined. In order to be compatible with the control system defined in Chapter 4 and to use the variables and frames already defined, $\dot{\psi}_e, \dot{x}_e, \dot{y}_e, \dot{z}_e$ are chosen to be the prescribed variables, where V_{fe}, γ_{fe} and β_e define $\dot{x}_e, \dot{y}_e, \dot{z}_e$ uniquely for the static case, so they are merely transformations of the conventional prescribed variables.

Considering the general case of transformation equations, the angular and linear velocities in the body frame are functions of Euler angles and navigation variables, so we can define a new frame between the body frame and vehicle-carried frame, which is oriented by ψ_e around z-axis, according to the vehicle-carried frame. In this frame yaw angle will always be zero, pitch and roll angles are to be determined with the trim algorithm. Although we can choose $\dot{z}_e$ arbitrarily, $\dot{\psi}_e$ and $\dot{x}_e\ \dot{y}_e$ cannot be chosen arbitrarily, resulting in two options as straight and rotational flight. In this work, only straight flight is inspected when calculating the trim points.

For straight flight $\dot{\psi}_e = 0$ and $\dot{x}_e, \dot{y}_e, \dot{z}_e$ can be chosen arbitrarily, and for the rotational flight $\dot{x}_e\ \dot{y}_e$ are functions of $\dot{\psi}_e \neq 0$. If a nonzero Earth frame velocity in the y-axes $\dot{y}_e \neq 0$, were to be considered, then $\psi_e = \arctan(\dot{y}_e / \dot{x}_e)$ and $\dot{xy}_e = \sqrt{(\dot{x}_e)^2 + (\dot{y}_e)^2}$: linear speed in the x-y plane of the vehicle-carried frame. Considering the new frame defined by ψ_e, linear velocities in x-axes and z-axes

being constant and zero in y-axes: results in $p_e = q_e = r_e = v_e = 0$ and $u_e, w_e =$ constant when θ_e is held fixed.

Considering the trim point calculation for the straight flight, the prescribed navigation variables reduce to; $\dot{\psi}_e = 0, \dot{y}_e = 0$, and $\dot{x}_e, \dot{z}_e =$ constant with $\psi_e = 0$. Also, roll angle is set to zero $\phi_e = 0$, since the Tiltrotor UAV has plane-symmetry property in x-z plane of the body frame, where 2 counter-rotating rotors balance the moments due to propeller rotation. Considering these, the transformation equations become:

$$\begin{bmatrix} p_e \\ q_e \\ r_e \end{bmatrix} = \begin{bmatrix} 0 \\ 0 \\ 0 \end{bmatrix}, \quad \begin{bmatrix} u_e \\ v_e \\ w_e \end{bmatrix} = \begin{bmatrix} \cos\theta_e & 0 & -\sin\theta_e \\ 0 & 1 & 0 \\ \sin\theta_e & 0 & \cos\theta_e \end{bmatrix} \begin{bmatrix} \dot{x}_e \\ 0 \\ \dot{z}_e \end{bmatrix}$$

where $v_e = 0$ and $u_e, w_e =$ constant when θ_e is held fixed.

Having zero angular velocities $p_e = q_e = r_e = 0$ in the body frame for the straight flight, the net moment acting on the aircraft must be equal to zero, since moment equations of RHS depend merely on angular velocities in the body frame. Both of the propellers must be set to the same tilt angles $\theta_{1e} = \theta_{2e} = \theta_{tilt,e}$ and same RPMs $\Omega_{1e} = \Omega_{2e} = \Omega_e$, in order to achieve moment balance for the aircraft, since they are counter-rotating. Eventually, we have 2 prescribed navigation variables $\dot{x}_e$ $\dot{z}_e$, 3 aerodynamical variables, θ_e, u_e, w_e (u_e, w_e are functions of θ_e and $\dot{x}_e$ $\dot{z}_e$) and 2 control inputs $\theta_{tilt,e}, \Omega_e$, resulting in 3 effective variables $\theta_e, \theta_{tilt,e}, \Omega_e$ that must be determined by the trim algorithm for the straight flight. The trim equations for the straight flight can be rearranged as follows;

$$\begin{bmatrix} X_e \\ Y_e \\ Z_e \end{bmatrix} = \begin{bmatrix} m_B g \sin\theta_e \\ 0 \\ m_B g \cos\theta_e \end{bmatrix}, \qquad \begin{bmatrix} L_e \\ M_e \\ N_e \end{bmatrix} = \begin{bmatrix} 0 \\ 0 \\ 0 \end{bmatrix},$$

$$LHS_F = RHS_F \qquad LHS_M = RHS_M$$

$$\begin{bmatrix} p_e \\ q_e \\ r_e \end{bmatrix} = \begin{bmatrix} 0 \\ 0 \\ 0 \end{bmatrix}, \qquad \begin{bmatrix} u_e \\ v_e \\ w_e \end{bmatrix} = \begin{bmatrix} \dot{x}_e \cos\theta_e - \dot{z}_e \sin\theta_e \\ 0 \\ \dot{x}_e \sin\theta_e + \dot{z}_e \cos\theta_e \end{bmatrix},$$

where

$$\begin{bmatrix} X_e \\ Y_e \\ Z_e \end{bmatrix} = {}^{B}F\left(\Omega_e, \theta_{tilt,e}, \theta_e, u_e, w_e\ \dot{x}_e, \dot{z}_e\right),$$

$$\begin{bmatrix} L_e \\ M_e \\ N_e \end{bmatrix} = {}^{B}M\left(\Omega_e, \theta_{tilt,e}, \theta_e, u_e, w_e\ \dot{x}_e, \dot{z}_e\right),$$

with all of the other variables are set to zero. There were 12 equations initially, 7 of these equations became definitions as $p_e = q_e = r_e = v_e = Y_e = L_e = N_e = 0$, due to straight flight conditions, symmetric structure of Tiltrotor UAV and synchronization of the control inputs, leaving only 5 equations. This treatment of the trim problem for the straight flight leaves out 7 variables $\left(\Omega_e, \theta_{tilt,e}, \theta_e, u_e, w_e, \dot{x}_e, \dot{z}_e\right)$ to be determined, where 2 of them $\left(\dot{x}_e, \dot{z}_e\right)$ were prescribed. So we need only 5 equations to obtain a solution for $\left(\Omega_e, \theta_{tilt,e}, \theta_e, u_e, w_e\right)$, which uniquely determines the trim solution for a straight flight.

Considering the above espousals, the problem of finding trim solution can be stated as, "*Find* $\left(\Omega_e, \theta_{tilt,e}, \theta_e, u_e, w_e\right)$ *given* $\left(\dot{x}_e, \dot{z}_e\right)$*".* The algorithm constructed in order to obtain the trim solution for a straight flight is shown in Figure 29.

First, all of the variables are initialized for the straight flight using prescribed navigation variables. Then, a cost-map is constructed by changing $\Omega_e, \theta_{tilt,e}, \theta_e$ with fixed steps for a range of minimum and maximum values. Within the cost map, a feasible region is selected which minimizes the cost function; then a fine search is applied using Generalized Pattern Search (GPS) global optimization algorithm, in order to obtain the best result.

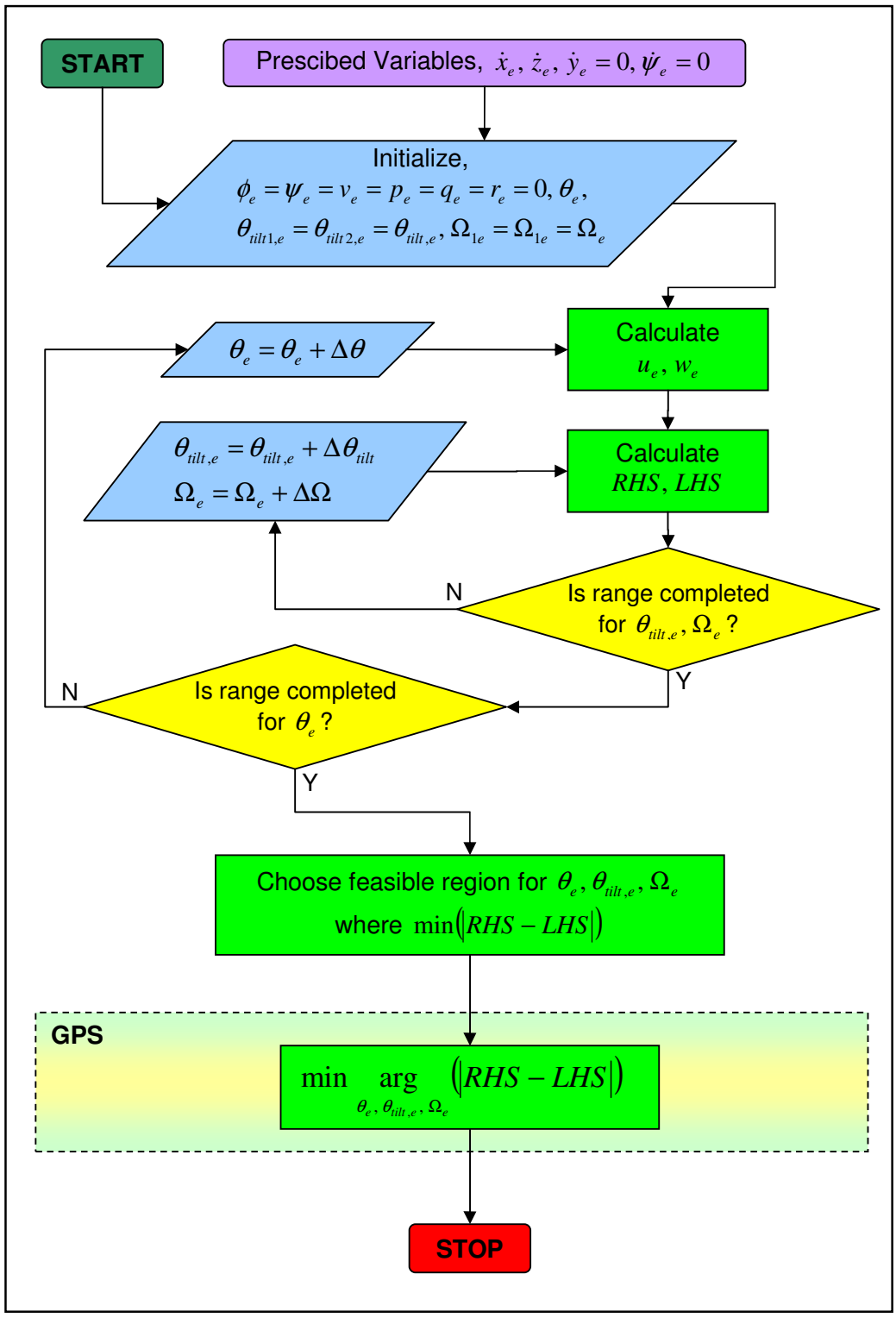

Figure 29. Trim algorithm for Tiltrotor UAV in straight flight.

GPS is one of the direct search methods for solving optimization problems that does not require any information about the gradient of the objective function. Unlike more traditional optimization methods that use information about the gradient or higher derivatives to search for an optimal point, a direct search algorithm searches a set of points around the current point, looking for one, where the value of the objective function is lower than the value at the other points. Since derivative calculation becomes computationally costly in numerical calculations, GPS is chosen over other optimization algorithms.

We consider pattern-search methods that choose a certain set of search directions at each iterate and evaluate cost at a given step length along each of these directions. These candidate points form a "frame" around the current iterate. If a point with a significantly lower function value is found, it is adopted as the new iterate, and the center of the frame is shifted to this new point. Whether shifted or not, the frame may then be altered in some way (the set of search directions may be changed, or the step length may grow or shrink), and the process repeats.

To define pattern-search methods, we introduce some notation. For the current iterate x_k, we define D_k to be the set of possible search directions and y_k to be the line search parameter. The frame consists of the points $x_k + y_k p_k$, for all $p_k \in D_k$. When one of the points in the frame yields a significant decrease in f, we take the step and may also increase y_k, so as to expand the frame for the next iteration. If none of the points in the frame has a significantly better function value than f_k, we reduce y_k (contract the frame), set $x_{k+1} = x_k$, and repeat. In either case, we may change the direction set D_k prior to the next iteration, subject to certain restrictions. The algorithm of pattern search may be summarized by the following algorithm:

Given convergence tolerance y_{tol}*, contraction parameter* $\theta_{\max}$*, sufficient decrease function* $\rho : [0,\infty) \to R$ *with* $\rho(t)$ *an increasing function of* t *and* $\rho(t)/t \to 0$ *as* $t \to 0$*;*
Choose initial point x_0*, initial step length* $y_0 > y_{tol}$*, initial direction set* D_0*;*
for $k = 1, 2, ...$
    if $y_k < y_{tol}$
        stop;

end (if)

if $f(x_k + y_k p_k) < f(x_k) - \rho(k)$ *for some* $p_k \in D_k$

Set $x_{k+1} \leftarrow x_k + y_k p_k$ *for some such* p_k *;*

Set $y_{k+1} \leftarrow \theta_k y_k$ *for some* $\theta_k \geq 1$*; (increase step length)*

else

Set $x_{k+1} \leftarrow x_k$ *;*

Set $y_{k+1} \leftarrow \theta_k y_k$ *, where* $0 < \theta_k \leq \theta_{\max} < 1$*; (decrease step length)*

end (if)

end (for).

3.2. Linearization

The motion model was constructed as below in a nonlinear form:

$$\dot{x} = F(x, u, t).$$

State variables: $x = \{u, v, w, p, q, r, \phi, \theta, \psi, x_e, y_e, z_e\}$,

Inputs: $u = \{X, Y, Z, L, M, N\}$.

For the stability analysis we are only interested in aerodynamical state variables $\{u, v, w, p, q, r, \phi, \theta\}$, so we can ignore navigation state variables $\{\psi, x_e, y_e, z_e\}$. After rearrangement of the motion model, it becomes:

$$\begin{bmatrix} \dot{u} \\ w \\ q \\ \theta \\ v \\ p \\ r \\ \phi \end{bmatrix} = \begin{bmatrix} rv - qw - g\sin\theta \\ qu - pv + g\cos\phi\cos\theta \\ pqI_{qpq} + qrI_{qqr} + prI_{qpr} + p^2 I_{qp^2} + q^2 I_{qq^2} + r^2 I_{qr^2} \\ q\cos\phi - r\sin\phi \\ pw - ru + g\sin\phi\cos\theta \\ pqI_{ppq} + qrI_{pqr} + prI_{ppr} + p^2 I_{pp^2} + q^2 I_{pq^2} + r^2 I_{pr^2} \\ pqI_{rpq} + qrI_{rqr} + prI_{rpr} + p^2 I_{rp^2} + q^2 I_{rq^2} + r^2 I_{rr^2} \\ p + q\sin\phi\tan\theta + r\cos\phi\tan\theta \end{bmatrix} + \begin{bmatrix} X/m_B \\ Z/m_B \\ I^t_{XY} L + I^t_{YY} M + I^t_{YZ} N \\ 0 \\ Y/m_B \\ I^t_{XX} L + I^t_{XY} M + I^t_{XZ} N \\ I^t_{XZ} L + I^t_{YZ} M + I^t_{ZZ} N \\ 0 \end{bmatrix}$$

with

u, w, q, θ : longitudinal state variables, v, p, r, ϕ : lateral state variables.

Using small perturbation theory we assume that, during disturbed motion, the aircraft's behavior can be described as a perturbation from the trim, written in the form:

$x = x_e + dx$,

where x_e : trim point, dx : perturbation.

The Taylor series is a representation of a function as an infinite sum of terms calculated from the values of its derivatives at a single point. The Taylor series of a function $f(x)$, that is infinitely differentiable in a neighborhood of a real or complex number a, is the power series:

$$f(x) = f(a) + \frac{f'}{1!}(x-a) + \frac{f''}{2!}(x-a)^2 + \frac{f'''}{3!}(x-a)^3 + \ldots,$$

which in a more compact form can be written as:

$$f(x) = \sum_{n=0}^{\infty} \frac{f^{(n)}(a)}{n!}(x-a)^n.$$

In our case, considering

$\dot{x} = F(x, u, t)$,

$x - x_e = dx$, $u - u_e = du$,

and the Taylor's expansion of $F(x,u,t)$ for two variables and for any t, is as follows;

$$F(x_e + dx, u_e + du) = F(x_e, u_e) + \left.\frac{dF}{dx}\right|_{x_e,u_e} dx + \left.\frac{dF}{du}\right|_{x_e,u_e} du + H.O.T.$$

$$H.O.T. = \frac{1}{2!}\left(\left.\frac{d^2F}{dx^2}\right|_{x_e,u_e} dx^2 + 2\left.\frac{d^2F}{dx\,du}\right|_{x_e,u_e} dx\,du + \left.\frac{d^2F}{du^2}\right|_{x_e,u_e} du^2 \right) + \ldots$$

Considering $F(x_e, u_e) = 0$ for the trim point, small disturbances $x = x_e + dx$, and neglecting $H.O.T.$ since the disturbances $\{dx, du\}$ are small making $\{dx^2, dx\,du, du^2, ..., dx^\infty, ..., du^\infty\}$ even much smaller, the equation becomes;

$$F(x_e + dx, u_e + du) = \left.\frac{dF}{dx}\right|_{x_e, u_e} dx + \left.\frac{dF}{du}\right|_{x_e, u_e} du .$$

The linearized equations of motion for the six degree of freedom, describing the perturbed motion about a trim condition can be written as:

$\dot{x} = Ax + Bu$,

where

$x = \{u, v, w, p, q, r, \phi, \theta\}$: 8×1 vector,

$u = \{\Omega_1, \theta_1, \theta_2, \Omega_2\}$: 4×1 vector,

A: 8×8 matrix,

B: 8×4 matrix,

and

$$A = \left.\frac{dF(x, u)}{dx}\right|_{x_e, u_e}, \quad B = \left.\frac{dF(x, u)}{du}\right|_{x_e, u_e} .$$

Since we have obtained the equations of motions as follows, we can divide it into two parts F_1 and F_2, where F_1 is analytically differentiable, and F_2 is not. F_1 is analytically differentiable because it is explicitly defined in terms of aerodynamic state variables. F_2 is not analytically differentiable because it is consisted of net forces and moments acting on the aircraft, obtained numerically based on the complex model of the Tiltrotor UAV.

$$F(x,u)=F_1(x)+F_2(x,u)$$

$$=\begin{bmatrix} rv-qw-g\sin\theta \\ qu-pv+g\cos\phi\cos\theta \\ pqI_{qpq}+qrI_{qqr}+prI_{qpr}+p^2I_{qp^2}+q^2I_{qq^2}+r^2I_{qr^2} \\ q\cos\phi-r\sin\phi \\ pw-ru+g\sin\phi\cos\theta \\ pqI_{ppq}+qrI_{pqr}+prI_{ppr}+p^2I_{pp^2}+q^2I_{pq^2}+r^2I_{pr^2} \\ pqI_{rpq}+qrI_{rqr}+prI_{rpr}+p^2I_{rp^2}+q^2I_{rq^2}+r^2I_{rr^2} \\ p+q\sin\phi\tan\theta+r\cos\phi\tan\theta \end{bmatrix}+\begin{bmatrix} X/m_B \\ Z/m_B \\ I^t_{XY}L+I^t_{YY}M+I^t_{YZ}N \\ 0 \\ Y/m_B \\ I^t_{XX}L+I^t_{XY}M+I^t_{XZ}N \\ I^t_{XZ}L+I^t_{YZ}M+I^t_{ZZ}N \\ 0 \end{bmatrix}.$$

Then A and B matrices can be written as follows;

$$A=A_1+A_2=\left.\frac{dF_1(x)}{dx}\right|_{x_e}+\left.\frac{dF_2(x,u)}{dx}\right|_{x_e,u_e},$$

$$B=\left.\frac{dF_2(x,u)}{du}\right|_{x_e,u_e}.$$

Since $F_1(x)$ is algebraic, its derivative can be obtained analytically, and $F_2(x,u)$ is a very complex function, so its derivative can not be obtained analytically. The derivative of $F_1(x)$ for the trim point is calculated as follows:

$$F_1(x)=\begin{bmatrix} rv-qw-g\sin\theta \\ qu-pv+g\cos\phi\cos\theta \\ pqI_{qpq}+qrI_{qqr}+prI_{qpr}+p^2I_{qp^2}+q^2I_{qq^2}+r^2I_{qr^2} \\ q\cos\phi-r\sin\phi \\ pw-ru+g\sin\phi\cos\theta \\ pqI_{ppq}+qrI_{pqr}+prI_{ppr}+p^2I_{pp^2}+q^2I_{pq^2}+r^2I_{pr^2} \\ pqI_{rpq}+qrI_{rqr}+prI_{rpr}+p^2I_{rp^2}+q^2I_{rq^2}+r^2I_{rr^2} \\ p+q\sin\phi\tan\theta+r\cos\phi\tan\theta \end{bmatrix},$$

$$A_1=\left.\frac{dF_1(x)}{dx}\right|_{x=x_e},$$

$$A_1 = \begin{bmatrix} 0 & -q_e & -w_e & -g\cos\theta_e \\ q_e & 0 & u_e & -g\cos\phi_e\sin\theta_e \\ 0 & 0 & p_e I_{qpq} + r_e I_{qqr} + 2q_e I_{qq^2} & 0 \\ 0 & 0 & \cos\phi_e & 0 \\ -r_e & p_e & 0 & -g\sin\phi_e\sin\theta_e \\ 0 & 0 & p_e I_{ppq} + r_e I_{pqr} + 2q_e I_{pq^2} & 0 \\ 0 & 0 & p_e I_{rpq} + r_e I_{rqr} + 2q_e I_{rq^2} & 0 \\ 0 & 0 & \sin\phi_e\tan\theta_e & \left(1+\tan^2\theta_e\right)\left(q_e\sin\phi_e + r_e\cos\phi_e\right) \end{bmatrix}$$

$$\begin{bmatrix} r_e & 0 & v_e & 0 \\ -p_e & -v_e & 0 & -g\sin\phi_e\cos\theta_e \\ 0 & q_e I_{qpq} + r_e I_{qpr} + 2p_e I_{qp^2} & q_e I_{qqr} + p_e I_{qpr} + 2r_e I_{qr^2} & 0 \\ 0 & 0 & -\sin\phi_e & -q_e\sin\phi_e - r_e\cos\phi_e \\ 0 & w_e & -u_e & g\cos\phi_e\cos\theta_e \\ 0 & q_e I_{ppq} + r_e I_{ppr} + 2p_e I_{pp^2} & q_e I_{pqr} + p_e I_{ppr} + 2r_e I_{pr^2} & 0 \\ 0 & q_e I_{rpq} + r_e I_{rpr} + 2p_e I_{rp^2} & q_e I_{rqr} + p_e I_{rpr} + 2r_e I_{rr^2} & 0 \\ 0 & 1 & \cos\phi_e\tan\theta_e & \tan\theta_e\left(q_e\cos\phi_e - r_e\sin\phi_e\right) \end{bmatrix}.$$

$F_2(x,u)$ has only forces and moments, as functions of state variables and aircrafts inputs. Since these forces and moments are produced with the interaction of all of the components of the aircraft, an analytic solution is not feasible. But, its derivatives according to state variables and inputs must be computed, in order to find A_2 and B matrices. A general approach is as follows;

$$A_2 = \begin{bmatrix} \frac{1}{m_B}\frac{dX}{dx} \\ \frac{1}{m_B}\frac{dZ}{dx} \\ I'_{XY}\frac{dL}{dx} + I'_{YY}\frac{dM}{dx} + I'_{YZ}\frac{dN}{dx} \\ 0 \\ \frac{1}{m_B}\frac{dY}{dx} \\ I'_{XX}\frac{dL}{dx} + I'_{XY}\frac{dM}{dx} + I'_{XZ}\frac{dN}{dx} \\ I'_{XZ}\frac{dL}{dx} + I'_{YZ}\frac{dM}{dx} + I'_{ZZ}\frac{dN}{dx} \\ 0 \end{bmatrix}_{x=x_e}, B = \begin{bmatrix} \frac{1}{m_B}\frac{dX}{du} \\ \frac{1}{m_B}\frac{dZ}{du} \\ I'_{XY}\frac{dL}{du} + I'_{YY}\frac{dM}{du} + I'_{YZ}\frac{dN}{du} \\ 0 \\ \frac{1}{m_B}\frac{dY}{du} \\ I'_{XX}\frac{dL}{du} + I'_{XY}\frac{dM}{du} + I'_{XZ}\frac{dN}{du} \\ I'_{XZ}\frac{dL}{du} + I'_{YZ}\frac{dM}{du} + I'_{ZZ}\frac{dN}{du} \\ 0 \end{bmatrix}_{u=u_e}.$$

A fundamental assumption of aircraft motion linearization is that the external forces X, Y, Z and moments L, M, N can be represented as analytic functions of the disturbed motion variables and their derivatives, in the vicinity of the trim point. We assume that the forces and moments are first-order functions of the translational, rotational velocities and control inputs. Taylor's theorem for analytic functions then implies that if the force and moment functions and all its derivatives are known at any one point (i.e. the trim condition), then the behavior of that function anywhere in its analytic range can be estimated from an expansion of the function in a series about the known point (Padfield [17]). The requirement that the aerodynamic and dynamic loads be analytic functions of the motion and control variables is generally valid, except for the extreme conditions like stall, sharp discontinuities and hysteresis where the analytic behavior is not valid. The validity of linearization depends on the behavior of the perturbations at small amplitude, i.e., the motion and control disturbances become very small, then the dominant effect should be a linear one. The linear approximation also contains terms in the rates of change of perturbations with time, but we can neglect these considering all other degrees of freedom held fixed. Considering these approximations and Taylor's theorem, the forces and moments can then be written in the approximate form (square and products of disturbances are neglected, since they get smaller in magnitude) as follows:

$$\left.\frac{dX}{dx}\right|_{x=x_e} dx = \frac{dX}{du}du + \frac{dX}{dw}dw + \frac{dX}{dq}dq + \frac{dX}{d\theta}d\theta + \frac{dX}{dv}dv + \frac{dX}{dp}dp + \frac{dX}{dr}dr + \frac{dX}{d\phi}d\phi$$

$$\left.\frac{dX}{du}\right|_{u=u_e} du = \frac{dX}{d\Omega_1}d\Omega_1 + \frac{dX}{d\theta_1}d\theta_1 + \frac{dX}{d\theta_2}d\theta_2 + \frac{dX}{d\Omega_2}d\Omega_2 \quad ,$$

In the following discussions, we will use a more convenient notation for derivatives in the following form:

$$\frac{dX}{du} = X_u, \quad \frac{dL}{dq} = X_q, \quad \frac{dY}{d\Omega_1} = Y_{\Omega 1}, \quad \frac{dN}{d\theta_2} = N_{\theta 2}, \text{ etc.}$$

All six forces and moments can be expanded in this manner as follows:

$$\frac{d}{dx}\begin{bmatrix} X \\ Y \\ Z \\ L \\ M \\ N \end{bmatrix}_{x=x_e} = \begin{bmatrix} X_u & X_w & X_q & X_\theta & X_v & X_p & X_r & X_\phi \\ Y_u & Y_w & Y_q & Y_\theta & Y_v & Y_p & Y_r & Y_\phi \\ Z_u & Z_w & Z_q & Z_\theta & Z_v & Z_p & Z_r & Z_\phi \\ L_u & L_w & L_q & L_\theta & L_v & L_p & L_r & L_\phi \\ M_u & M_w & M_q & M_\theta & M_v & M_p & M_r & M_\phi \\ N_u & N_w & N_q & N_\theta & N_v & N_p & N_r & N_\phi \end{bmatrix}_{x=x_e},$$

$$\frac{d}{du}\begin{bmatrix} X \\ Y \\ Z \\ L \\ M \\ N \end{bmatrix}_{u=u_e} = \begin{bmatrix} X_{\Omega 1} & X_{\theta 1} & X_{\theta 2} & X_{\Omega 2} \\ Y_{\Omega 1} & Y_{\theta 1} & Y_{\theta 2} & Y_{\Omega 2} \\ Z_{\Omega 1} & Z_{\theta 1} & Z_{\theta 2} & Z_{\Omega 2} \\ L_{\Omega 1} & L_{\theta 1} & L_{\theta 2} & L_{\Omega 2} \\ M_{\Omega 1} & M_{\theta 1} & M_{\theta 2} & M_{\Omega 2} \\ N_{\Omega 1} & N_{\theta 1} & N_{\theta 2} & N_{\Omega 2} \end{bmatrix}_{u=u_e}.$$

Analytic differentiation of the force and moment expressions is required to deliver the exact values of the derivatives. Since the force and moment calculations are very complex in nature, in practice a numerical method is employed for derivative calculations, leading to equivalent linearizations for finite amplitude motion. The forces and moments are perturbed by each of the states in turn, using two-sided backward - forward differencing method as follows:

$$X_u = \frac{X(u_e + du) - X(u_e - du)}{2du}.$$

The numerical derivatives will converge to the analytic, true values as the perturbation size reduces to zero. If there is any significant nonlinearity at small amplitude, then the slope at the trim may not give the best 'fit' to the force over the amplitude range of interest.

Following the calculation of the derivatives, A_2 and B matrices are obtained as shown below;

,

$$
A_2 = \begin{bmatrix}
\frac{X_u}{m_B} & \frac{X_w}{m_B} & \frac{X_q}{m_B} & \frac{X_\theta}{m_B} & \frac{X_v}{m_B} & \frac{X_p}{m_B} & \frac{X_r}{m_B} & \frac{X_\phi}{m_B} \\
\frac{Z_u}{m_B} & \frac{Z_w}{m_B} & \frac{Z_u}{m_B} & \frac{Z_\theta}{m_B} & \frac{Z_v}{m_B} & \frac{Z_p}{m_B} & \frac{Z_r}{m_B} & \frac{Z_\phi}{m_B} \\
I'_{XY}L_u & I'_{XY}L_w & I'_{XY}L_q & I'_{XY}L_\theta & I'_{XY}L_v & I'_{XY}L_p & I'_{XY}L_r & I'_{XY}L_\phi \\
0 & 0 & 0 & 0 & 0 & 0 & 0 & 0 \\
\frac{Y_u}{m_B} & \frac{Y_w}{m_B} & \frac{Y_q}{m_B} & \frac{Y_\theta}{m_B} & \frac{Y_v}{m_B} & \frac{Y_p}{m_B} & \frac{Y_r}{m_B} & \frac{Y_\phi}{m_B} \\
I'_{XX}L_u & I'_{XX}L_w & I'_{XX}L_q & I'_{XX}L_\theta & I'_{XX}L_v & I'_{XX}L_p & I'_{XX}L_r & I'_{XX}L_\phi \\
I'_{XZ}L_u & I'_{XZ}L_w & I'_{XZ}L_q & I'_{XZ}L_\theta & I'_{XZ}L_v & I'_{XZ}L_p & I'_{XZ}L_r & I'_{XZ}L_\phi \\
0 & 0 & 0 & 0 & 0 & 0 & 0 & 0
\end{bmatrix}
$$

$$
+ \begin{bmatrix}
0 & 0 & 0 & 0 & 0 & 0 & 0 & 0 \\
0 & 0 & 0 & 0 & 0 & 0 & 0 & 0 \\
I'_{YY}M_u & I'_{YY}M_w & I'_{YY}M_q & I'_{YY}M_\theta & I'_{YY}M_r & I'_{YY}M_p & I'_{YY}M_r & I'_{YY}M_\phi \\
0 & 0 & 0 & 0 & 0 & 0 & 0 & 0 \\
0 & 0 & 0 & 0 & 0 & 0 & 0 & 0 \\
I'_{XY}M_u & I'_{XY}M_w & I'_{XY}M_q & I'_{XY}M_\theta & I'_{XY}M_r & I'_{XY}M_p & I'_{XY}M_r & I'_{XY}M_\phi \\
I'_{YZ}M_u & I'_{YZ}M_w & I'_{YZ}M_q & I'_{YZ}M_\theta & I'_{YZ}M_r & I'_{YZ}M_p & I'_{YZ}M_r & I'_{YZ}M_\phi \\
0 & 0 & 0 & 0 & 0 & 0 & 0 & 0
\end{bmatrix}
$$

$$
+ \begin{bmatrix}
0 & 0 & 0 & 0 & 0 & 0 & 0 & 0 \\
0 & 0 & 0 & 0 & 0 & 0 & 0 & 0 \\
I'_{YZ}N_u & I'_{YZ}N_w & I'_{YZ}N_q & I'_{YZ}N_\theta & I'_{YZ}N_r & I'_{YZ}N_p & I'_{YZ}N_r & I'_{YZ}N_\phi \\
0 & 0 & 0 & 0 & 0 & 0 & 0 & 0 \\
0 & 0 & 0 & 0 & 0 & 0 & 0 & 0 \\
I'_{XZ}N_u & I'_{XZ}N_w & I'_{XZ}N_q & I'_{XZ}N_\theta & I'_{XZ}N_r & I'_{XZ}N_p & I'_{XZ}N_r & I'_{XZ}N_\phi \\
I'_{ZZ}N_u & I'_{ZZ}N_w & I'_{ZZ}N_q & I'_{ZZ}N_\theta & I'_{ZZ}N_r & I'_{ZZ}N_p & I'_{ZZ}N_r & I'_{ZZ}N_\phi \\
0 & 0 & 0 & 0 & 0 & 0 & 0 & 0
\end{bmatrix}
$$

$$B=\begin{bmatrix} \frac{X_{\Omega 1}}{m_B} & \frac{X_{\theta 1}}{m_B} & \frac{X_{\theta 2}}{m_B} & \frac{X_{\Omega 2}}{m_B} \\ \frac{Z_{\Omega 1}}{m_B} & \frac{Z_{\theta 1}}{m_B} & \frac{Z_{\theta 2}}{m_B} & \frac{Z_{\Omega 2}}{m_B} \\ I^{'}_{XY}L_{\Omega 1}+I^{'}_{YY}M_{\Omega 1}+I^{'}_{YZ}N_{\Omega 1} & I^{'}_{XY}L_{\theta 1}+I^{'}_{YY}M_{\theta 1}+I^{'}_{YZ}N_{\theta 1} & I^{'}_{XY}L_{\theta 2}+I^{'}_{YY}M_{\theta 2}+I^{'}_{YZ}N_{\Omega 2} & I^{'}_{XY}L_{\Omega 2}+I^{'}_{YY}M_{\Omega 2}+I^{'}_{YZ}N_{\Omega 2} \\ 0 & 0 & 0 & 0 \\ \frac{Y_{\Omega 1}}{m_B} & \frac{Y_{\theta 1}}{m_B} & \frac{Y_{\theta 2}}{m_B} & \frac{Y_{\Omega 2}}{m_B} \\ I^{'}_{XX}L_{\Omega 1}+I^{'}_{XY}M_{\Omega 1}+I^{'}_{XZ}N_{\Omega 1} & I^{'}_{XX}L_{\theta 1}+I^{'}_{XY}M_{\theta 1}+I^{'}_{XZ}N_{\theta 1} & I^{'}_{XX}L_{\theta 2}+I^{'}_{XY}M_{\theta 2}+I^{'}_{XZ}N_{\Omega 2} & I^{'}_{XX}L_{\Omega 2}+I^{'}_{XY}M_{\Omega 2}+I^{'}_{XZ}N_{\Omega 2} \\ I^{'}_{XZ}L_{\Omega 1}+I^{'}_{YZ}M_{\Omega 1}+I^{'}_{ZZ}N_{\Omega 1} & I^{'}_{XZ}L_{\theta 1}+I^{'}_{YZ}M_{\theta 1}+I^{'}_{ZZ}N_{\theta 1} & I^{'}_{XZ}L_{\theta 2}+I^{'}_{YZ}M_{\theta 2}+I^{'}_{ZZ}N_{\Omega 2} & I^{'}_{XZ}L_{\Omega 2}+I^{'}_{YZ}M_{\Omega 2}+I^{'}_{ZZ}N_{\Omega 2} \\ 0 & 0 & 0 & 0 \end{bmatrix}$$

In order to summarize, the linear model is obtained using the algorithm presented in Figure 30.

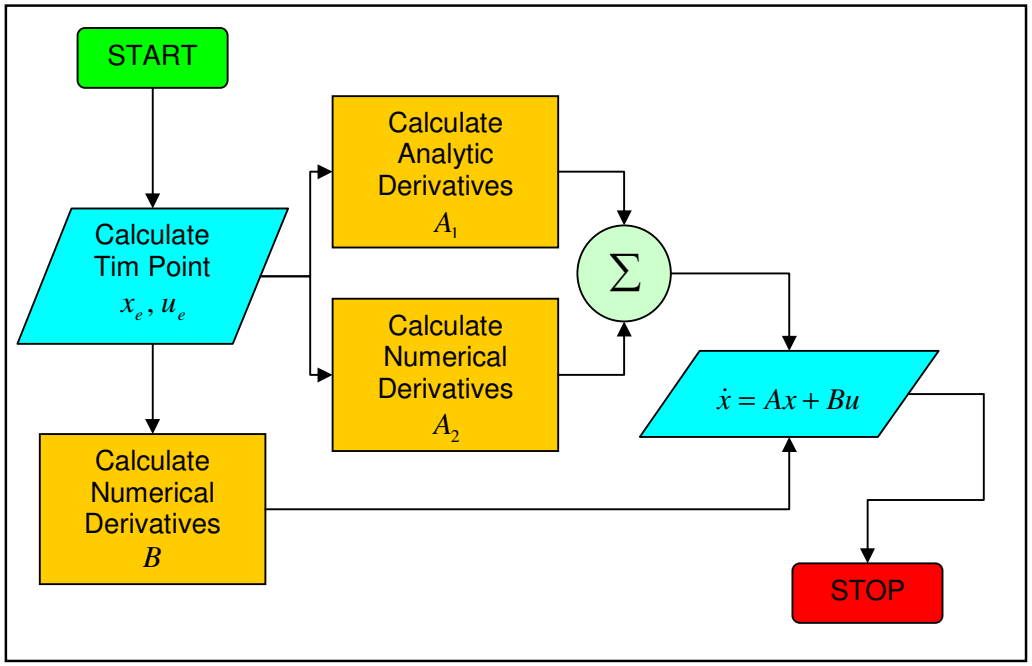

Figure 30. Linearization algorithm.

3.3. Stability

Considering all modes of operations of Tiltrotor UAV, both static stability and dynamic stability contribute to the flying qualities of an aircraft. Static stability refers to the initial tendency of the aircraft to return to its trimmed condition following a displacement. Dynamic stability considers the subsequent motion in time. Here we consider static stability of the aircraft with eigenvalues analysis considering zero-input response, and BIBO (Bounded Input Bounded Output) stability considering zero-state response, where the initial conditions of the state variables are zero, while applying a non-zero control input.

Following a general approach (Chen [27]), considering linear time-invariant dynamical equation,

$$\dot{x}(t) = Ax(t) + Bu(t),$$
$$y(t) = Cx(t),$$

where A, B, C are constant matrices and $t \geq 0$, the system is;

- BIBO stable, if and only if all of the poles of every entry of $G(s)$ have negative real parts (impulse response is bounded), where $G(s) = C(sI - A)^{-1}B$,
- Stable in the sense of Lyapunov, if and only if all of the eigenvalues of A matrix have non-positive real parts and those with zero real parts are distinct roots of the minimal polynomial of A,
- Asymptotically stable, if and only if all of the eigenvalues of A matrix have negative real parts.

For stability analysis, the aircraft motion can be considered to comprise a linear combination of natural modes, each having its own unique frequency, damping and distribution of the response variables. The linear approximation that allows this interpretation is extremely powerful in enhancing the physical understanding of the complex motions in disturbed flight. Free motion (unforced by the control inputs) of

the aircraft is defined by the homogeneous form of linearized motion model, using aerodynamic state variables:

$\dot{x} = Ax$, $x = \{u, v, w, p, q, r, \phi, \theta\}$,

where

$\det[\lambda I - A] = 0$,

$Aw_i = \lambda_i w_i$,

λ_i : eigenvalues of A ,

w_i : eigenvectors of A .

Therefore, the free motion is a linear combination of natural modes, each with an exponential character in time defined by the eigenvalues, and a distribution among the states, defined by the eigenvectors where a positive real part indicates instability, a negative real part stability.

CHAPTER 4

CONTROL SYSTEM DESIGN

Optimal control theory, a modern extension of the calculus of variations, is a mathematical optimization method for deriving control policies. A standard optimal control problem involves a scalar performance index, a set of differential constraints (system dynamics), and boundary conditions. In the differential equations, the differentiated variables are called the states and the undifferentiated variables are called the controls. The objective is to find the control histories that drive the system from the initial conditions to the final conditions while optimizing the performance index (Hull [18]).

Due to the desired features like, optimality, stability of the closed-loop system, good gain and phase margins, Linear Quadratic Regulator (LQR) is preferred in designing the control system of the Tiltrotor UAV. For the linear models of the Tiltrotor UAV, the results obtained in Chapter 3 are used. The controllers are obtained by the proper selection of LQR weighting matrices, for different trim points and transitions between them are obtained with gain scheduling method.

4.1. Linear Quadratic Regulator

The LQR algorithm is, at its core, just an automated way of finding an appropriate state-feedback controller. The advantage of a quadratic performance index, is that for a linear system it has a mathematical solution that yields a control law of the matrix form, K, where $u^*(t) = Kx(t)$. Although the performance index may be chosen to define the problem as minimum-time control, terminal control, minimum-energy control; tracking control is chosen in order to track the command history $r(t)$, which reduces to regulator problem when command is not changing at the trim point.

The problem for the LQR is stated as follows;

Design an optimal state-feedback controller, with finding the control law $u^*(t) = k(x(t))$*, which causes the system*

$$\dot{x}(t) = Ax(t) + Bu(t),$$

to follow an optimal trajectory $x^*(t)$ *that minimizes the performance index;*

$$J(u(t)) = \frac{1}{2}\int_0^{t_f} \left(x(t)^T Q x(t) + u(t)^T R u(t) \right) dt,$$

providing that,

- (A, B) *is controllable,*
- (Q, A) *is observable,*
- $Q = Q^T \geq 0$ *is symmetric and positive semi-definite,*
- $R = R^T > 0$ *is symmetric and positive definite,*
- $t_f = \infty,$

where

$x = \{u, v, w, p, q, r, \phi, \theta\}$*:* 8×1 *vector,* $u = \{\Omega_1, \theta_1, \theta_2, \Omega_2\}$*:* 4×1 *vector,*

A*:* 8×8 *matrix,* B*:* 8×4 *matrix,* Q*:* 8×8 *matrix,* R*:* 4×4 *matrix.*

The optimal control law for this problem is obtained by applying Hamilton-Jacobi-Bellman approach, which satisfies the necessary condition for optimality. The Hamilton-Jacobi equation to be solved for the linear time-invariant plant with quadratic performance index, takes the form of the matrix Riccati equation. This produces an optimal control law as a linear function of the state vector, which is always stable, providing that the system is controllable (Burns [19]).

Considering the Hamiltonian function as,

$$H(t) = \frac{1}{2}\left(x(t)^T Qx(t) + u(t)^T Ru(t)\right) + \lambda(t)^T \left(Ax(t) + Bu(t)\right),$$

where $u : [0, t_f] \in R^4$ is optimization variable,

$\dot{x} : [0, t_f] \in R^8$ is equality constraint,

$\lambda : [0, t_f] \in R^8$ is Lagrange multiplier.

Using Pontryagin's necessary conditions for optimality (Geering [20]),

$$\frac{\partial H}{\partial x}(t) = -\frac{d}{dt}\lambda(t)^T, \quad \frac{\partial H}{\partial \lambda}(t) = \frac{d}{dt}x(t), \quad \frac{\partial H}{\partial u}(t) = 0$$

Then, equality constraints are,

$$\frac{d}{dt}\lambda(t)^T = -\lambda(t)^T A - x(t)^T Q, \qquad \text{(Costate equation)}$$

$$\frac{d}{dt}x(t) = Ax(t) + Bu(t), \qquad \text{(State equation)}$$

$$u(t) = -R^{-1}B^T \lambda(t), \qquad \text{(Control equation)}$$

When the control equation is inserted into state equation, the problem becomes a set of differential equations with boundary constraints,

$$\frac{d}{dt}\lambda(t)^T = -\lambda(t)^T A - x(t)^T Q,$$

$$\frac{d}{dt}x(t) = Ax(t) - BR^{-1}B^T \lambda(t),$$

$x(0) = x_0$, (Initial condition)

$\lambda(t_f) = P(t_f)x(t_f) = 0$, (Final condition, $x(t_f) = 0$, $P(t_f)$ = constant or $x(t_f)$ = constant, $P(t_f) = 0$)

where P: 8×8 matrix.

The two differential equations are homogeneous in (x, λ) and at the final time t_f, the costate vector $\lambda(t_e)$ is a linear function of the final state vector $x(t_e)$. This leads

to the conjecture that the costate vector might be a linear function of the state vector at all times. Thus, introducing the transformation,

$\lambda(t) = P(t)x(t)$ with $P(t_f) = 0$,

differentiating with respect to time,

$$\frac{d}{dt}\lambda(t)^T = \frac{d}{dt}P(t)x(t) + P(t)\frac{d}{dt}x(t),$$

inserting costate and state equations,

$$-A^T P(t)x(t) - Qx(t) = \frac{d}{dt}P(t)x(t) + P(t)\left(Ax(t) - BR^{-1}B^T P(t)x(t)\right),$$

writing in a more compact form,

$$\left(\dot{P}(t) + Q + A^T P(t) + P(t)A - P(t)BR^{-1}B^T P(t)\right)x = 0.$$

Thus, the vector $x \in R^l$ in this equation may be an arbitrary vector, providing that the expression in the parenthesis is zero for all times, so that the states converge to the desired final state irrespective of the initial state. So the expression in the parenthesis may be written as follows;

$$\dot{P}(t) = -Q - A^T P(t) - P(t)A - P(t)BR^{-1}B^T P(t), \quad \text{with } P(t_f) = 0.$$

Kalman has shown that, if the system is completely controllable, if A, B, R, Q are constant matrices, $P(t) \to P$ a constant matrix as $t_f \to \infty$ (Kirk [28]). This means that satisfying the above conditions, then the optimal control law for an infinite-duration process is stationary resulting in the Algebraic Riccati Equation (ARE). For this special case, P has a solution for,

$$0 = -Q - A^T P - PA - PBR^{-1}B^T P,$$

Solving ARE for P, and insertion of this to the control equation yields the control law;

$$u(t) = -Kx(t),$$
$$K = R^{-1}B^T P,$$

where $K : 4 \times 8$ matrix. Considering the stability of the closed loop system,

$$\dot{x}(t) = (A - BK)x(t)$$
$$\lambda_i = eig(A - BK), \quad i = 1..8,$$
$$real(\lambda_i) < 0,$$

guarantees the closed loop stability. Considering the Lyapunov function, $V = x^T Px$,

- $V \geq 0$ for all $x \in R^8$, is satisfied,
- $\dot{V} < 0$, is satisfied with

$$\begin{aligned} \dot{V} &= x^T P\left(Ax + B\left(-R^{-1}B^T Px\right)\right) + \left(Ax + B\left(-R^{-1}B^T Px\right)\right)^T Px \\ &= x^T \left(A^T P + PA - 2PBR^{-1}B^T P\right)x \\ &= x^T \left(-Q - PBR^{-1}B^T P\right)x \end{aligned} .$$

Thus, satisfying both conditions, LQR stabilizes the system asymptotically.

Considering the tracking control, the problem is directed at applying a control $u(t)$ to drive the system, so that the state vector $x(t)$ follows a desired state trajectory $r(t)$ in optimal manner. This problem reduces to LQR problem when the command inputs are zero. Then the performance index becomes,

$$J(u(t)) = \frac{1}{2}\int_0^{t_f} \left((r(t) - x(t))^T Q(r(t) - x(t)) + u(t)^T Ru(t) \right) dt.$$

It is shown by Burns [19] that the constrained functional minimization of the cost function yields again the matrix Riccati equation obtained for the LQR, and the additional set of reverse-time state tracking equations;

$$\dot{s}(t) = \left(A - BR^{-1}B^T P\right)^T s(t) - Qr(t) \text{ for } t_{present} < t < t_{final},$$

and command input is,

$$v(t) = -R^{-1}B^T s(t).$$

Then the optimal control law becomes,

$$u(t)^* = v(t) - Kx(t).$$

Hence, when the desired state vector $r(t)$ is known in advance, tracking errors are reduced by allowing the system to follow a command vector $v(t)$ computed in advance using the reverse-time equation. In Chapter 3, we have calculated the trim points of the states for a range of navigation states. Consider that the aircraft operates in a trimmed navigation state, when we command the autopilot to move the aircraft from the current navigation state to another, we find the next state trim point to be reached from the previously calculated values. Then we have a prior knowledge of the desired state vector to be reached. Gain-scheduling is used while changing the navigation state, with employing small fixed steps for $r(t)$. The controller waits until the states deviations are minimized in order to go to the next step. So, keeping the fixed steps very small, the overall trajectory of the states becomes like a continuous response. For the simulations, the control system block diagram is shown in Figure 31.

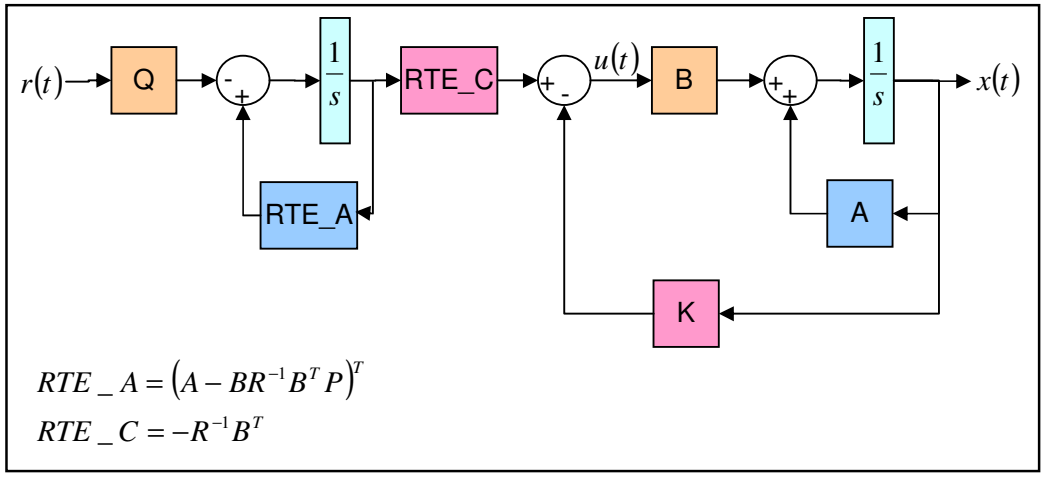

Figure 31. Tracking LQR block diagram.

4.2. LQR Weight Selection

In selecting a performance measure the designer attempts to define a mathematical expression which, when minimized indicates that the system is performing in the most desirable manner. Thus, choosing a performance measure is a translation of the system's physical requirements into mathematical terms. In fact, the numerical value of the performance measure does not represent a physically meaningful quantity.

The weighting matrices Q and R are used for shaping the compromise between keeping the state errors $(x(t)-x_e)$ and the control corrections $(u(t)-u_e)$, respectively small during the whole mission (Geering [20]).

Considering the cost function; Q is related with the energy of the states, R is related with the energy of the controlled inputs. In LQR, one seeks a controller that minimizes both energies; however, decreasing the energy of the states will require a large control signal and a small control signal will lead to large states deviation (Anderson [21]).

The choice for the matrices Q and R is given by the Bryron's rule; select Q and R diagonal with $\varepsilon > 0^+$:

$$Q_{ii} = \frac{1}{\text{Maximum acceptable value of } x_i^{\,2} + \varepsilon}, \quad i \in \{1,2,...,8\},$$

$$R_{jj} = \frac{1}{\text{Maximum acceptable value of } u_j^{\,2} + \varepsilon}, \quad j \in \{1,2,...,4\}.$$

In essence, the Bryson's rule scales the variables that appear in J, so that the weighting matrix is nondimensionalized, because the state and control vectors contain components of different units and magnitudes.

4.3. Performance of the Controller

In order to determine a performance criteria for the controller, the control effort is defined as follows;

$CE = \int_0^{t_f} \left(u(t) - u^*(t)\right)^2 \, dt$. u^* : trim inputs.

In order to determine the transient characteristics of the controller, power spectral density is inspected for the control deviations from the trim points, which tells about the frequency distribution of the control effort:

$$S(f) = \int_{-\infty}^{\infty} R(\tau) e^{-j2\pi f\tau} d\tau ,$$

where

$$R(\tau) = \lim_{T\to\infty} \frac{1}{T} \int_0^T \left(u(t) - u^*(t)\right)\left(u(t+\tau) - u^*(t+\tau)\right) dt$$

is the autocorrelation function.

CHAPTER 5

MODELING AND SIMULATION PROGRAMS

All of the programs are prepared in MATLAB 7.6.0 (R2008A), using GUIDE for the graphical user interface, standard MATLAB language, SIMULINK and Embedded MATLAB Editor for the control system simulations.

5.1. Airfoil Mapper

The main function of this program is to obtain and arrange the aerodynamical coefficients (C_l, C_d, C_m) for an airfoil type, and then construct appropriate tables for the other programs to use as look-up tables. The program has two modes; mapper and simulator. A screenshot of this program is given in Figure 32.

Before running the program, the aerodynamic coefficients for an airfoil type are obtained using XFOIL (Drela [15]), as shown in Figure 33, for the maximum range of applicable angles of attack and Reynolds numbers (i.e. $-30 \le AoA \le +30$, $0 \le \mathrm{Re} \le 2500000$). Airfoil's coordinates (geometry of the airfoil) and the results obtained with XFOIL simulations (Figure 34), are loaded into Airfoil Mapper program. Then, aerodynamical coefficients are interpolated for $\pm\pi$, with using the interpolation formulas for high angles of attack (Chapter 2.2.7). After the interpolation process, the data required for the simulation of the airfoil is stored.

In the simulation of the airfoil (Figure 35), the interpolated aerodynamical coefficients are used in order to ensure that no unidentified point is left in the angles of attack $-\pi < AoA \le +\pi$. Simulation uses the chord length and span as user-defined constants, in order to construct a wing of the same airfoil section type. When the translation velocity and pitch inputs are adjusted using the slidebars, the resulting inflow angle, angle of attack and Reynolds numbers are calculated.

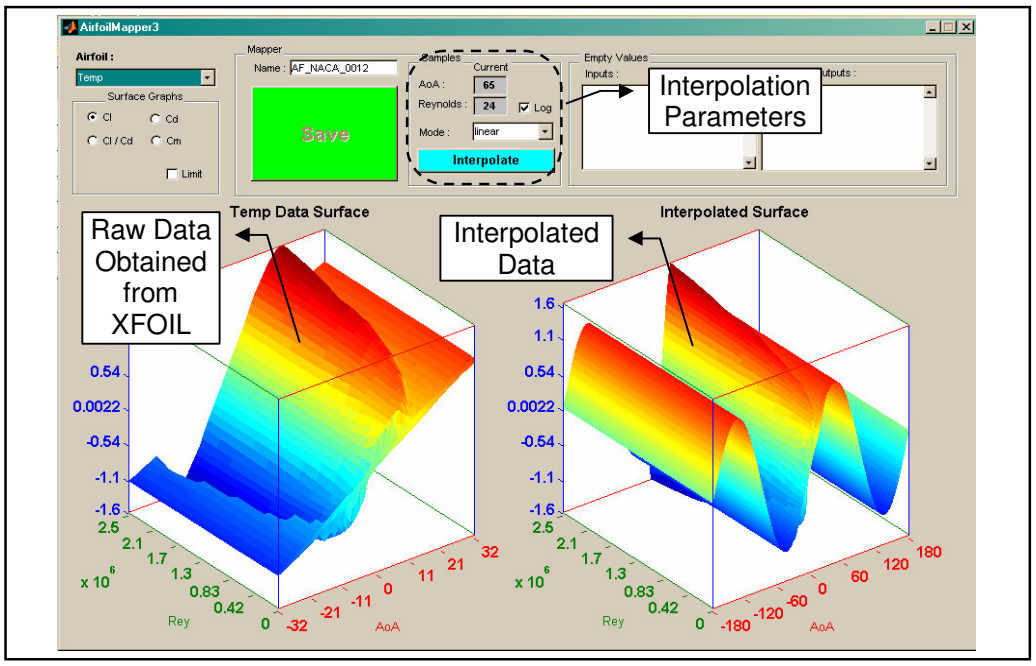

Figure 32. A screenshot of Airfoil Mapper program.

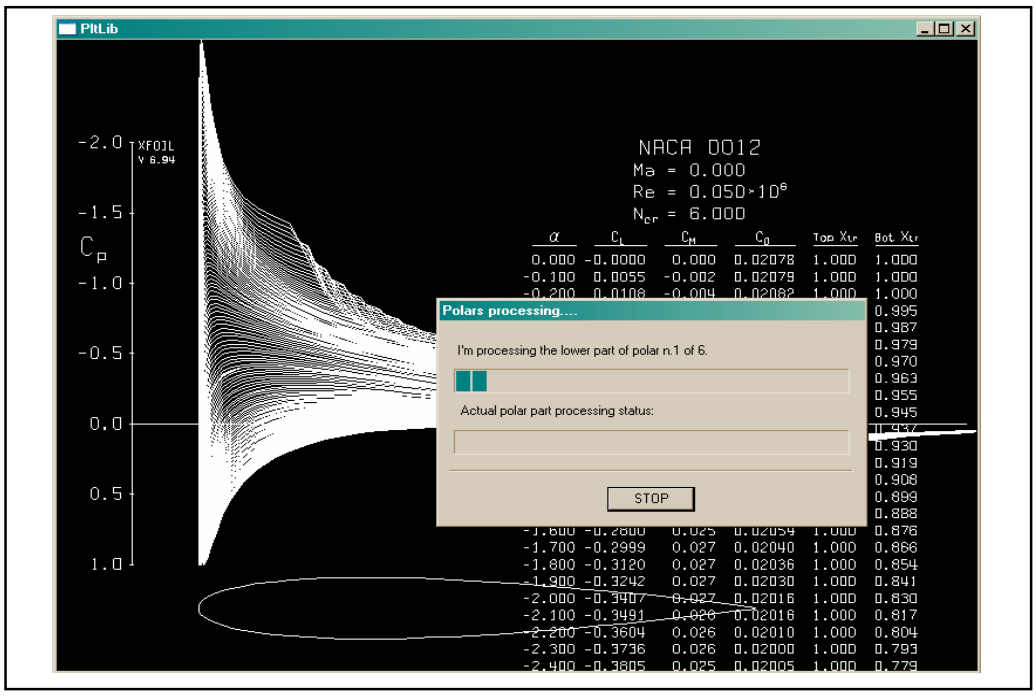

Figure 33. XFOIL simulation for NACA0012 airfoil.

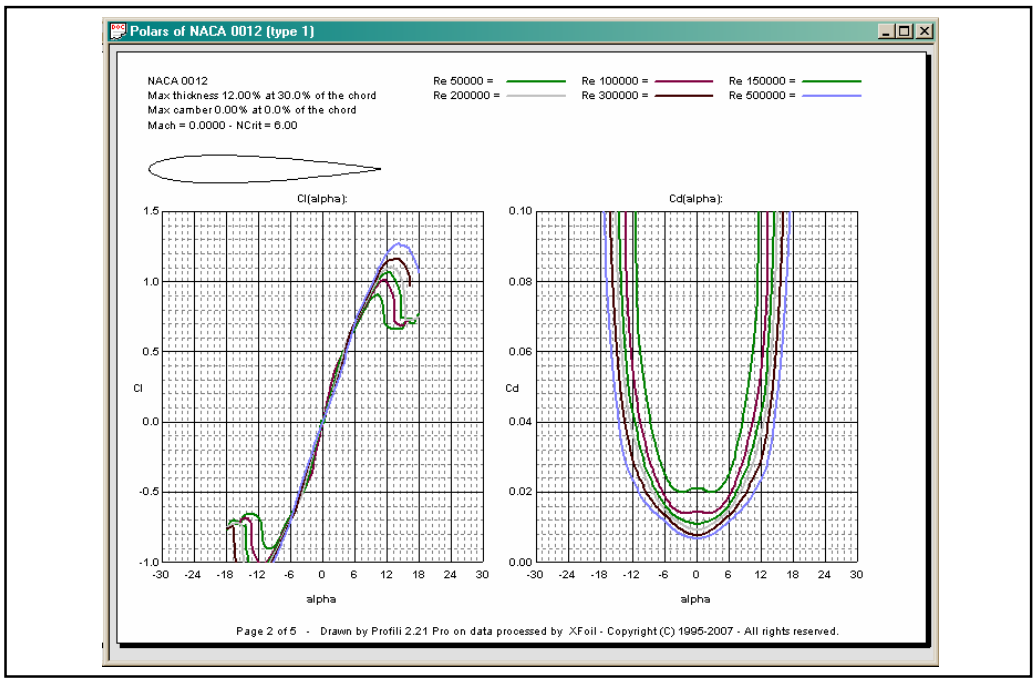

Figure 34. XFOIL simulation results for NACA0012 airfoil.

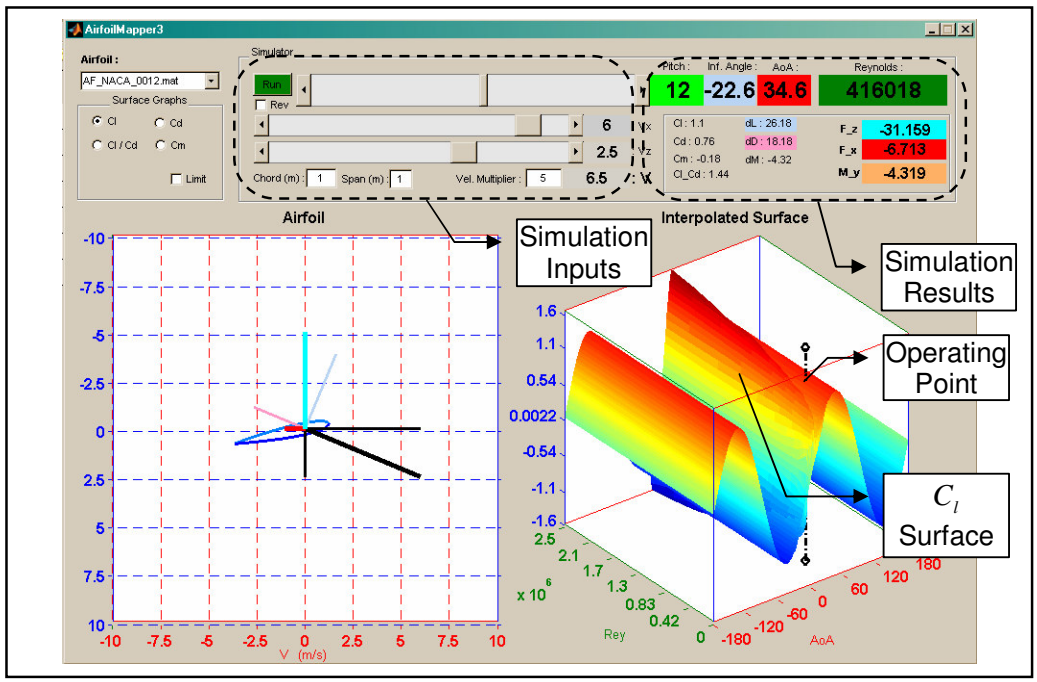

Figure 35. A screenshot of Airfoil Mapper program in simulation mode.

Using angles of attack and Reynolds numbers as the inputs of the look-up tables, the aerodynamical coefficients are obtained using *'2D-spline interpolation'* method. The resultant forces and moments are calculated as mentioned in Chapter 2.2.7.

5.2. Component Designer

The main function of this program is to construct the data for the component models (fuselage, wing propeller) individually, that constitute full UAV model when combined in Chapter 5.3. Component Designer program, with its user-friendly graphical user interface, eases modeling and gives the user the opportunity of analyzing different models and compare the changes in the performance of existing models when a modification is applied. The screenshot of this program is given in Figure 36.

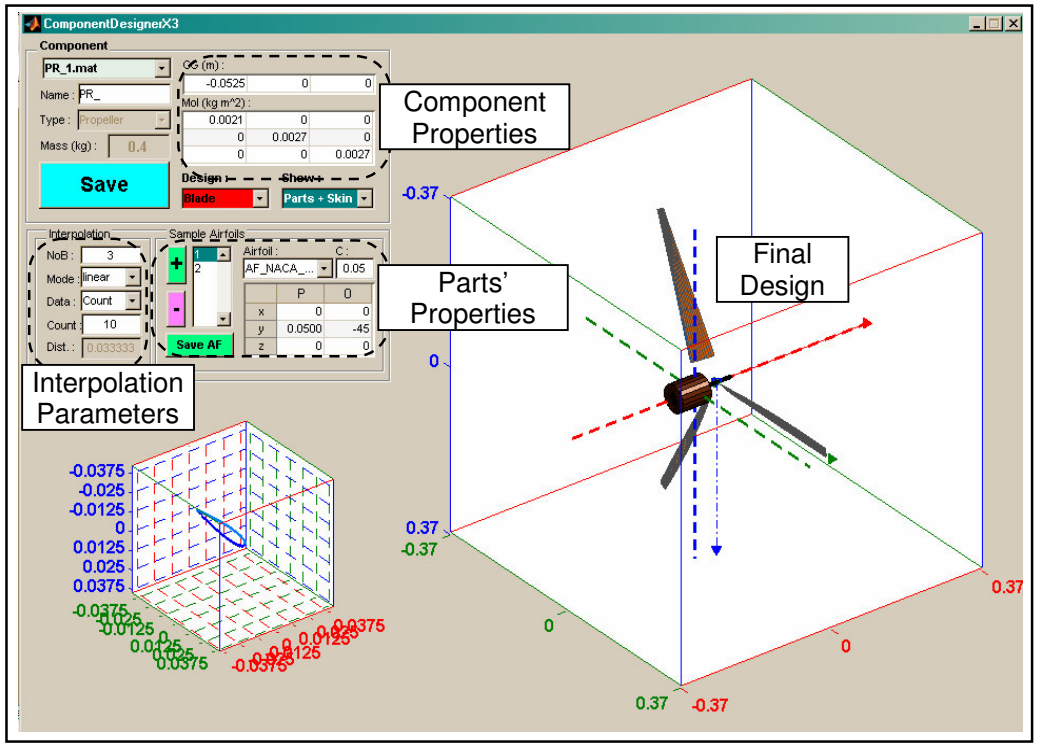

Figure 36. A screenshot of the Component Designer program.

The mass, center of gravity and moment of inertia of the components are computed according other parts' physical properties automatically. The moment of inertia of

the parts are calculated utilizing the standard prism, full cylinder, plate, and rod moment of inertia formulas. The effect of displacements of parts from c.g. of the component are taken into account using parallel axis theorem,

$$I_{displaced} = I_{center} + m\left[(R \cdot R)E_3 - R \otimes R\right].$$

The orientations of the parts according to component frame are considered using angular momentum of a rigid body,

$$^{A}H = {}^{A}I\,{}^{A}\omega,$$
$$^{B}H = {}^{B}I\,{}^{B}\omega,$$

$$\begin{aligned} {}^{B}H &= {}^{B}R_{A}\,{}^{A}H \\ &= {}^{B}R_{A}\,{}^{A}I\,{}^{A}\omega \\ &= {}^{B}R_{A}\,{}^{A}I\left[{}^{B}R_{A}^{-1}\,{}^{B}R_{A}\right]{}^{A}\omega \quad \Rightarrow \quad {}^{B}I = {}^{B}R_{A}\,{}^{A}I\,{}^{B}R_{A}^{-1}. \\ &= \left[{}^{B}R_{A}\,{}^{A}I\,{}^{B}R_{A}^{-1}\right]{}^{B}R_{A}\,{}^{A}\omega \\ &= {}^{B}I\,{}^{B}\omega \end{aligned}$$

The c.g. of the component is calculated using the distributions of positions and masses of the parts in 3-dimensions.

There are three main types of components that may be modeled in this program, with the following features;

- Fuselage: is the main component of an aircraft that holds all other components together. In addition to the fuselage cab, other parts like, battery, GPS antenna, avionic equipments, communication components may be added inside the fuselage as shown in Figure 37. For every part added to the component, the physical parameters, position, orientation, mass and part type must be determined.

- Wing: may be designed as main, horizontal or vertical tail wing, or different configurations like V-tail or canard, from the selected airfoil types. This versatility is obtained by entering the physical design parameters in the desired way. A wing is symmetrical in the x-z plane of the design axis. For one side of the wing, airfoil types are selected,

positioned and oriented at the desired geometry. Then interpolation technique is used to determine the airfoil samples between the entered ones. A sample of wing modeling is shown in Figure 38, with airfoils, airfoil axes and the final model.

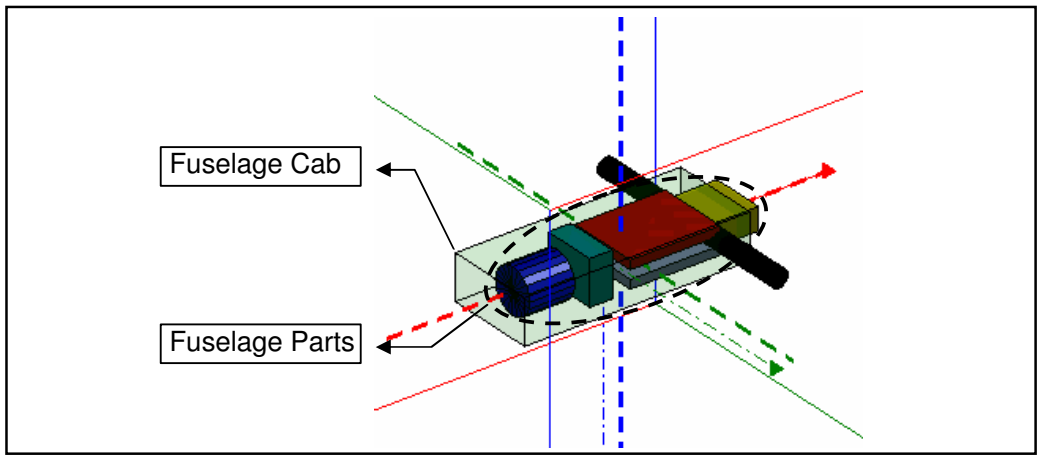

Figure 37. Fuselage design.

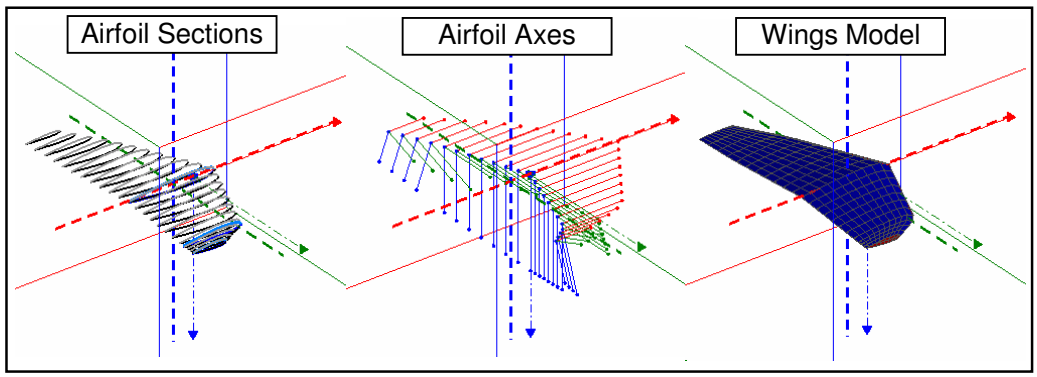

Figure 38. Wing design.

- Propeller: has a powerplant (an electric motor modeled as a cylinder), a drive shaft (modeled as a rod) connecting powerplant to the propeller and a number of propeller blades. Blades are modeled like wings, but the difference is that a blade is duplicated according to the number of blades

in the propeller around x-axis of design frame. A sample of propeller modeling is shown in Figure 39.

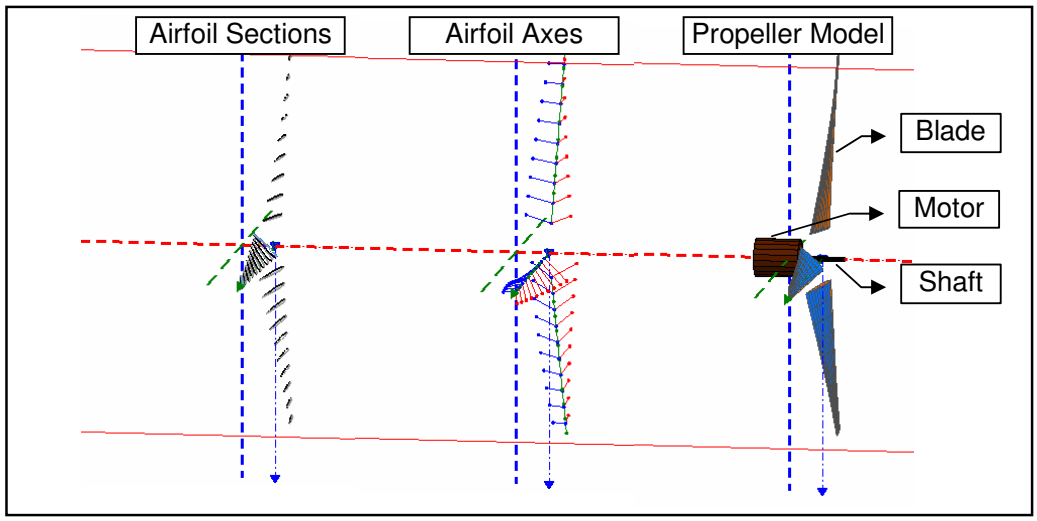

Figure 39. Propeller design.

5.3. UAV Designer

The main functions of this program (Figure 40) are to;

- Construct the data for a UAV model with the combination of components (wing, fuselage and propeller), and their properties,
- Run case simulations for given state and control inputs, resulting in the forces and moments,
- Calculate trim points for given navigation inputs, obtaining trim states and trim inputs,
- Linearize the UAV model at the trim point, resulting in state-space model and obtain eigenvalues,
- Calculate trim points and linearized models for a range of navigation inputs, forming look-up tables for the control simulations,
- Output the linearized model's look-up tables with graphs for observation.

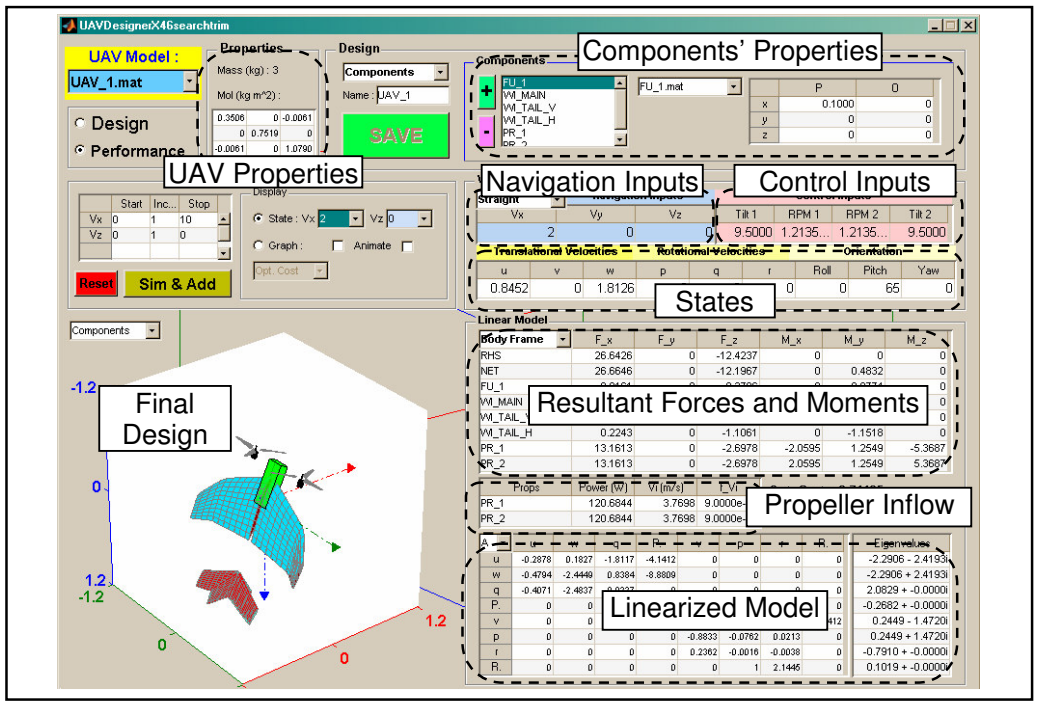

Figure 40. A screenshot of the UAV Designer program.

In order to obtain the model of Tiltrotor UAV, the components designed in Component Designer program are placed at the desired positions and orientations. The combination of these components gives the resultant mass and center of gravity and moment of inertia of the UAV, using the same principles as in Chapter 5.2.

Case simulations are run according to input states and control inputs using the algorithms stated in Chapter 2, resulting in the forces and moments of the components and the net forces and moments acting on the Tiltrotor UAV. In order to increase the computation speed, all of the component's airfoils are formed as an array, containing their positions and orientations according to c.g. as shown in Figure 41, and then airfoil model is used to compute the forces and moments of each airfoil section. After that, all forces and moments are combined in the c.g. of the aircraft. The trim point is calculated with the algorithm stated in Chapter 3.1. Linearization is performed according to Chapter 3.2., using small perturbation theory around the trim point.

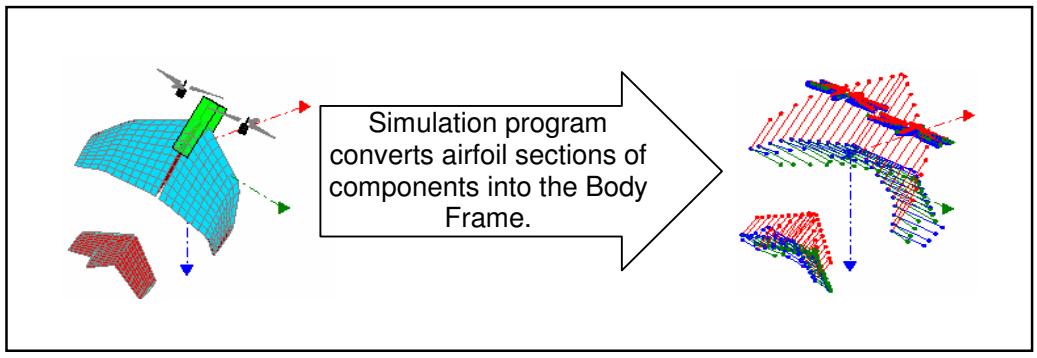

Figure 41. Airfoil sections in the Tiltrotor UAV.

When we run the program for trim point and linearization calculations for a range of navigation inputs, the look-up tables of trim states, trim inputs, power required and state-space models are obtained and graphed for inspection as shown in Figure 42.

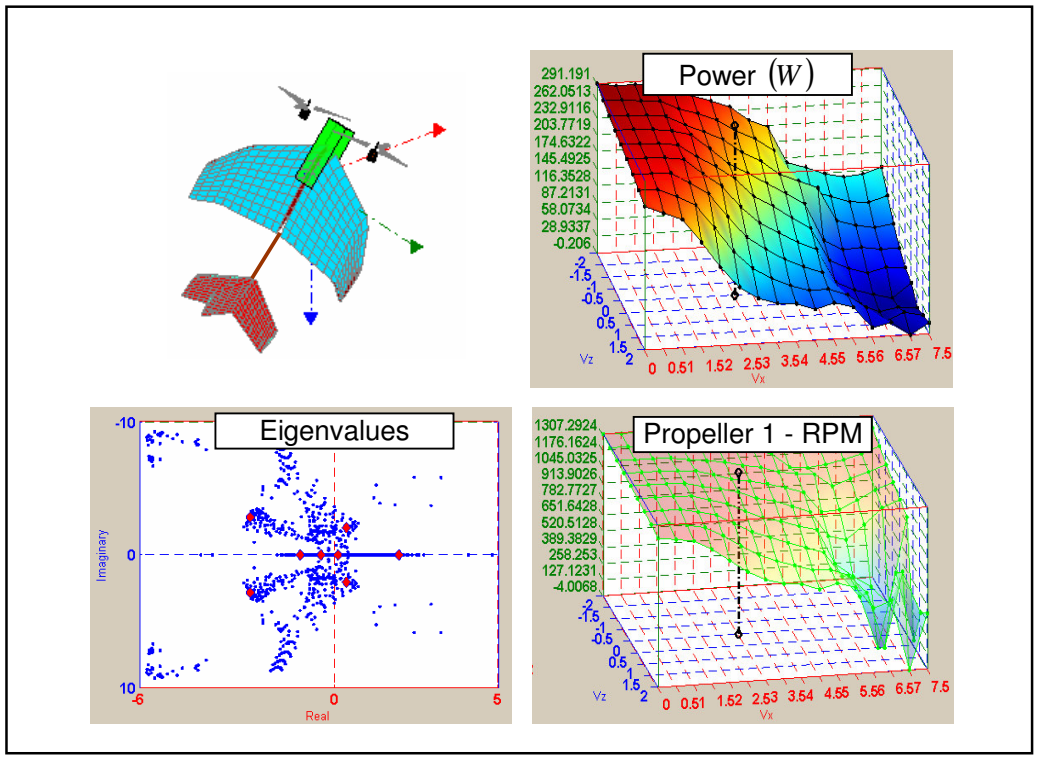

Figure 42. Tiltrotor UAV, trimmed and linearized for a range of navigation states.

5.4. LQR Control

The main objective of this program (Figure 43) is to calculate the gains of the full-state controller and to run simulations in order to follow command inputs in the vehicle-carried frame. The gains of the controller for the trim points are calculated, using the algorithm stated in Chapter 4.2. Algebraic Riccati equation formed in this algorithm is solved by using standard Matlab functions. When the linear controllers are computed, a Simulink model (Figure 44) is called from this program, with predetermined time dependent disturbances acting directly on the states, and navigation commands, which constitutes the initial navigation state and next navigation state to be reached. Simulation outputs the state and control variables in graphs for observation as shown in Figure 43.

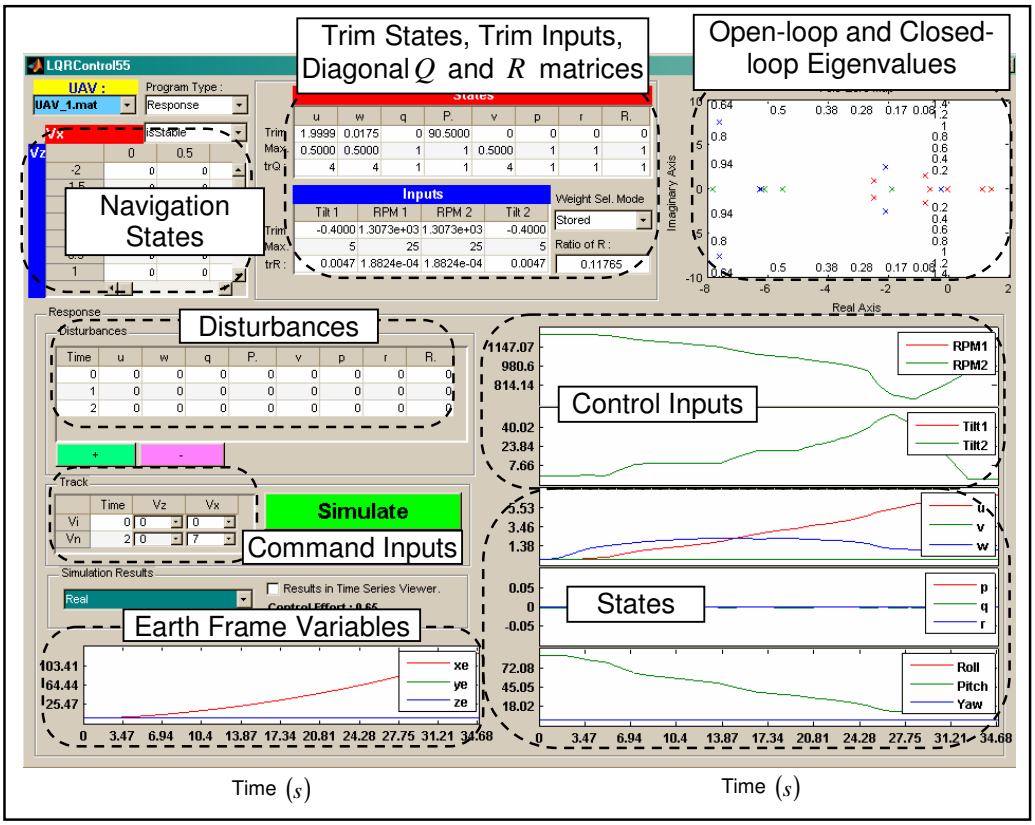

Figure 43. A screenshot of the LQR Control program.

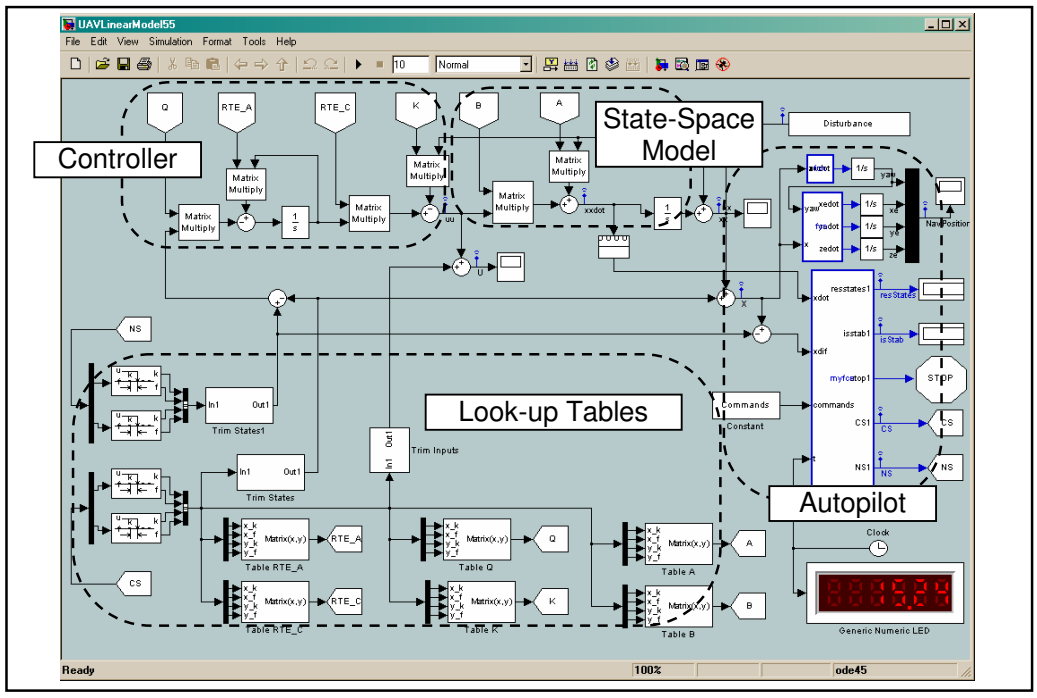

Figure 44. SIMULINK model for LQR Control of Tiltrotor UAV.

Before running the simulation, LQR Control program sets all of the aircraft's related informations (trim states, trim inputs, linearized state-space models, controller parameters) as look-up tables for the Simulink model. Simulation model starts simulation with setting the initial condition of Tiltrotor UAV. Then the controller switches to tracking mode and sets the current navigation state incrementally in order to reach next navigation state. The controller monitors the changes in the states continuously, not knowing the time and magnitude of the disturbance. When there is a great change (which may be caused by a disturbance) in the states, the controller switches to regulator mode with setting the next navigation state to current navigation state, and stays in this mode until the deviations are minimized with the controls. When the next navigation state is reached, the simulation stops autonomously. Simulink model uses gain-scheduling in order to accomplish transitions between navigation states.

CHAPTER 6

RESULTS AND DISCUSSIONS

6.1. NACA 0012 Airfoil Simulation

A sample simulation is run for NACA0012 airfoil, at 12 degrees of pitch angle, with chord length and span length of 1 m. forming a wing, moving with velocity $V = [6 \quad 0 \quad 2.5]\, m/s$, results $F = [-31.2 \quad 0 \quad -6.7]\, N$ and $M = [0 \quad -4.3 \quad 0]\, Nm$. The operating point on the lift coefficient surface is shown with a black dotted line in Figure 45.

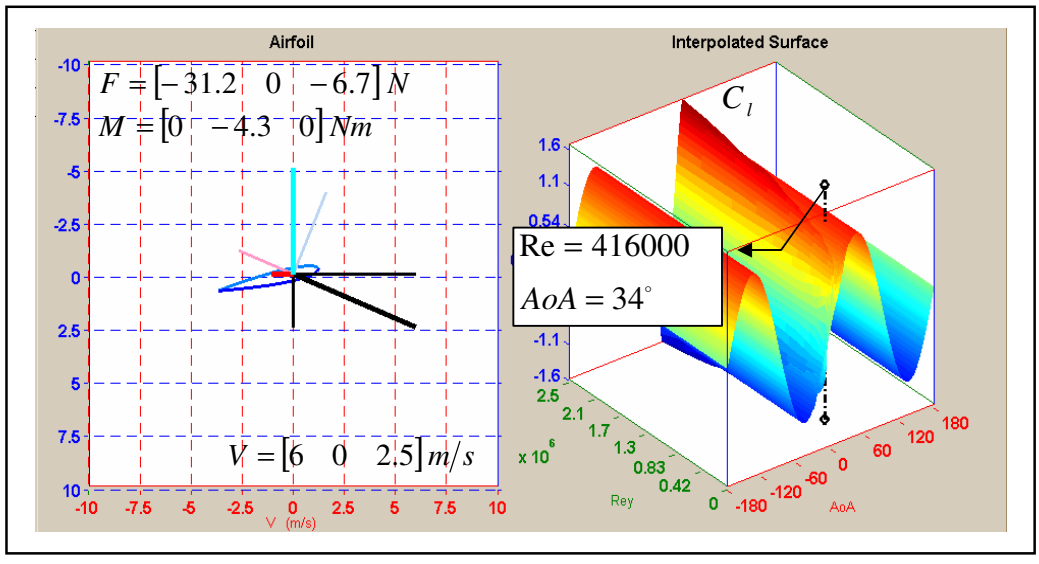

Figure 45. Simulation results for NACA0012 airfoil at 20° pitch.

The aerodynamical coefficient surfaces obtained (Figure 46) are compared to the data obtained by Sheldahl [16] and Cunningham [22], and similar trends of data are observed. If we consider the ratio of the lift coefficient to the drag coefficient as a performance criteria, it is clear that operating this airfoil for $|AoA| > 12^\circ$ and low Reynolds numbers is not efficient. When we look at the change of coefficients with Reynolds numbers, bigger numbers are desirable, forming a linear slope in the before-stall range, which are used as a linear coefficient slope in the simulation of large-scale helicopters and airplanes. But since we can not reach big velocities and Reynolds numbers in small-scale, the change of coefficients in this range forms a nonlinear trend. So, using look-up table method, as in this work, performs well in reflecting more realistic simulations.

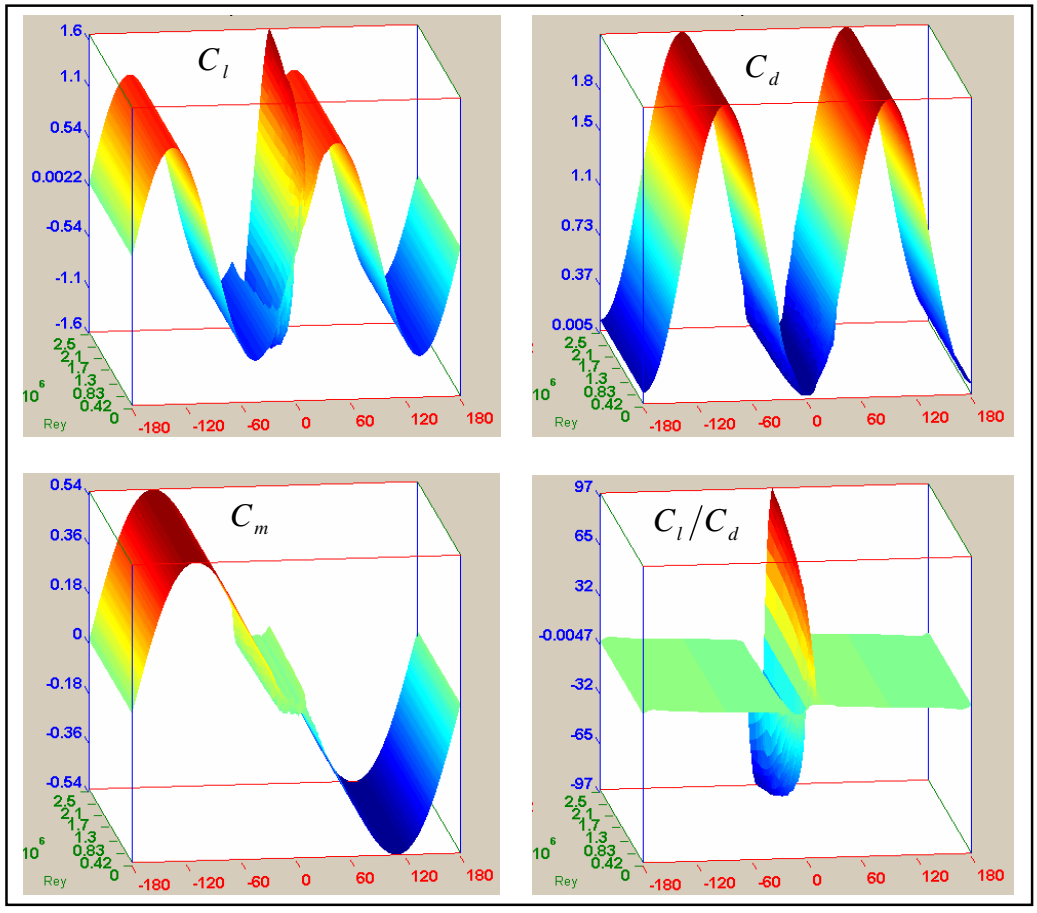

Figure 46. Aerodynamical coefficient surfaces of NACA0012 airfoil.

6.2. Tiltrotor UAV

Tiltrotor UAV model is constructed using Component Designer and UAV Designer programs with properties given in Chapter 2.2.3.2. Using the body frame, x-axis pointing forward from the center of gravity, forms a plane of symmetry with z-axis pointing downwards, providing that y-axis being normal to this plane with the right-hand rule. This symmetry forms the moment of inertia in the following form Philips [23]. Considering the moment of inertia calculated for Tiltrotor UAV, we see that the method used in the calculation gives parallel results to that of Philips [23],

$$ {}^{B}I = \begin{bmatrix} I_{xx} & 0 & -I_{xz} \\ 0 & I_{yy} & 0 \\ -I_{zx} & 0 & I_{zz} \end{bmatrix} = \begin{bmatrix} 0.3506 & 0 & -0.0061 \\ 0 & 0.7193 & 0 \\ -0.0061 & 0 & 1.0463 \end{bmatrix}. $$

6.3. Propeller Performance

Looking at the inflow characteristics of the propeller as shown in Figure 46, the results obtained are similar to that of Seddon [13], for small descent, hover and forward velocities. This shows that the momentum theory has been successfully applied in the propeller simulation. Although, momentum theory can not simulate higher descent velocities, this problem is eliminated with limiting the navigation state velocities.

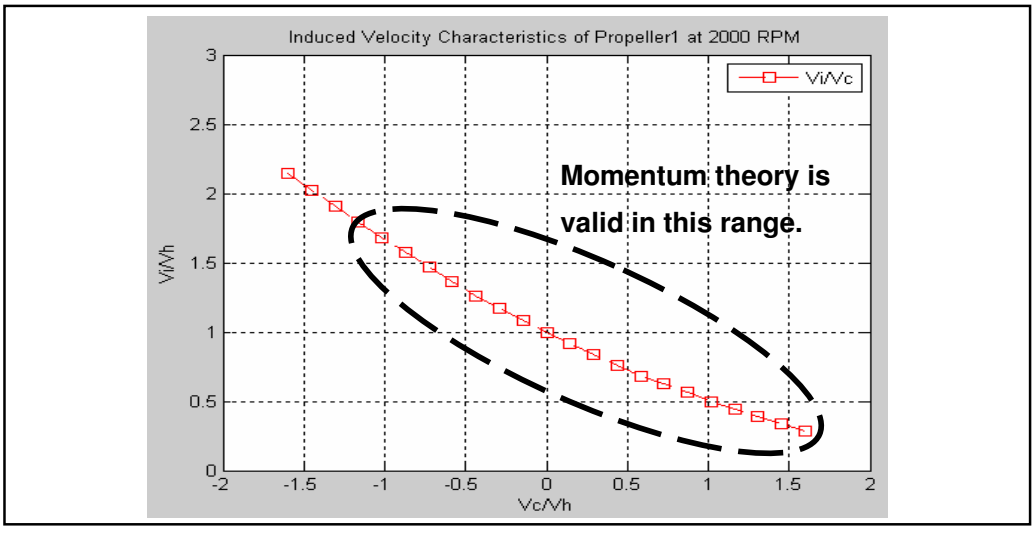

Figure 47. Inflow characteristics of Propeller 1 operating at 2000 RPM.

The propeller generates thrust and moment symmetrically, in the case of axial velocities along x-axis; for a non-axial velocity the forces and moments become dissymmetrical, due to the periodic motion of the operating points of airfoil sections on the aerodynamical coefficients' surfaces as shown in Figure 48. Although, this level of detail gives more realistic results, it makes calculation for the trim points more difficult.

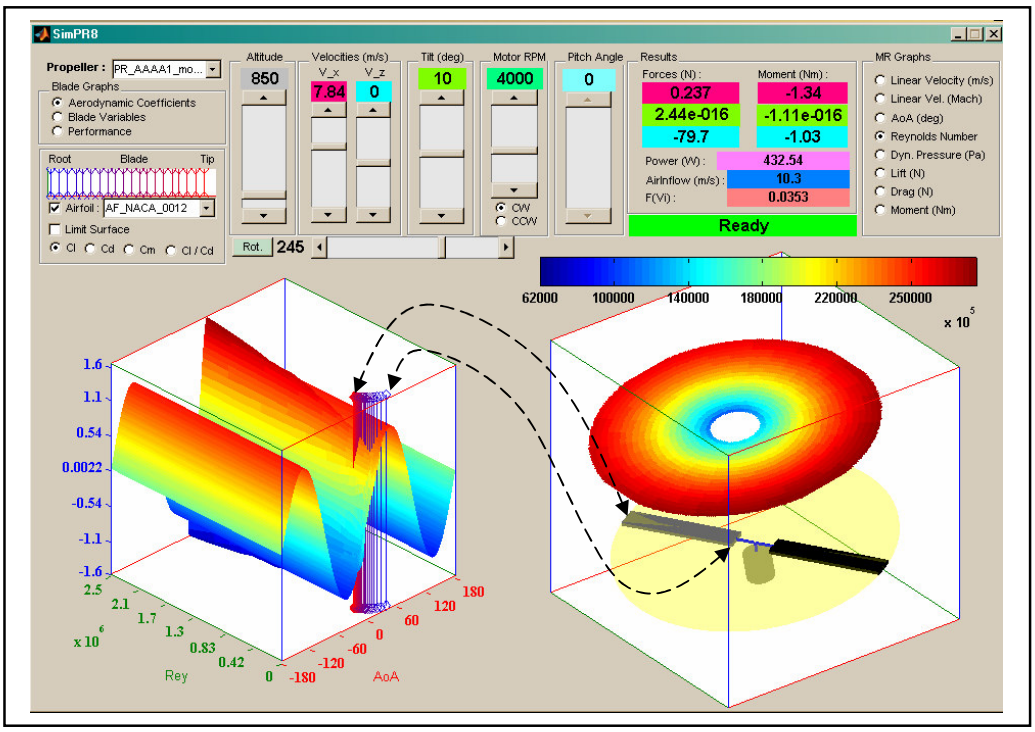

Figure 48. Non-axial motion of the propeller.

Thinking of the power requirements and thrust capacities of the Propeller 1, simulation results in Figure 49 show that, as RPM is increased then power and thrust increases. As the velocity in x-axis is increased, the power and thrust decreases. These characteristics, allow us to have enough thrust capacity for the overall flight envelope of Tiltrotor UAV.

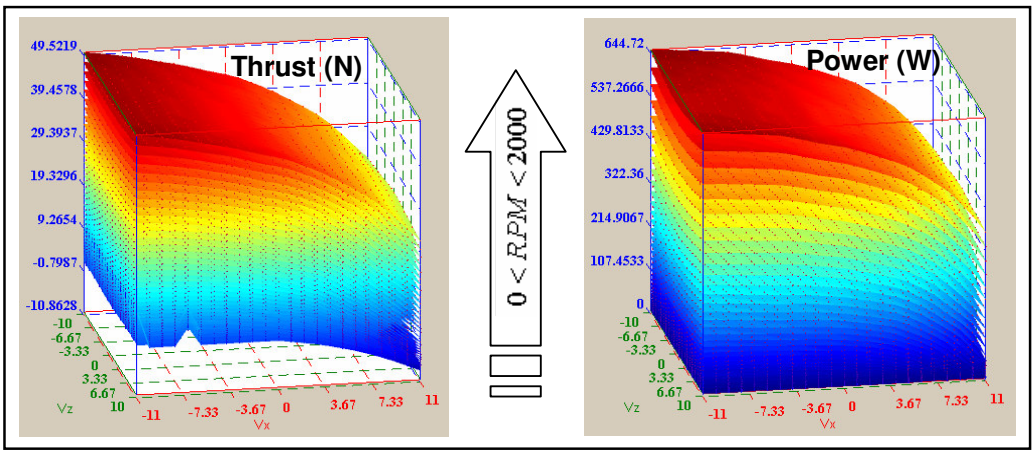

Figure 49. Power requirements and thrust capacities of Propeller 1.

If we consider the overall performance of the propeller, a performance plot is obtained using the same methods as previously performed by Merchant [6], whose results were obtained in wind tunnel tests for different model airplane propellers. Merchant [6] defined the following performance variables;

Advance Ratio: $\mu = \frac{V}{nD}$, $n = \frac{RPM}{60}$, $D =$ Prop. Dia. (m), ρ : Air density $\left(kg/m^3\right)$,

Thrust Coefficient: $C_T = \frac{T}{\rho n^2 D^4}$, T : Thrust (N),

Torque Coefficient: $C_M = \frac{M}{\rho n^2 D^5}$, M : Moment (Nm),

Power Coefficient: $C_P = \frac{P}{\rho n^3 D^5}$, P : Power (W),

Efficiency = $\mu \frac{C_T}{C_P}$.

Although a direct comparison is not possible, since the specifications (airfoil sections and their distributions) of the model propellers are proprietary informations of the manufacturer companies, a comparison may be performed with the Master Air Screw 16-8 (3-blade) whose data were obtained by Merchant [6] in wind tunnel experiments. Figure 50 shows that the trends of the data are consistent.

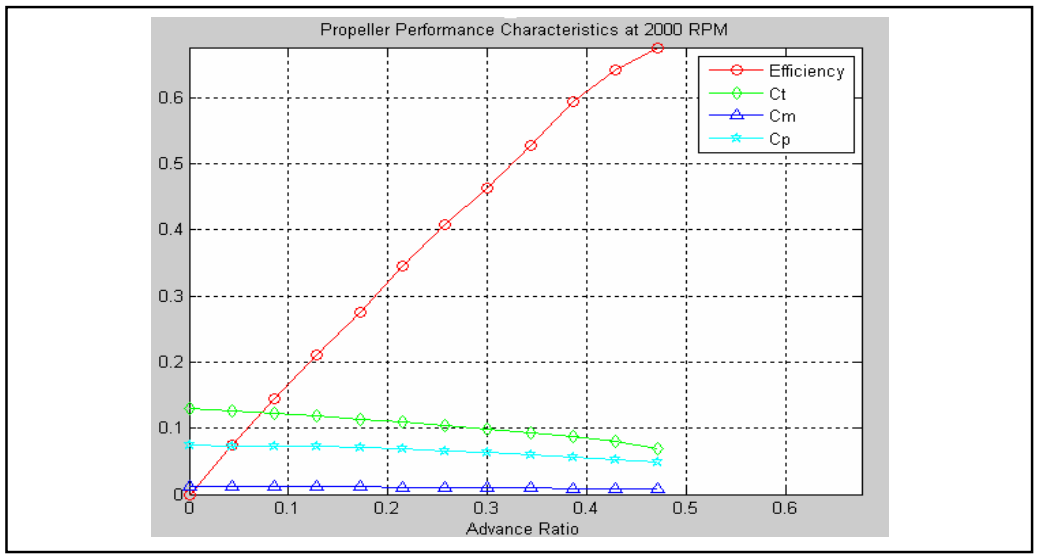

Figure 50. Propeller performance graph.

6.4. Trim Points

The trim points are calculated with the algorithm stated in Chapter 3.1. A sample of the trim point simulation results is given in Table 6.

Table 6. The trim point solution for $V = [7 \quad 0 \quad 0]\, m/s$.

States	u (m/s)	w (m/s)	q $(\deg/s)$	θ $(\deg)$	v (m/s)	p $(\deg/s)$	r $(\deg/s)$	ϕ $(\deg)$
	6.9152	1.0866	0	8.9297	0	0	0	0
Inputs	$\theta_1\,(\deg)$		$\Omega_1\,(RPM)$		$\Omega_2\,(RPM)$		$\theta_2\,(\deg)$	
	-1.3516		930.5000		930.5000		-1.3516	
Outputs	*Name*		${}^{B}F_x$ (N)	${}^{B}F_y$ (N)	${}^{B}F_y$ (N)	${}^{B}M_x$ (Nm)	${}^{B}M_y$ (Nm)	${}^{B}M_z$ (Nm)
	RHS		4.5630	0	-29.0406	0	0	0
	NET		4.5691	0	-29.0400	0	0	0
	Fuselage		-1.0789	0	-0.1332	0	0.0238	0
	Main Wing		3.9795	0	-30.1626	0	-2.0313	0
	Vertical Tail		-0.0778	0	0	0	0	0
	Horizontal Tail		-0.3970	0	1.8167	0	1.7429	0
	Propeller 1		1.0716	0	-0.2805	-0.2844	0.1325	-0.5627
	Propeller 2		1.0716	0	-0.2805	0.2844	0.1325	0.5627

A total number of 135 trim points are calculated for a map of the navigation states as $\dot{x}_e = 0.0, 0.5, 1.0, ..., 7.0, 7.5$ and $\dot{z}_e = -2.0, -1.5, -1.0, ..., 1.5, 2.0$. Considering the trim points calculated, as the forward velocity is increased in the vehicle-carried frame, the velocities in body frame change with u being increased, θ being decreased, w increasing initially in the conversion mode, and then decreasing gradually as getting closer the airplane mode as shown in Figure 50, and v, p, q, r, ϕ all being equal to 0. These trends show that, as we gain speed forward in the vehicle-carried frame, Tiltrotor UAV trim points guide the aircraft from helicopter mode to conversion mode, and when the cruise velocity is reached to the airplane mode, as expected.

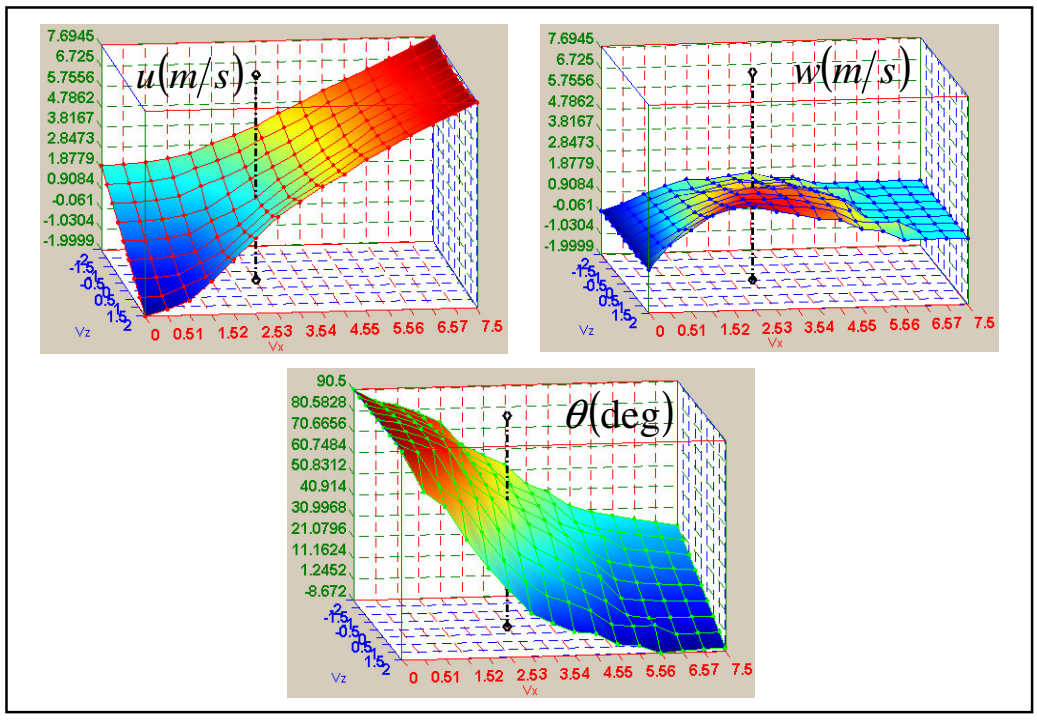

Figure 51. Trim state transitions.

Thinking of trim inputs, as Tiltrotor UAV enters airplane mode, the tilt inputs of the rotors make them perpendicular to the Earth surface as expected. As observed in Figure 52, RPMs get smaller together with power, this is just because, the lift source

being only propellers for hover, and main wings for the level flight. When the airplane mode is achieved, trying to reach higher speeds will make the inflow of the propellers get bigger, resulting that the propellers can not sustain the thrust for small RPMs, since blades are not pitch-controlled. This problem could be solved with the choice of a variable-pitch propeller, or just selecting more tilted propellers, with loosing some performance in hover. When the power requirements are examined, it is clear that Tiltrotor UAV would be needing much power in ascends and helicopter mode, and less power in descends and airplane mode as expected.

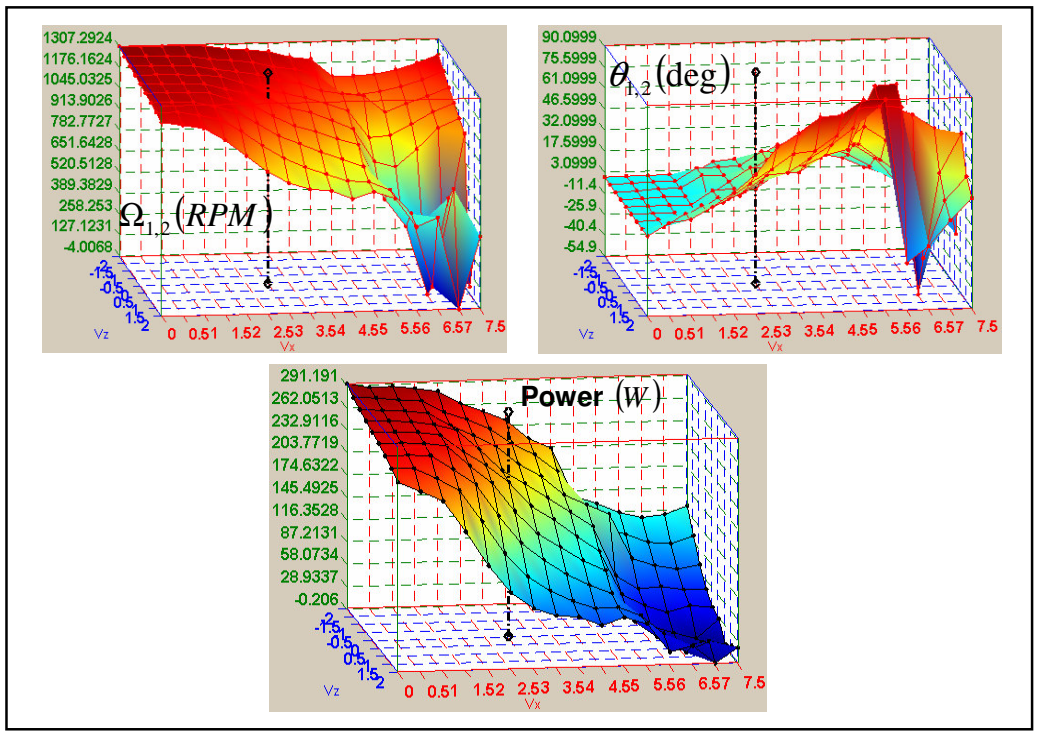

Figure 52. Trim input transitions.

6.5. State-Space Models

The linear models are obtained by linearizing Tiltrotor UAV model at the trim points, according to algorithm stated in Chapter 3.2. The state-space model for the trim point in Table 6. is given in the following equation. Although we see that, the longitudinal and lateral states are uncoupled, we can not say the same thing for the

control inputs, so the state-space models are handled as a whole, instead of separating them into longitudinal and lateral equations. The control inputs $\theta_1, \Omega_1, \Omega_2, \theta_2$ are not independent of each other, so one can not change them arbitrarily.

$$\dot{x} = \begin{bmatrix} -1.4571 & 2.6990 & -1.0686 & -9.6725 & 0 & 0 & 0 & 0 \\ -0.9746 & -10.4193 & 6.5791 & -1.5692 & 0 & 0 & 0 & 0 \\ 3.0435 & -17.4890 & -0.3278 & 0 & 0 & 0 & 0 & 0 \\ 0 & 0 & 1 & 0 & 0 & 0 & 0 & 0 \\ 0 & 0 & 0 & 0 & -3.2966 & 1.0736 & -6.6068 & 9.6725 \\ 0 & 0 & 0 & 0 & -3.4674 & -0.3167 & 0.0669 & 0 \\ 0 & 0 & 0 & 0 & 8.2477 & -0.0269 & -0.1555 & 0 \\ 0 & 0 & 0 & 0 & 0 & 1 & 0.1622 & 0 \end{bmatrix} x$$

$$+ \begin{bmatrix} 0.0053 & 0.0068 & 0.0068 & 0.0053 \\ -0.0214 & 0.0002 & 0.0002 & -.0.0214 \\ 0.0409 & -0.0003 & -0.0003 & 0.0409 \\ 0 & 0 & 0 & 0 \\ 0 & 0 & 0 & 0 \\ 0.0810 & -0.0041 & 0.0041 & 0.0810 \\ -0.0198 & -0.0080 & 0.0080 & -0.0198 \\ 0 & 0 & 0 & 0 \end{bmatrix} u, \quad \text{with roots:} \quad \lambda = \begin{bmatrix} -5.6641 - 9.4754i \\ -5.6641 + 9.4754i \\ -0.7179 - 1.7200i \\ -0.7179 + 1.7200i \\ -1.6318 - 7.7562i \\ -1.6318 + 7.7562i \\ -0.7681 \\ 0.0939 \end{bmatrix}$$

6.6. Stability

Considering the stability of the Tiltrotor UAV, for all of the trim points calculated, the aircraft is not BIBO stable, nor stable in the sense of Lyapunov, nor asymptotically stable. Tiltrotor UAV has poor stability as an overall flight envelope criticisms, as shown in Figure 53. Hovering is unstable, as the aircraft gains speed in the conversion mode it becomes even more unstable, but as the speed increases more, letting the wings do work, it becomes more stable entering airplane mode. Thinking of level flight, increasing forward speed makes it more stable to some point, and after that point the stability decreases. The selection of the most stable trim point as the cruise speed, would be a wise choice. In our case, the cruise speed is determined as $V = [7 \quad 0 \quad 0] m/s$.

Comparing the placements of the eigenvalues with the results obtained by Kleinhesselink [4], for the XV-15 and Generic Tiltrotor Simulation model (GTRS),

Tiltrotor UAV has similar pole placements in helicopter and airplane modes, also faster, due to small weight and smaller moment of inertia. For the conversion mode, Tiltrotor UAV is very unstable compared to the XV-15, this difference comes from the structural properties and the method of conversion. The XV-15 keeps its fuselage always parallel to Earth frame, and achieves conversion by only tilting the rotors. But Tiltrotor UAV uses its big main wings and the resulting moment to accomplish conversion, which makes it very unstable, where tiltrotors are only used for balance.

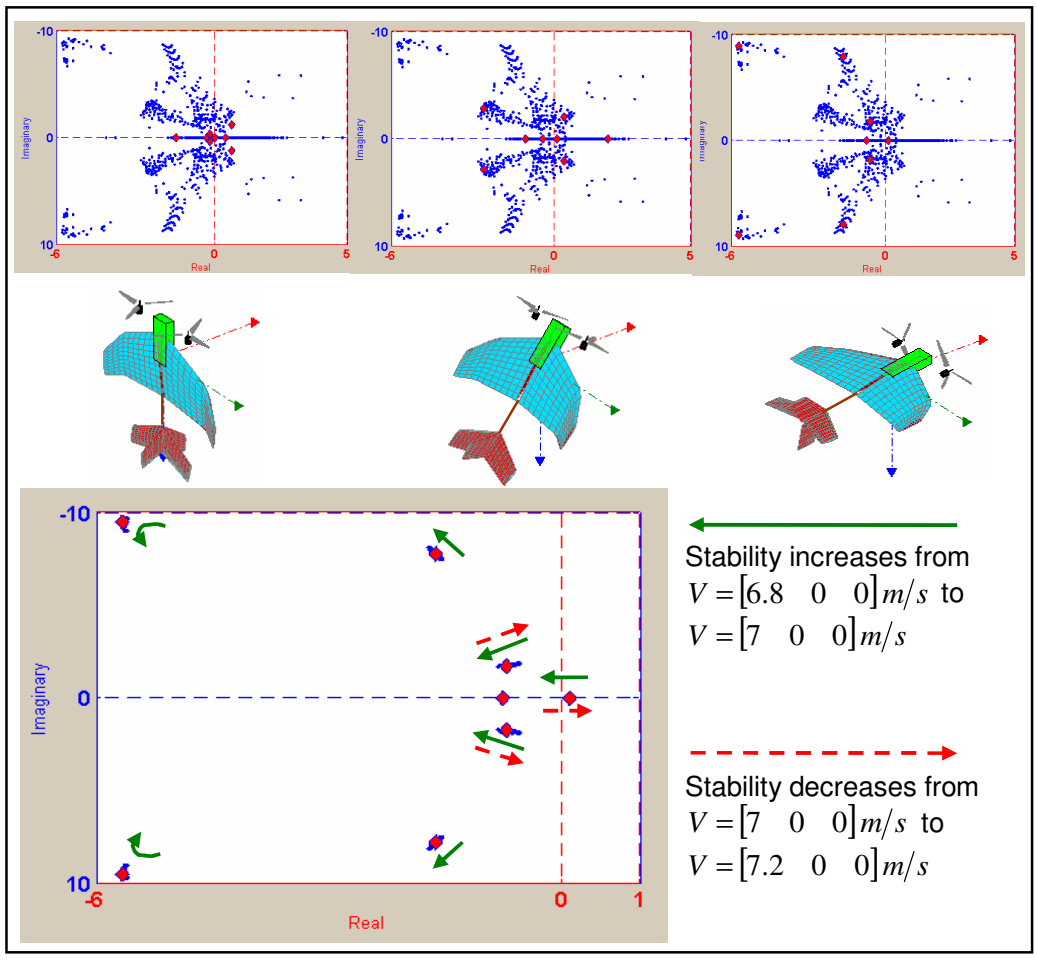

Figure 53. Changes in the stability of Tiltrotor UAV in different modes.

The eigenvalue trajectories of Tiltrotor UAV starting from helicopter mode, and converting to airplane mode, is given in Figure 54.

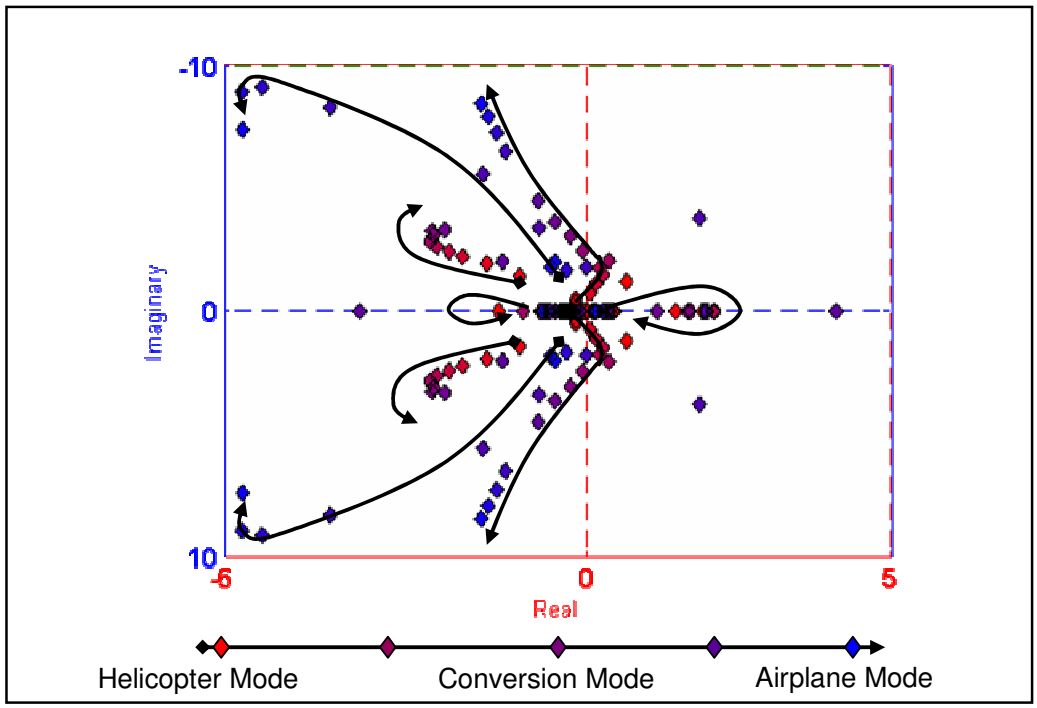

Figure 54. Eigenvalue trajectories from Helicopter to Airplane Mode.

6.7. Flight Simulations

A navigation system is not implemented in LQR Control simulation program, but using the method of changing next navigation state continuously and monitoring the current state with appropriate navigation algorithms, it may be applied in a way to reach the navigation purposes. The controller only controls the aerodynamical state variables, where yaw angle can be controlled with an outer-loop navigation controller, since roll and yaw is coupled when pitch is fixed. Although, command filtering needs to be employed in order to guarantee that the actuators follow the control inputs, it is not used in this simulation in order to see the ideal case.

Before the control system design, the linearized models are inspected using the concepts, controllability and observability. It is observed that all navigation states

are controllable, and observable since full-state feedback is used in a way that we can measure the states perfectly. Also, the necessary conditions, stated in Chapter 4.1, for being able to use LQR method are inspected, which are found to be applicable.

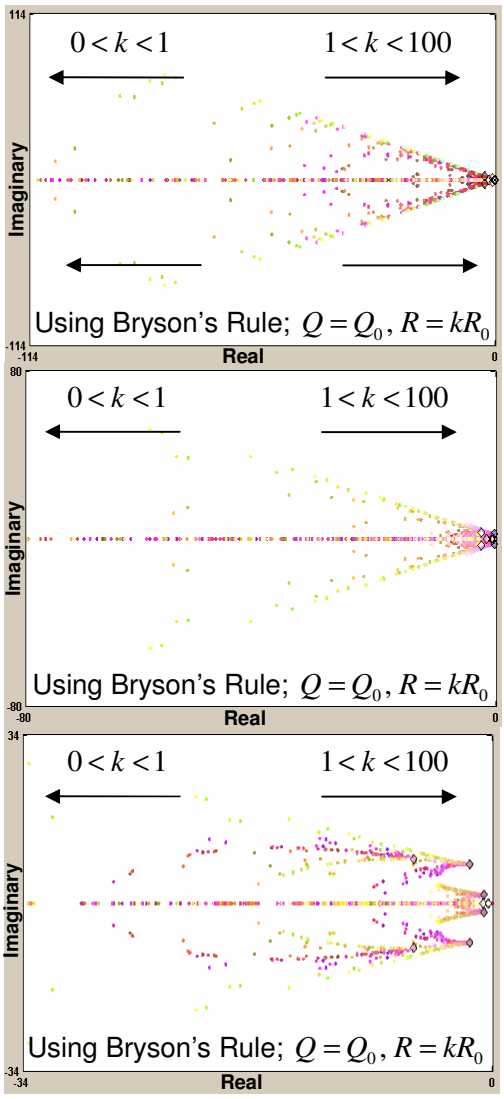

Helicopter Mode ${}^{V}V = [0 \quad 0 \quad 0] m/s$

$k = 1,$

$$K = \begin{bmatrix} -5.6983e04 & +0.0127 & +0.0127 & -5.6983e04 \\ -0.1646 & -4.2329e05 & -4.2329e05 & -0.1646 \\ +8.9590 & -5.3941e05 & -5.3941e05 & +8.9590 \\ +13.8118 & +3.7604e04 & +3.7604e04 & +13.8118 \\ +0.6325 & -0.6337 & +0.6337 & -0.6325 \\ -0.5852 & -0.3410 & +0.3410 & +0.5852 \\ +127.2927 & -88.8010 & +88.8010 & -127.2927 \\ -0.6026 & +0.3785 & -0.3785 & +0.6026 \end{bmatrix}$$

Conversion Mode ${}^{V}V = [3.5 \quad 0 \quad 0] m/s$

$k = 1,$

$$K = \begin{bmatrix} -1.9495 & -0.0713 & -0.0713 & -1.9495 \\ -7.7773 & -0.3162 & -0.3162 & -7.7773 \\ +11.4659 & +0.4629 & +0.4629 & +11.4659 \\ +36.7200 & +1.4912 & +1.4912 & +36.7200 \\ +0.1431 & +0.0125 & -0.0125 & -0.1431 \\ -3.3932 & -0.3060 & +0.3060 & +3.3932 \\ -2.3429 & -0.2691 & +0.2691 & +2.3429 \\ -3.0665 & -0.2160 & +0.2160 & +3.0665 \end{bmatrix}$$

Airplane Mode ${}^{V}V = [7 \quad 0 \quad 0] m/s$

$k = 1,$

$$K = \begin{bmatrix} +0.0081 & +0.0033 & +0.0033 & +0.0081 \\ -0.0163 & -2.9357e04 & -2.9357e04 & -0.0163 \\ +0.0140 & +2.9330e04 & +2.9330e04 & +0.0140 \\ +0.0812 & +9.4552e04 & +9.4552e04 & +0.0812 \\ +0.0011 & -4.0358e04 & +4.0358e04 & -0.0011 \\ -2.0737 & -0.1741 & +0.1741 & +2.0737 \\ -0.8332 & -0.0719 & +0.0719 & +0.8332 \\ -1.0255 & -0.0841 & +0.0841 & +1.0255 \end{bmatrix}$$

Figure 55. The movement of closed-loop pole locations according to LQR weights.

The movement of the roots of the closed-loop system is observed in Figure 54, with changing the weighting ratios of the Q and R matrices of the LQR method. The result of this inspection is that the main contributor to the placement of the closed loop poles is the ratio between Q and R matrices, as the weights of the Q matrix get bigger compared to the weights of R matrix, the poles tend to move to more negative region, making the system more stable. The ratios changing within Q and R matrices just change the location of eigenvalues relative to each other, making the related state variable more stable. Although this method directs us to make the system more stable, it has a serious drawback; which is as we increase the weights of states compared to inputs, the norm of the feedback matrix K gets bigger and bigger, resulting in very fast and large control deviations in the presence of small state disturbances, which sets us off the track from applicability. When we inspect the case of unit Q and R matrices, while changing the aircraft's modes, studying the trends in the K matrix (Figure 55);

- For the helicopter mode, the biggest values indicate that the controller strives to maintain $r\,(\deg/s)$, yaw rate, in order to keep the propellers parallel to the Earth surface.

- For the conversion mode, the biggest values indicate that the controller tries control $q\,(\deg/s), \theta\,(\deg)$ pitch rate and pitch heavily, meaning that the conversion is accomplished with strictly controlling these state variables.

- For the airplane mode, all feedback gains are smaller compared to the other modes, because of the reduced unstability of the natural system.

Applying Bryson's rule as the method for the selection of LQR weights, allowing more deviations in the control inputs, in order to control states more strictly, the selected matrices are obtained using maximum allowable deviations,

$$X_{\text{maxdev}} = [0.5 \quad 0.5 \quad 1 \quad 1 \quad 0.5 \quad 1 \quad 1 \quad 1],\ U_{\text{maxdev}} = [5 \quad 25 \quad 25 \quad 5],$$

$$Q=\begin{bmatrix} 4 & 0 & 0 & 0 & 0 & 0 & 0 & 0 \\ 0 & 4 & 0 & 0 & 0 & 0 & 0 & 0 \\ 0 & 0 & 1 & 0 & 0 & 0 & 0 & 0 \\ 0 & 0 & 0 & 1 & 0 & 0 & 0 & 0 \\ 0 & 0 & 0 & 0 & 4 & 0 & 0 & 0 \\ 0 & 0 & 0 & 0 & 0 & 1 & 0 & 0 \\ 0 & 0 & 0 & 0 & 0 & 0 & 1 & 0 \\ 0 & 0 & 0 & 0 & 0 & 0 & 0 & 1 \end{bmatrix}, \quad \text{and} \quad R=\begin{bmatrix} 0.04 & 0 & 0 & 0 \\ 0 & 0.0016 & 0 & 0 \\ 0 & 0 & 0.0016 & 0 \\ 0 & 0 & 0 & 0.04 \end{bmatrix}.$$

Full-state feedback matrices, and system's closed-loop eigenvalues are calculated using these weights (Figure 56). As seen from the graphs, Tiltrotor UAV is unstable in helicopter mode, becomes more unstable in conversion, and gains stability in the airplane mode. Looking at the closed-loop eigenvalues, we see that the closed-loop system is stable in all modes. Inspection of control inputs' power spectral density gives us the idea of how fast the controller must be assuming that actuators follow the commands perfectly. It is expected that, the controller will be fastest in the conversion mode, due to aircraft's high unstability. As a general deduction, controller speed is the trade-off for making the unstable system stable; when the system is more unstable, faster controls are required.

Running the simulation model with initial navigation state ${}^{V}V_i=\begin{bmatrix}0 & 0 & 0\end{bmatrix}m/s$ (helicopter mode) and next navigation state ${}^{V}V_n=\begin{bmatrix}7 & 0 & 0\end{bmatrix}m/s$ (airplane mode), we expect that, the control and state deviations should follow the trim points, as shown in Chapter 6.4. The control and state deviations obtained from the simulation are plotted in Figure 57, power spectral density of input deviations are plotted in Figure 58. The graphs tell that conversion from helicopter to airplane mode is accomplished within 33 seconds of time and 120 meters of displacement in x-axis of Earth frame, with a total control effort of 0.65, following the trim points as expected. The biggest control effort is spent at times $t=7s$ and $t=26s$. Considering the velocity at those times in vehicle-carried frame, ${}^{V}V(7)=\begin{bmatrix}2 & 0 & 0\end{bmatrix}m/s$, ${}^{V}V(26)=\begin{bmatrix}5 & 0 & 0\end{bmatrix}m/s$. Looking at Figure 55., we see that the open-loop system was most unstable in these velocities, which explains the increase in the control effort.

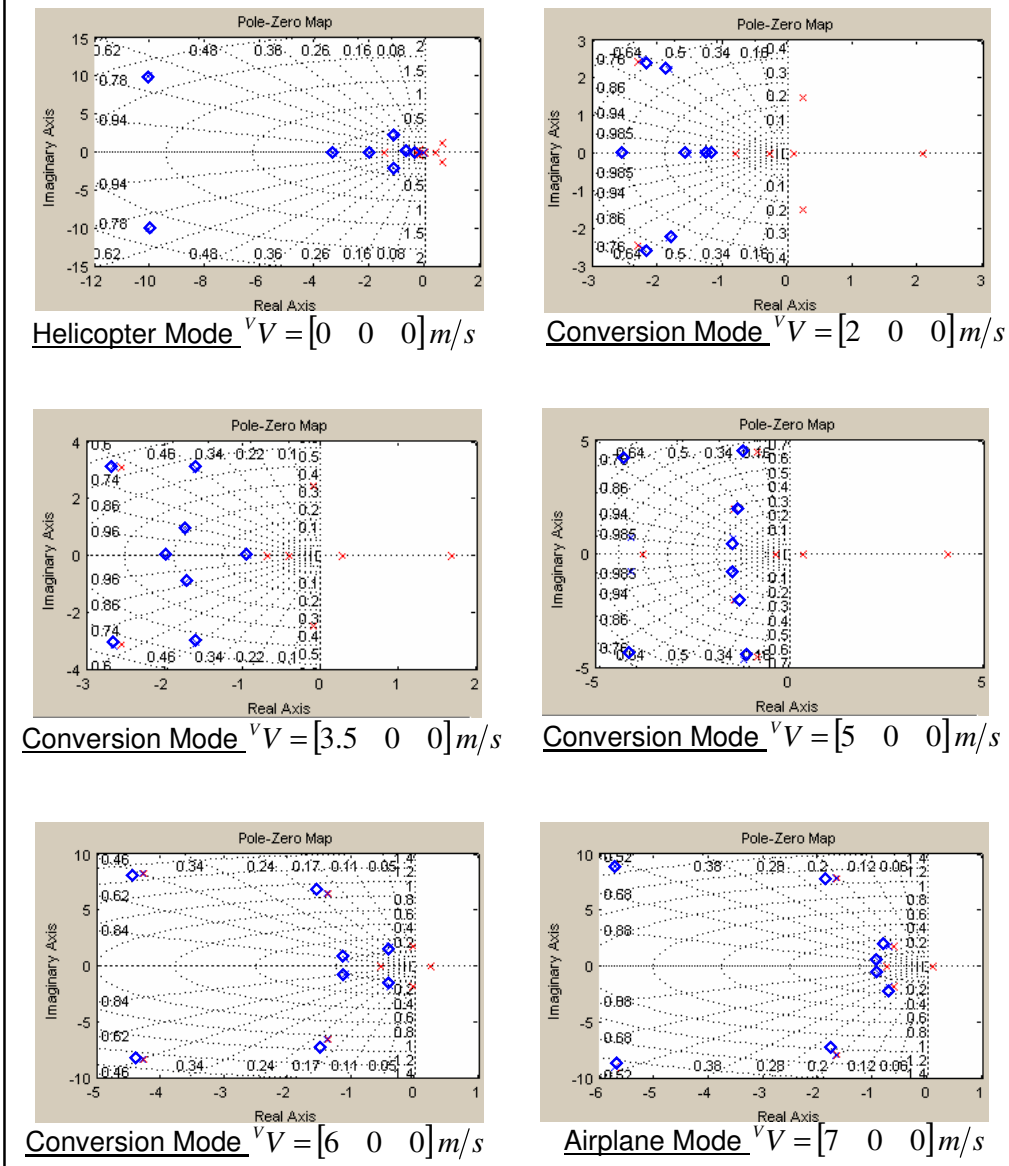

Figure 56. Tiltrotor UAV's open-loop and closed-loop eigenvalues.

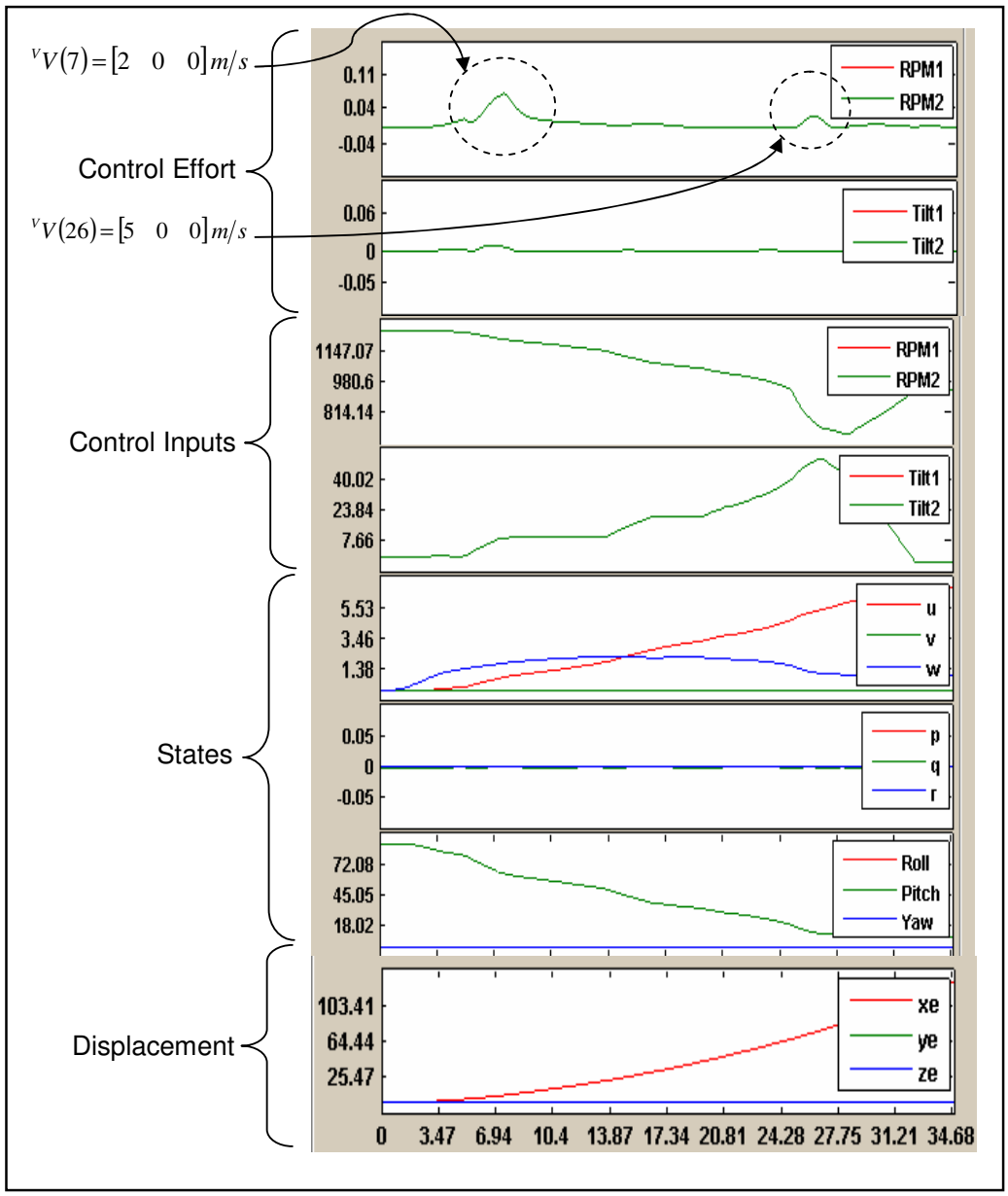

Figure 57. Simulation results for conversion from Helicopter to Airplane Mode.

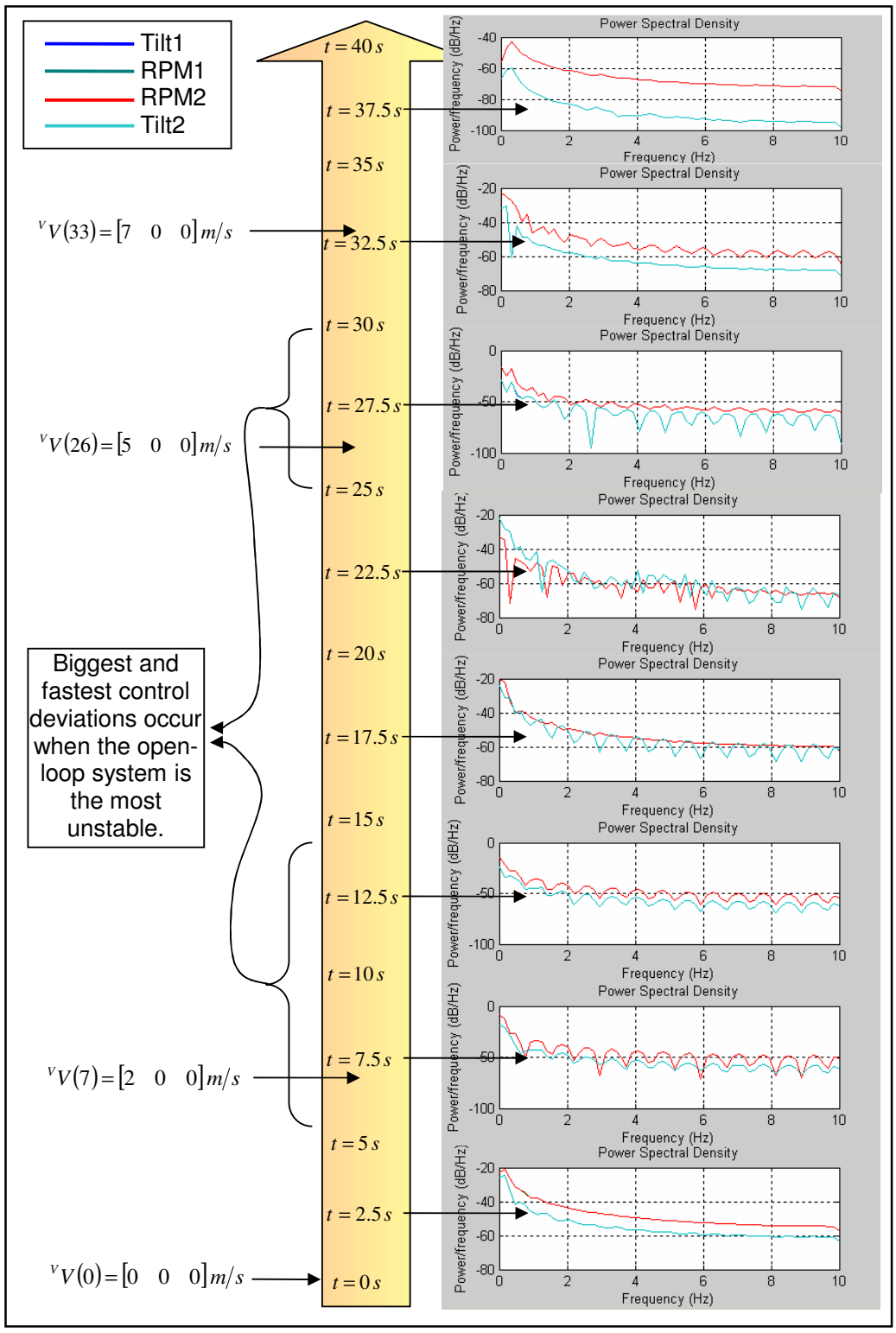

Figure 58. PSD of the inputs for conversion from Helicopter to Airplane Mode.

The power spectral densities for control deviations are calculated for consecutive intervals of $5s$. As seen in Figure 59, control deviations are bigger and faster for navigation states ${}^{V}V(7)=[2 \quad 0 \quad 0]m/s$, ${}^{V}V(26)=[5 \quad 0 \quad 0]m/s$, compared the other navigation states. As a result, we will be needing faster control deviations when the open-loop system is more unstable.

Running the same simulation with a triangle shaped disturbance of $x_d=[0 \quad 0 \quad 0 \quad 0 \quad 0 \quad 0 \quad 0 \quad 1]$ (roll disturbance) between $11 \le t \le 13\,s$, we expect that the controller should quit tracking mode in the presence of a disturbance, get into regulator mode and continue tracking after disturbance and its adverse affects are minimized. Results are graphed in Figure 59. This time, conversion is accomplished in 39 seconds of time and 145 meters of displacement with a control effort of 97.15. The results show that when the disturbance has affected the system, making the system feel rolling CCW around x-axis of body frame, it initially increased RPM1 and Tilt1, and reduced RPM2 and Tilt2. This change gave Tiltrotor UAV a negative roll rate $p\,(\deg/s)$ in order to turn aircraft in the negative direction. After the disturbance vanished in 2 seconds, the controller reversed the control deviations in order to get back to the trim state, and reaching to the trim point in about 4 seconds. In fact, the controller left the tracking mode for the regulator mode, and waited in this mode until the disturbance and its adverse affects are minimized. Then, the controller got back to the tracking mode and finished conversion in 39 seconds. As a result, the disturbance delayed the conversion, increased the displacement in the Earth frame, and total control effort, as expected.

The power spectrum densities of control input deviations in the presence of disturbance are shown in Figure 60. It is clear that, the controller applies faster and bigger control deviations, when a disturbance is detected.

This controller works properly if the disturbances have small magnitudes, small enough not to disturb the states of the system far away from the trim points. If such conditions occur, the linearized model is no longer valid, and control inputs slip out of the operating region. In order to overcome this problem, larger sets of linearized data, for both straight and rotational flight are required.

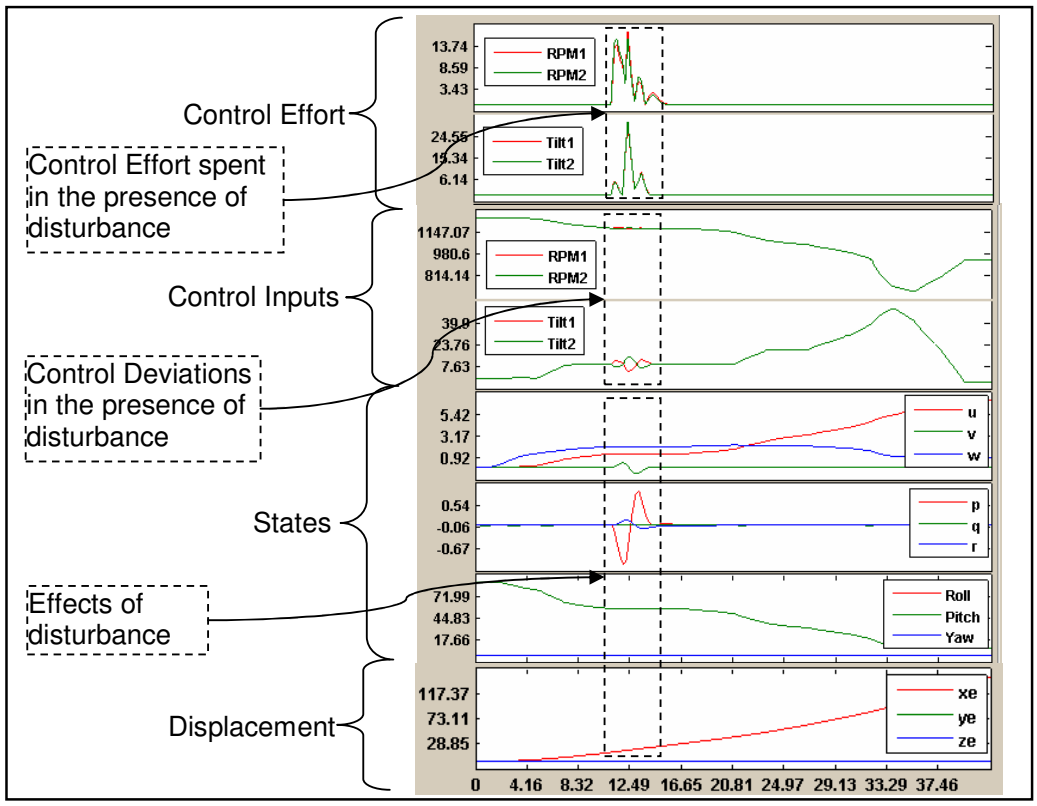

Figure 59. Conversion from Helicopter to Airplane Mode with disturbance.

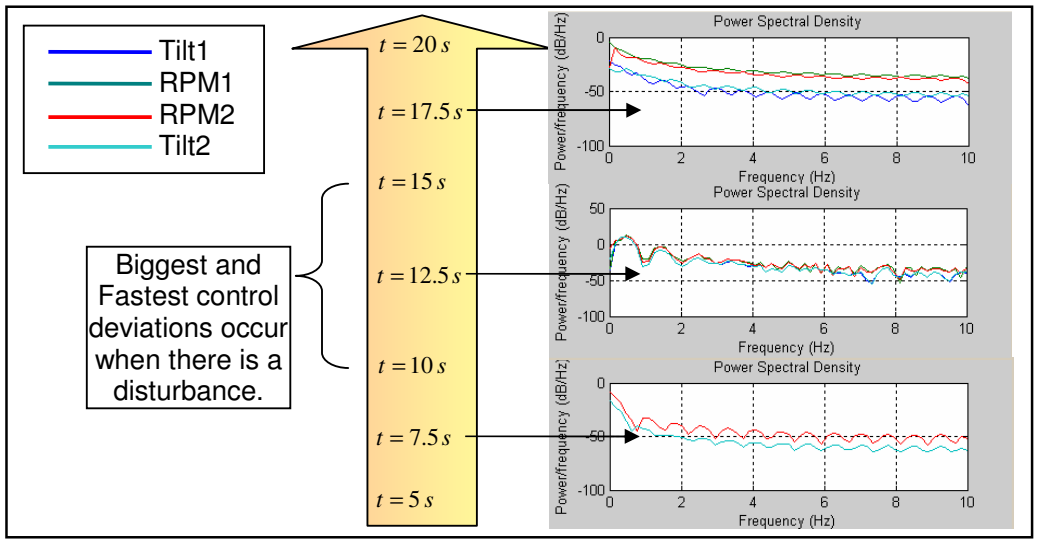

Figure 60. PSD of control input deviations for conversion from Helicopter to Airplane Mode with disturbance.

CHAPTER 7

CONCLUSIONS

The main purpose of this study was to assert an initial conceptual design for a small-sized Tiltrotor UAV, explore its dynamics, determine control strategies and requirements. With that purpose, simulation programs are prepared in order to obtain the numerical results for the design phases.

Airfoil Mapper program gave the opportunity to model and analyze any type of airfoil, resulting with sufficient data for using airfoils as a structural element to compose wings and propeller blades. *Component Designer* program formed a backbone to design basic components of an aircraft. *UAV Designer* program equipped with trimming and linearization routines, provided the ability to design new types of conceptual UAVs with simulation and analysis tools. *LQR Control* program enabled the design of different optimal control strategies, for the control of designed UAVs. Although, these programs have a lot to add and improve, they have a lot more to offer for new designs and analysis.

The initial conceptual design of the Tiltrotor UAV, performed well in simulations, accomplishing the conversion from helicopter mode to airplane mode in a reasonable amount of time and distance. But, the analysis showed the requirements for very fast actuators for the tilt and RPM changes, which are not easy to achieve in the real world; although slower controls may perform well in certain conditions, this makes it more vulnerable to disturbances. These high standard requirements resulted from the unstable nature of Tiltrotor UAV, which may be reduced with the addition of new control surfaces like a tail stabilizer or a free-wing design.

Although a navigation algorithm is not implemented in this work, the controller is designed to follow velocity commands in the Earth frame, so that an outer controller for navigation may be implemented easily.

CHAPTER 8

FUTURE WORKS

Due to the popularity of UAVs, they have become the focus of the cutting-edge technologies. New designs emerge all over the world, with only limitations being the human mind. For example, “The Vulture Project” managed by DARPA (Defense Advanced Research Projects Agency - USA) is claiming to overtake the missions of satellites, with flying non-stop at high altitudes at least for 5 years, using only the sunlight as the power source. Considering military applications, operational UAVs have become ready for service, but there is a growing demand for crucial missions, in the heart of the battlefield. As the new sensor technologies are developed, new UAV designs are required in order to make the sensors accomplish its mission efficiently, where the sensor is the limiting factor, not UAV. It seems that, this trend will continue until UAVs take over even the throne of automobiles in transportation, who knows what is to come in the future.

The ideas asserted in this thesis, have a lot more to study than performed in this work. With the help of the prepared simulation programs, the possibility of different design, analysis and simulation studies seems limitless.

Considering the problems faced in this work, if the tail wings were designed with a degree of freedom to move or designed with rudder and elevators as in airplanes, or stabilizers in helicopters, the stability of the Tiltrotor UAV would be increased in a way making the control easier for the conversion modes near the plane mode, and the plane mode itself. This idea may be followed as an extension of this work in the future.

One of the difficulties faced in this study, was finding a good trim point. This difficulty arose mostly from the complexity of the propeller model. When the trends of the

outputs of the propeller model is inspected, it is observed that the model could be simplified with polynomials of some degree. Model simplifications may be applied to the components and Tiltrotor UAV as a future work.

From the inexpert practitioner's point of view, the results of this work showed that, it is not easy to make a small-scale tiltrotor in one attempt, due to its unstable characteristics. First of all, one may analyze the characteristics of propellers experimentally as performed by Merchant [6], in order to fortify the propeller model used here. Then a quadrotor application may follow, which forms more stable characteristics at hover, making the practitioner experienced with the vertical flight. After that, experiments may be followed with model airplanes, for getting familiar with straight flight. Eventually the combinations of these two aircrafts may be practiced, finally resulting in a tiltrotor. Considering that V-22 Osprey, as said to be built upon the experience gained from XV-15, was available for service 15 years after, than initially planned (Leishman [1]), these steps seem to be a logical way to follow.

REFERENCES

[1] G. Leishman, “Is There a Case for the Tiltrotor?”, Rusi Defence Systems, vol.10, no. 2, pp. 52-55, October 2007.

[2] Bell Helicopter, *Bell’s Eagle Eye*, Texas, USA: Bell Helicopter Textron Inc. Pub., 2005.

[3] R. Preator, “Conceptual Design Studies of a Mono Tiltrotor”, M.Sc. thesis, University of Maryland, USA, 2005.

[4] K. M. Kleinhesselink, “Stability and Control Modeling of Tiltrotor Aircraft”, M.Sc. thesis, University of Maryland, USA, 2007.

[5] G. D. Klein, “Linear Modeling of Tiltrotor Aircraft (In Helicopter and Airplane Modes) for Stability Analysis and Preliminary Design”, M.Sc. thesis, California, USA: Naval Postgraduate School, 1996.

[6] M. P. Merchant, “Propeller Performance Measurement for Low Reynolds Number Unmanned Aerial Vehicle Applications”, M.Sc. thesis, Wichita State University, Kansas, USA, 2005.

[7] I. D. Cowling, Whidborne, J.F., Cooke, A.K., “Optimal Trajectory Planning and LQR Control for a Quadrotor UAV”, Cranfield University, Oxfordshire, UK, 2006.

[8] Ç. Karasu, “Small-Size Unmanned Model Helicopter Guidance and Control”, M.Sc. thesis, Middle East Technical University, Ankara, Turkey, 2004.

[9] B. Etkin, *Dynamics of Atmospheric Flight*, Toronto, Canada: John Wiley and Sons, Inc., 1972.

[10] ISA (International Standard Atmosphere), International Organization for Standardization (ISO) Publication, ISO 2533:1975.

[11] G. Leishman, *Principles of Helicopter Aerodynamics*, 2nd ed., England: Cambridge University Press, 2006.

[12] W. Johnson, *Helicopter Theory*, Toronto, Canada: Dover Publications Inc., 1994.

[13] J. Seddon, *Basic Helicopter Aerodynamics*, USA: Blackwell Science Pub., 1996.

[14] J. Nocedal, *Numerical Optimization*, 2nd ed., Illinois, USA: Springer Pub., 2006.

[15] M. Drela, XFOIL 6.96 (GPL): An Interactive Program For the Design and Analysis of Subsonic Isolated Airfoils, Massachusetts Institute of Technology, USA, 2008.

[16] R. E. Sheldahl and P. C. Klismas, "Aerodynamic Characteristics of Seven Airfoil Sections Through 180-degree Angle of Attack for Use in Aerodynamic Analysis of Vertical Axis Wind Turbines", Sandia National Laboratories, SAND80-2114, 1981.

[17] G. D. Padfield, *Helicopter Flight Dynamics: The Theory and Application of Flying Qualities and Simulation Modeling*, Bedford, UK, AIAA Education Series, 1996.

[18] D. G. Hull, *Optimal Control Theory for Applications*, Texas, USA: Springer, 2003.

[19] R. Burns, *Advanced Control Engineering*, Oxford, UK: Butterworh-Heinemann Pub. 2001.

[20] H. P. Geering, *Optimal Control with Engineering Applications*, Zurich, Switzerland: Springer Pub. 2007

[21] B. D. O. Anderson, *Optimal Control Linear Quadratic Methods*, Canbera, Australia: Prentice-Hall, 1989.

[22] K. Cunningham, “Simulation Study of Flap Effects on a Commercial Transport Airplane in Upset Conditions”, NASA Langley Research Center, Langley, USA, AIAA 2005: 5908, 2005.

[23] W. F. Philips, *Mechanics of Flight*, New Jersey, USA: John Wiley and Sons, Inc., 2007.

[24] J. J. Craig, *Introduction to Robotics*, 2nd ed., USA: Addison-Wesley Pub. Co., 1989.

[25] P. Castillo, *Modeling and Control of Mini-Flying Machines,* Compiegne, France, Springer, 2005.

[26] F. Çakıcı and K. Leblebicioğlu, “Modeling, Stability Analysis and Control System Design of A Small-Sized Tiltrotor UAV”, presented at the 50th Annual Conference of National Committee of Automatic Control, Istanbul Technical University, Turkey, 2008.

[27] T. C. Chen, *Linear System Theory and Design,* New York, USA: Saunders Collage Pub., 1984.

[28] D. E. Kirk, *Optimal Control Theory: An Introduction,* New York, USA: Dover Pub., 2004.

[29] “Drag Coefficient’s of different body shapes”, Jan. 25 , 2009. [Online]. Available: http://en.wikipedia.org/wiki/Drag_coefficient. [Accessed: Feb.09, 2009].

[30] J. J. Bertin, *Aerodynamics for Engineers,* New Jersey, USA: Prentice-Hall Pub.,1998.

APPENDICES

A. NOTATIONS FOR VARIABLES

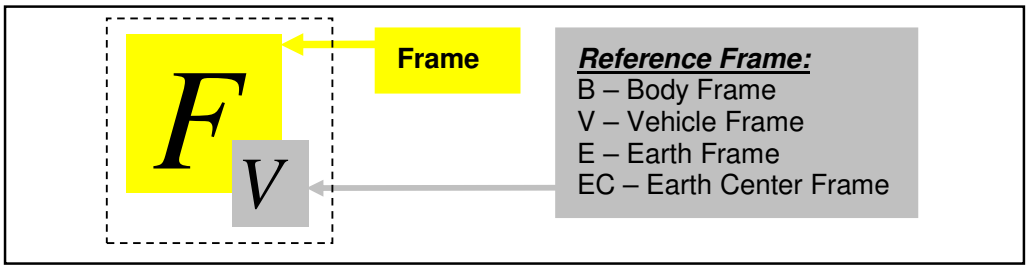

Figure 61. Notation for frames.

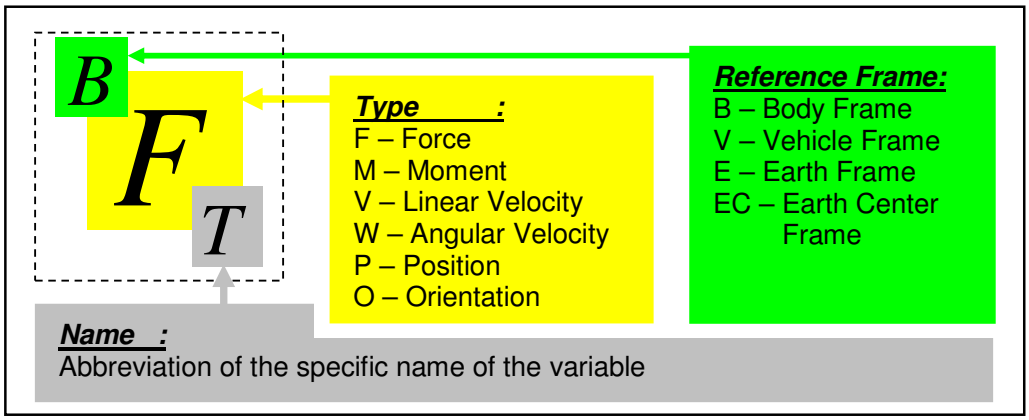

Figure 62. Notation for vectoral variables.

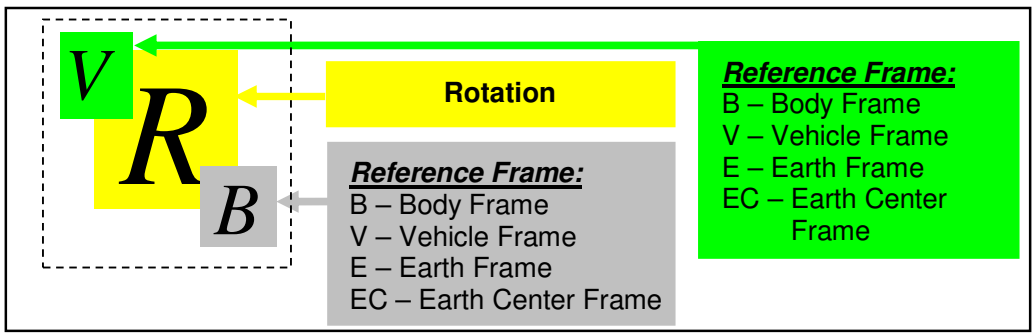

Figure 63. Notation for rotational operators.